Inter-regional synchronization in the hippocampal system by oscillations: unit and LFP studies

by

David W. Sullivan

A Dissertation submitted to the

Graduate School-Newark

Rutgers, The State University of New Jersey

in partial fulfillment of the requirements

for the degree of

Doctor of Philosophy

Graduate Program in Behavioral and Neural Sciences

written under the direction of

György Buzsáki

and approved by

_____

_____

_____

_____

_____

Newark, New Jersey

May 2013

Abstract of the Dissertation

Inter-regional synchronization in the hippocampal system by oscillations: unit and LFP studies

By David W. Sullivan

Dissertation Director:

György Buzsáki

This dissertation investigated how several different types of oscillation organize neural activity in the hippocampus and the entorhinal cortex. I used recordings performed by myself and others to explore the nature of the ripple, sharp wave, fast gamma, theta, and spindle oscillations, the manner in which these oscillations propagate through the hippocampal network, and how behavior affects the properties of these oscillations.

The first study concerned two types of high frequency oscillation in CA1: fast gamma and ripples, their relationship to sharp waves, the nature of their emergence in CA3 and propagation to CA1, and their interaction with slow oscillations during sleep. I found that the ripple oscillation emerges de novo in CA1 rather than being transmitted wave-by-wave from CA3 to CA1. I also found that there is an inverted-U shaped relationship between the peak frequency of ripple oscillations and the amplitude of sharp waves.

The second study extended the observations of the first study by taking the behavioral state of the animal into account. I found that the ripples that occur intermidst active

behavior oscillate at a higher frequency than those that occur during sleep and quiescence, and that the relationship between sharp wave amplitude and ripple frequency differs depending on behavioral state. I also found that ripples that are detected during running are due to recording artifacts, whereas ripples occasionally occur during REM sleep.

The third study examined the nature of sleep spindles in the hippocampus, and is an exploration (and ultimately, a rejection) of the hypothesis that the mechanisms of sleep spindles are the same. I found that many neurons prefer different oscillation phases of theta and spindles, suggesting that different sets of inputs drive neurons. I also found that principal cells are not rhythmically entrained by spindle oscillations; this and the lack of phase precession during spindles led to the conclusion that spindles should not be considered as a special case of theta.

Acknowledgements

Many thanks to my advisor, György Buzsáki, whose bottomless well of inspiration is itself an inspiration. Thanks to my former advisor, Chip Levy, who facilitated my entrance to this field. Thanks for my parents and family and friends for love and support. Many thanks to my thesis committee for your patience and feedback.

Contents

Section 1 – Introduction

1.1 Overview

In the hippocampus and in the brain in general, communication is facilitated and organized by several different types of neural oscillations, operating during different behaviors, at different timescales, and at different frequencies (Buzsáki and Draguhn, 2004). There are multiple putative functions of neural oscillations such as the temporal coordination of neurons that they provide, leading to the transfer of information between brain regions, regulation of plasticity, and homeostatic processes.

This thesis comprises three studies that expand and refine our knowledge of how several different types of oscillations (sharp wave-ripples, fast gamma, gamma, spindles, theta) organize activity in the hippocampus and its "upstream" and "downstream" region, the entorhinal cortex. For the introduction, I present a brief overview of hippocampal and entorhinal anatomy, followed by an overview of oscillations in the hippocampus, followed by an overview of hippocampal function.

1.2 Basic anatomy of the rat hippocampus

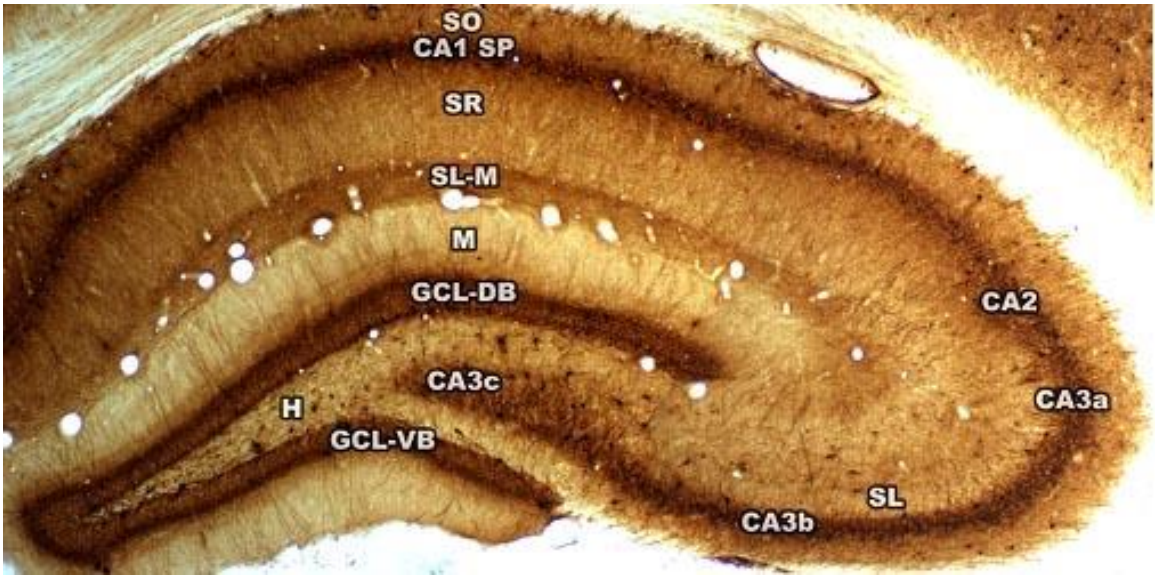

Figure 1.1 A coronal section (50 µm thick) through the dorsal hippocampus, stained for parvalbumin, illustrating the major anatomical features of the hippocampus (from one of my first practice brains). Left is medial, right is lateral. Abbreviations: SO: CA1 stratum oriens; CA1 SP: CA1 stratum pyramidale (pyramidal layer); SR: CA1 stratum radiatum; SL-M: stratum lacunosum-moleculare; M: dentate gyrus molecular layer; GCL-DB: dentate gyrus granule cell layer (dorsal blade); H: dentate gyrus hilus (polymorphic layer); SL: stratum lucidum; CA3c: CA3c pyramidal layer; CA3b: CA3b pyramidal layer; CA3a: CA3a pyramidal layer, CA2: CA2 pyramidal layer. Image was created by digitally merging two photomicrographs (4x).

Although there is some disagreement as to which specific neural structures fall under the umbrella of the term "hippocampus" (Amaral and Witter, 1995), for the purposes of this document the hippocampus consists of two folded, interlocking neural structures: the Cornu Ammonis and the dentate gyrus. The hippocampal cross-section in figure 1.1 illustrates the subregions and layers of the hippocampus. The anatomical organization depicted in this cross-section is largely repeated throughout the third dimension, or septo-temporal axis of the hippocampus.

Perhaps the most well-known aspect of hippocampal connectivity is the feed-forward excitatory "tri- or multi-synaptic loop", comprising glutamatergic projections from the

entorhinal cortex to the dentate gyrus, dentate gyrus to CA3, CA3 to CA1, and CA1 back to entorhinal cortex (Amaral and Witter, 1995)

1.2.1 Cornu ammonis

The Cornu Ammonis, or "Ammon's horn", sometimes referred to as the "hippocampus proper", is traditionally divided into three subregions, abbreviated as CA1, CA2, and CA3. Each subregion consists of 4 or 5 layers. From outside to inside, the layers and their most notable features are: the stratum oriens, which contains the basal dendrites of pyramidal cells and collaterals of hippocampal CA3 pyramidal cells; the stratum pyramidale, which contains the pyramidal cell bodies; the stratum lucidum, which is a layer only found in CA3 that contains the axons from dentate gyrus granule cells (also referred to as mossy fibers); the stratum radiatum, which contains pyramidal cell dendrites and inputs from hippocampal CA3 pyramidal cells; and the stratum lacunosum-moleculare, which contains distal pyramidal cell dendrites and "perforant path" inputs: in CA3 from entorhinal cortex layer 2 cells, in CA1 from entorhinal cortex layer 3 cells as well as inputs from various anterior thalamic nuclei.

The CA1 and CA3 regions have different circuitry. The pyramidal cells of CA3 project bilaterally to the pyramidal cells of both CA3 and CA1. Although there is some topographic organization to the pattern of CA3 connections (Ishizuka et al., 1990), it is more diffuse than in most cortical regions, and in fact is considered by some researchers to be essentially random (Li et al., 1994; Levy, 1996; Wittner et al., 2007). Aside from the hilus of the dentate gyrus (see below), CA3 is the only region to receive inputs from the granule cells of the dentate gyrus. The only known extrahippocampal projection of

CA3 pyramidal cells is to the lateral septal nucleus (Swanson and Cowan, 1977). CA1, in contrast to CA3, has widespread, topographically organized projections to structures outside the cornu Ammonis. The best described projections of CA1 are to the subiculum and the deep layers of the entorhinal cortex. However, recent studies have demonstrated that CA1 projects to a surprisingly large number of neocortical areas (Cenquizca and Swanson, 2007), and also projects to various hypothalamic and thalamic structures (Cenquizca and Swanson, 2006).

The CA2 region, a narrow sector between CA3 and CA1, has pyramidal cells with axonal projections much like those of CA3 cells; however, CA2 pyramidal cells do not receive mossy fiber inputs, and CA2 is the only Cornu Ammonis region to receive inputs from the supramammillary nucleus (Vertes and McKenna, 2000).

The extrahippocampal inputs to CA3 are limited. The only extrahippocampal, non-subcortical input to CA3 is from layer 2 of the entorhinal cortex. CA3 receives GABAergic and cholinergic inputs from the medial septum (Gulyas et al 1990), noradrenergic input from the locus coeruleus (Swanson et al 1987), and serotonergic inputs from the median raphe (Acsady et al 1996).

The major cortical projection to CA1 arises from layer III of the entorhinal cortex. Similarly to CA3, CA1 receives noradrenergic and serotonergic projections, but also receives a weak dopaminergic projection (Swanson et al., 1987). CA1 receives subcortical inputs that CA3 does not, including afferents from the nucleus reuniens (Herkenham, 1978) and the amygdala projects to temporal levels of CA1 (Krettek and Price, 1977).

Until recently, pyramidal cells in the cornu Ammonis subregions were generally assumed to constitute a single class of cells. However, new studies indicate that there may be two classes of pyramidal cell in CA1, which differ in their morphological and electrophysiological properties and may constitute separate, parallel output streams (Mizuseki et al., 2011; Graves et al., 2012).

1.2.3 Dentate gyrus

The anatomy of the dentate gyrus was recently reviewed in thorough detail in a number of studies contained within Scharfman (2007); what follows here is an overview of the main features. The dentate gyrus is a U- (in the horizontal plane) or V- (in the coronal plane) shaped structure wrapped around the proximal end of the CA3 field. It consists of three main layers: the molecular layer, the granule cell layer, and the hilus or polymorphic layer (the term "CA4" by Lorente de Nó has also been used to refer to the hilus but is now considered obsolete; Amaral, 1978). The molecular and granule cell layers together are sometimes referred to as the "fascia dentata". The molecular layer most notably contains the dendrites of the granule cells, intrinsic and extrinsic axon fibers, and also cell bodies and dendrites of some types of interneuron. The molecular layer can be divided into an outer, middle, and inner subdivision, corresponding to the termination zones of projections from the lateral entorhinal cortex, the medial entorhinal cortex (and also the presubiculum), and the commissural/associational projection from the hilus, respectively.

The granule cell layer is composed of the cell bodies of the granule cells and some types of interneurons. The portion of the granule cell layer situated between the CA3 and CA1

regions is commonly referred to as the dorsal blade, while the portion of the granule cell layer positioned ventral to the CA3c pyramidal layer is termed the ventral blade. The apical dendritic trees of the granule cells of the dorsal blade extend to the hippocampal fissure. The primary excitatory input to granule cells is from layer 2 cells of the medial and lateral entorhinal cortex, although granule cells also receive excitatory inputs from mossy cells (Buckmaster et al., 1992), presubicular cells (Amaral and Witter, 1995), and supramammillary cells (Kiss et al., 2000). Unlike the other principal cells of the hippocampus, the mature granule cells possess no basal dendritic tree in rodents (but do have basal dendritic trees in humans; Seress and Mrzljak, 1987), although such processes can develop in pathological conditions in rodents (Ribak et al., 2000). The axons of granule cells, the mossy fibers (not to be confused with mossy cells, see below), project into the hilus, where they collateralize and contact mossy cells and assorted interneurons before coursing parallel to the CA3 pyramidal layer. Most mossy fibers course in a layer termed stratum lucidum, which is situated directly above the CA3 pyramidal layer, although there are also weaker infra-pyramidal and sub-pyramidal bundles of mossy fibers in CA3c (Amaral et al., 2007). Although mossy fibers contact both pyramidal cells and interneurons in CA3, many more interneurons than pyramidal cells are contacted: the ratio of interneuron contacts to pyramidal cell contacts is approximately ten to one, although the terminal types are different (Acsady et al., 1998). The mossy fibers travel parallel to the transverse axis of the hippocampus, except at the CA3/CA2 border where they make an abrupt turn and project longitudinally toward the temporal pole (Swanson et al., 1978; Amaral and Witter, 1995; Acsady et al., 1998). Another distinction between granule cells and the pyramidal cells of the CA3 and CA1 regions is that the mossy fibers

do not project to any extrahippocampal structures, and have no contralateral projections. Finally, granule cells differ from pyramidal cells in that they are generated postnatally (Altman and Das, 1965; Zhao et al., 2008) and are maintained by circulating steroids (Sloviter et al., 1989).

1.2.4 Entorhinal cortex

The entorhinal cortex is a six-layer cortex that occupies the most posterior and medial portion of the rat brain. The laminar organization of entorhinal cortex is similar to that of neocortex, with populations of excitatory glutamatergic neurons in layers 2, 3, and 5, although the layer that corresponds to cortical layer 4 is mostly cell-free and is called lamina dessicans. On the basis of connectivity, the entorhinal cortex is subdivided into medial and lateral areas.

The entorhinal cortex layers 2 and 3 project topographically to the hippocampus via the perforant path. Whereas there is a radial topography to the projection to the dentate gyrus and CA3, there is a transverse topographic organization of the perforant path projection to CA1, with medial entorhinal cortex projecting to the proximal portion of CA1 (closer to CA2) and lateral entorhinal cortex projecting to the distal portion of CA1 (closer to the subiculum).

Within the entorhinal cortex, there are projections from deep layers to superficial layers. Because entorhinal projections to the hippocampus mostly arise from layers 2 and 3, and projections from the hippocampus to the entorhinal cortex terminate mostly on layer 5 neurons, the connectivity between the hippocampus and entorhinal cortex forms a loop involving all subregions of these two structures.

On the basis of its inputs, the entorhinal cortex can be considered to be near the top of a processing hierarchy – most of the cortical inputs to entorhinal cortex are from polymodal associational areas, including the perirhinal and postrhinal cortices, although there are some inputs from gustatory and piriform cortex, as well as direct inputs from the olfactory bulb. There is evidence that the lateral entorhinal cortex processes primarily non-spatial information whereas the medial entorhinal cortex is more concerned with spatial information (Hargreaves et al., 2005). Recently the medial entorhinal cortex has received a great amount of attention due to the discovery of neurons that fire in a grid pattern relative to the animal's spatial location (Hafting et al., 2005) beside neurons that seem to respond preferentially to head direction and borders (or combinations of these features) in the environment (Solstad et al., 2008).

1.2.5 Hippocampal interneurons

A menagerie of GABAergic interneuron types is present in the hippocampus, and they are distinguished by several characteristics, including the domain of principal cells they target, as well as their morphology, (co-)transmitters, and immunocytochemical markers (Freund and Buzsáki, 1996). Most hippocampal interneuron cell types have analogous cell types in the neocortex. The major classes of hippocampal interneurons are basket cells (targeting the perisomatic region), axo-axonic cells (targeting the axon initial segment), axo-dendritic cells (targeting the dendrites of principal cells), and interneuron-specific interneurons.

Within these broad classes of interneurons are specific cell types that are noted for the laminar specificity of their axonal projections, and in some cases, their dendritic

arborization. For example, in CA1 the axons of a class of interneurons referred to as "O-LM cells" are found mainly in s. lacunosum moleculare, whereas their dendrites are confined to s. oriens -- a feed-back arrangement with CA1 pyramidal cells that leads to inhibition their own dendrites and presumably counterbalances the excitation by entorhinal inputs (Leão et al., 2012). An analogous cell type exists in the dentate gyrus: the HIPP cell's dendrites are mostly confined to the hilus and its axons mostly arborize in the outer two thirds of the molecular layer, putatively providing feedback inhibition of entorhinal inputs to granule cells (Han et al., 1993; Halasy & Somogyi, 1993; Sik et al., 1997).

A major subdivision exists within the class of basket cells: those that express the calcium binding protein parvalbumin, and those that express cholecystokinin (CCK). The fast firing rates and membrane time constants of parvalbumin-expressing basket cells are ideal for providing fast feedback inhibition, whereas CCK expressing basket cells seem more ideally situated for state-dependent patterns of inhibition (Földy et al 2007).

1.3 Oscillations

The hippocampal LFP is dominated by oscillations associated with specific behaviors. These oscillations, which reflect the summation of synchronous membrane potential fluctuations in the parallel oriented dendritic trees of principal cells and some classes of interneurons, occur over a wide range of frequencies, including theta (4-8 Hz), spindle (9-18 Hz), gamma (30-80 Hz), and epsilon (90-200 Hz). Oscillations are thought to be key to neural computation, synchronizing neural activity, enhancing synaptic plasticity (Huerta and Lisman, 1995), and coordinating cell assemblies (Dragoi and Buzsáki, 2006).

1.3.1 Large irregular activity (LIA)

During non-REM sleep, the hippocampal EEG is characterized by large-amplitude irregular patterns occurring over a variety of frequencies, and unit activity is characterized by periods of relatively high activity interspersed with periods of near-silence, reminiscent of the neocortical slow oscillation However, in contrast to the bimodal distribution of the membrane potential of neocortical (Steriade et al., 1993) and entorhinal (Isomura et al., 2006) principal cells, hippocampal cells do not show such bimodality; it remains to be determined whether this arises from differences at the cell or network level. Nevertheless, the neocortical slow oscillation present during non-REM sleep (Steriade et al., 1993) can bias the timing of hippocampal patterns in an organized fashion (Isomura et al., 2006).

1.3.2 Theta

Theta oscillations (4-8 Hz), which occur mostly during exploration and REM sleep, emerge from a complex network including the nucleus pontis oralis, the median raphe nucleus, the supramammillary nucleus, and the medial septum/diagonal band of Broca (Vertes et al., 2004). During exploration, firing of hippocampal principal cells is dynamically modulated by the phase of the theta oscillation such that the phase of firing correlates with animal's position (O'Keefe & Reece, 1993; Huxter et al., 2008) and within each theta cycle, the sequence of place cells that fires represents the animal's immediate past and future trajectory (Skaggs et al., 1996; Tsodyks et al., 1996; Jensen and Lisman 1996; Dragoi and Buzsáki, 2006).

Recent studies have demonstrated that different classes of interneurons in the CA1 region of the hippocampus preferentially fire during different theta phases in anesthetized animals (Klausberger et al., 2003). Additionally, some hippocampal interneurons dramatically change their firing rates depending on the presence or absence of the theta rhythm (Buzsáki and Eidelberg, 1983; Colom & Bland, 1987). Because different interneuron classes target different compartments of primary cells, cell class-specific theta phase preferences and state-dependent firing rates may have major implications for the impact of the theta rhythm on physiological processes in individual principal cells (Klausberger & Somogyi, 2008).

1.3.3 Sleep spindles

Sleep spindles (9-20 Hz) are a prominent EEG feature of non-REM sleep (Loomis, 1937; Steriade, 1993). Sleep spindles are generated by interactions between the thalamic reticular nucleus and thalamocortical nuclei (Steriade et al., 1993). Although sleep spindles have not been widely studied in the hippocampus, it has been demonstrated that the occurrence of sharp wave-ripple oscillations in the hippocampus is correlated with sleep spindles (Siapas and Wilson, 1998), and that hippocampal neurons and field potentials are entrained by spindles detected in the neocortex, both in the rat (Sirota et al., 2003) and in humans (Nir et al., 2011). Sleep spindles are most common in intermediate sleep, a sleep stage that occurs preceding the transition from non-REM to REM sleep (Gottesmann, 1973).

1.3.4 Gamma

The gamma oscillation (30-80Hz) is generated by the hippocampal network itself and also by entorhinal afferents (Bragin et al., (1995b); Csiscvari et al., 2003; Buzsáki and Wang, 2012). Gamma oscillations can occur simultaneously with the theta rhythm, or in the absence of it, and are nearly ubiquitous in the dentate gyrus. Hippocampal gamma oscillations are thought to be important as a mechanism for the coordination of assemblies (Harris et al., 2003), and for memory encoding (Sederberg et al, 2007) and retrieval (Montgomery et al., 2007). The firing of some but not all hippocampal neurons is modulated by the phase of the gamma oscillation (Tukker et al., 2007), and in behaviors where the theta oscillation is present, the power of the gamma oscillation is modulated by the phase of the theta oscillation (Bragin et al., 1995b), and by behavior (Montgomery et al., 2007).

1.3.3 Sharp wave / ripples (SPW-R)

A major feature of the hippocampal EEG during non-REM sleep and quiet resting behaviors are transient (~50 ms) ~200Hz oscillations (“ripples”; O’Keefe and Nadel, 1978; Buzsáki et al., 1983, 1992), which appear in the CA1 pyramidal layer LFP, accompanied by large amplitude sharp waves (SPW) in stratum CA1 and CA3 radiatum (Buzsáki et al., 1983). These events are thought to originate from self-organized population bursts in the CA3 region (Csicsvari et al., 2000, 2003). Although sharp waves and ripples are often discussed as if they are a unitary phenomenon, they are indeed dissociable – sharp waves emerge in the developing animal before ripples (Leinekugel et al., 2002; Buhl and Buzsáki, 2005).

SPW-R is a mechanism by which the hippocampus can synchronize neurons in distant brain areas, including entorhinal cortex (Chrobak and Buzsáki, 1996) and prefrontal cortex (Wierzynski et al., 2009). Principal cells and interneurons in entorhinal cortex layers 2, 3, and 5 are recruited during SPW-R. The SPW-R evoked gain in firing rate by interneurons is close to or greater than that by principal cells in EC layers 2 and 3, supporting the idea that excitation generated by SPW-R does not complete the HPC-EC-HPC loop (Buzsáki and Lopes da Silva, 2012). Although dentate granule cells show increases in firing rate related to the occurrence of SPW (Penttonen et al., 1997); this effect is likely mediated by projections from the CA3 region to the hilus (Scharfman, 1994).

The physiological mechanism of sharp waves is relatively straightforward – a population burst of CA3 pyramidal cells leads to depolarization in the apical dendrites of CA1 and CA3 neurons, which is reflected by the large amplitude negative sharp wave and current sink observed in CA1 and CA3 stratum radiatum (Ylinen et al., 1995). The mechanism of ripple oscillations, on the other hand, is more complicated. Ripples are thought to emerge from the dynamics of fast interaction between synaptically connected CA1 pyramidal cells and interneurons (Ylinen et al., 1995; Csicsvari et al, 2000; Brunel and Wang, 2003), but ephaptic effects may also play a role (Anastassiou et al., 2010). SPW-R are not a global pattern in the hippocampus; the spatial extent of SPW-R is limited the septotemporal axis and SPW-R do not usually occur simultaneously in both hemispheres (Chrobak and Buzsáki 1996; Csicsvari et al., 2003; Patel 2013).

1.4 Hippocampal function

The function of the hippocampus has been widely debated, but almost all researchers agree that it is critically involved in some types of learning and memory. In humans, lesions to the hippocampal region can lead to severe deficits in declarative and episodic memory (Scoville and Milner, 1957); i.e., the ability to recall facts and personal experiences. Because damage to the hippocampus and other closely connected areas often results in retrograde amnesia (i.e., recent memories are abolished while older memories are preserved), it is thought that memories that are initially hippocampus-dependent are gradually transferred to the cortex, a process termed "memory consolidation" (Squire, 1987; Buzsáki, 1989). Supporting of the hippocampal role in memory consolidation, sequences of neurons that fire during SPW-R both during sleep (Skaggs and McNaughton, 1996) and wakeful states (Foster and Wilson, 2006; Diba and Buzsáki, 2007) reflect previously experienced spatial trajectories. Furthermore, on-line disruption of SPW-R in CA1 during sleep following learning (Girardeau et al., 2009) or during waking (Jadhav et al., 2012) decreases performance on a hippocampus-dependent spatial reference memory tasks.

Single unit recording studies in the hippocampi of epileptic patients have provided evidence that hippocampal cells are selectively responsive to abstract concepts, such as specific famous people (Quiroga et al., 2005), as well as specific places in a navigational task (Ekstrom et al., 2003) and episodic recall (Gelbard-Sagiv et al., 2008). Such abstract neural correlates are consistent with a hippocampal role in declarative and episodic memory, and that the function of a "place cell" in rodents may be more general in humans.

The rodent hippocampal literature has focused primarily but not exclusively on a role for the hippocampus in spatial navigation. Principal cells from all hippocampal subregions selectively fire in one or more regions of the animal's environment; cells that exhibit this mode of firing are referred to as "place cells" (O'Keefe & Dostrovsky, 1971; Jung & McNaughton, 1993). Many of the behavioral tasks that are dependent on an intact hippocampus have a component that requires spatial navigation component, such as the Morris water maze (Morris et al, 1982).

There are two main aspects to the spatial navigation role of the hippocampus: providing information about the animal's location that is acquired and updated from environmental cues; i.e., allocentric (world-centered) mapping, and providing information about the distance of the animal from places that have been allocentrically mapped based on self-motion cues; i.e. path integration or egocentric exploration. A recent review argues that there are strong parallels between these two facets of spatial navigation in rats and the two types of memory that the hippocampus is thought to support in humans, such that declarative memory is an internalized version of allocentric mapping and episodic memory is an internalization of egocentric mapping (Buzsáki and Moser, 2013).

Conflicting with a purely spatial role for the hippocampus, it has been shown that hippocampal lesions interfere with configural tasks (i.e., tasks that require learning rules based on the relationships of environmental features) such as transverse patterning (Alvarado & Rudy, 1995) and transitive inference (Dusek & Eichenbaum, 1997). Additionally, the hippocampus seems to be required for explicitly non-spatial tasks such as trace fear conditioning (McEchron et al., 1998), and hippocampal neurons fire in specific sequences that bridge temporal gaps between discontiguous task events

(Pastalkova et al., 2007; MacDonald et al. 2011). Many attempts have been made to develop a theory of hippocampal function that can account for the role of the hippocampus in learning and memory in both spatial and non-spatial behaviors, and many of such theories consider hippocampal function in terms of the types of information processing it might perform (e.g., Levy, 1989; Treves & Rolls, 1994; Hasselmo & McClelland, 1999).

1.5 Figure Legends

Figure 1.1

Figure 1.1 A coronal section (50 μm thick) through the dorsal hippocampus, stained for parvalbumin, illustrating the major anatomical features of the hippocampus (from one of my first practice brains). Left is medial, right is lateral. Abbreviations: SO: CA1 stratum oriens; CA1 SP: CA1 stratum pyramidale (pyramidal layer); SR: CA1 stratum radiatum; SL-M: stratum lacunosum-moleculare; M: dentate gyrus molecular layer; GCL-DB: dentate gyrus granule cell layer (dorsal blade); H: dentate gyrus hilus (polymorphic layer); SL: stratum lucidum; CA3c: CA3c pyramidal layer; CA3b: CA3b pyramidal layer; CA3a: CA3a pyramidal layer, CA2: CA2 pyramidal layer. Image was created by digitally merging two photomicrographs (4x).

Section 2 - Synchronization by sharp waves-ripples and fast gamma oscillations in the hippocampal-entorhinal loop

Published: Sullivan D, Csicsvari J, Mizuseki K, Montgomery S, Diba K, Buzsáki G. 2011 J Neurosci 31:8605–8616.

2.1 Abstract

Hippocampal sharp waves (SPW) and associated fast ('ripple') oscillations in the CA1 region are among the most synchronous physiological patterns in the mammalian brain. Using two-dimensional arrays of electrodes for recording local field potentials and unit discharges in freely moving rats, we studied the emergence of ripple oscillations (140-220 Hz) and compared their origin and cellular-synaptic mechanisms with fast gamma oscillations (90-140 Hz). We show that (a) hippocampal SPW-Rs and fast gamma oscillations are quantitatively distinct patterns but involve the same networks and share similar mechanisms, (b) both the frequency and magnitude of fast oscillations is positively correlated with the magnitude of SPWs, (c) during both ripples and fast gamma oscillations the frequency of network oscillation is higher in CA1 than in CA3, (d) SPWs and associated firing of neurons are synchronous in the dorsal hippocampus and dorso-medial entorhinal cortex but ripples are confined to the CA1 pyramidal layer and its downstream targets and (e) the emergence of CA3 population bursts, a prerequisite for SPW-ripples, is biased by activity patterns in the dentate gyrus and entorhinal cortex, with highest probability of ripples associated with an 'optimum' level of dentate gamma power. We hypothesize that each hippocampal subnetwork possesses distinct resonant properties, tuned by the magnitude of the excitatory drive.

2.2 Introduction

Large amplitude local field potentials (‘sharp waves’; SPWs) occur irregularly in the hippocampal CA1 stratum radiatum when the animal has minimal interaction with its environment, such as immobility, consummatory behaviors or slow wave sleep (Buzsáki et al., 1983; Suzuki and Smith, 1987). SPWs are associated with fast-field oscillations (~140-200 Hz), or “ripples” in the CA1 pyramidal cell layer (SPW-R; Buzsáki et al., 1992; Csicsvari et al., 2000; O'Keefe and Nadel, 1978; Ylinen et al., 1995) In the time window of SPW-R (50-150 msec), 50,000 to 100,000 neurons (10-18% of all neurons) discharge synchronously in the CA3-CA1-subicular complex-entorhinal cortex (Chrobak and Buzsáki, 1996; Csicsvari et al., 1999), representing a several-fold increase of population synchrony compared to theta oscillations (Csicsvari et al., 1999a). Neuronal participation in the population discharge of SPW-R is biased by previous experience of the animal (Buzsáki, 1989; Kudrimoti et al., 1999; Nadasdy et al., 1999; Skaggs and McNaughton, 1996; Wilson and McNaughton, 1994; Lee and Wilson 2002; Foster and Wilson, 2006; Diba and Buzsáki, 2007; O'Neill et al., 2006; 2008; Dupret et al., 2010; Karlsson and Frank, 2008; 2009; Singer and Frank, 2009). Largely because of the behaviorally relevant spike content and the large gain in network excitability (Csicsvari et al., 1999a), SPW-Rs have been postulated to play a critical role in consolidating memory traces within the hippocampus and in transferring memories from the hippocampus to the neocortex (Buzsáki, 1989; 1996; Wilson and McNaughton, 1994; Ji and Wilson, 2007; McClelland et al., 1995; Siapas and Wilson, 1998; Axmacher et al., 2008; Eschenko et al., 2008; Mölle et al., 2009; Ramadan et al., 2009; but see Lubenov and Siapas, 2008). In support of this hypothesis, selective elimination of SPW-Rs during post-learning sleep

results in impairment of memory (Girardeau et al., 2009; Ego-Stengel and Wilson, 2010; Nokia et al., 2010). The importance of SPW-R is further illustrated by the observation that the temporal patterning of ripples is altered in epilepsy; in human temporal lobe epilepsy, the super-fast ripples that emerge are pathognomonic (Bragin et al., 1999 a, b; 2000; Staba et al., 2002; Jiruska et al., 2010).

A related hippocampal pattern in the absence of the theta rhythm is the gamma oscillation. Gamma oscillations are supported by multiple mechanisms (Bartos et al., 2007; Wang 2010), and occur in at least two varieties: gamma (or low frequency gamma; 30-90 Hz) and fast or 'high' gamma (> 90 Hz; Csicsvari et al., 1999b; Canolty et al., 2006; Colgin et al., 2009), which occupy different frequency bands and possibly utilize different mechanisms. While the origin and mechanisms of 'slow' gamma oscillations are relatively well-characterized (Csicsvari et al., 2003; Mann et al. 2005; Whittington et al., 2011), the mechanisms supporting fast gamma oscillations and especially their relationship to SPW-Rs are not well understood (Csicsvari et al., 1999b). In the present experiments, we investigated the physiological features of SPWs, ripples and fast gamma oscillations in the CA1 and CA3 regions of the hippocampus and the impact of the activity in the dentate gyrus and entorhinal cortex on these rhythms in the sleeping rat.

2.3 Materials and Methods

2.3.1 Animals and surgery

Ten male Long-Evans (5-8 months old) and 2 male Sprague-Dawley rats (350-500g; 5-8 months) were used in these experiments. Behavioral training, surgery details and data obtained from subgroups of the present rats have been reported earlier (Csicsvari et al.,

2002; Diba and Buzsáki, 2007; Montgomery et al., 2009; Mizuseki et al., 2009). After maze training, recording and stimulation electrodes were implanted. In six rats, a 96-site silicon probe was implanted in the right hemisphere parallel to the transverse axis of the hippocampus (45° parasagittal). These probes had recording sites spaced regularly over a 1.5mm X 1.5mm area with 6 shanks spaced at 300 µm, each with 16 recording sites at 100µm spacing. A bipolar stimulating electrode was implanted into the angular bundle (perforant path) at AP 1.0 mm, ML 1.0 mm from the junction between lambda and the right lateral ridge and DV 3.5 mm from the dura. Another stimulating electrode was implanted in the ventral hippocampal commissure at AP 1.2mm,ML 1.0mm from bregma and 3.8mm from the dura (Csicsvari et al., 2000; Montgomery et al., 2009). Three other rats were implanted with 32- and/or 64-site silicon probes in the left or right dorsal hippocampus. The silicon probes, consisting of 4 or 8 individual shanks (spaced 200 µm apart) each with 8 staggered recording sites (20 µm spacing), were lowered to CA1, CA3 pyramidal cell layers (Diba and Buzsáki, 2007) and dentate gyrus. Additional 3 rats were implanted with a 4-shank silicon probe in the right dorsocaudal medial entorhinal cortex (EC; Hafting et al., 2005) and another 4- or 8-shank probe into the CA1-dentate axis (Mizuseki et al., 2009). All silicon probes were attached to a microdrive, which allowed precise positioning of the probe tips into the desired layer. Two stainless steel screws inserted above the cerebellum were used as indifferent and ground electrodes during recordings.

Postmortem electrode location was verified using thionin, fluorescent Nissl (Invitrogen), or DAPI (Invitrogen) staining in combination with DiI (Invitrogen)-labeled electrode tracks. The histological reconstruction of the electrode tracks is available in Montgomery

et al. (2008; 2009). All protocols were approved by the Institutional Animal Care and Use Committee of Rutgers University.

2.3.2 Data collection

After recovery from surgery (~1 week), physiological signals were recorded in the home cage and included waking immobility and sleep epochs. During sleep the rat curled up in one of the corners with eyes closed. REM and slow wave sleep epochs were separated as described earlier (Montgomery et al., 2008). During the recording sessions, neurophysiological signals were amplified (1,000X), bandpass-filtered (1 Hz – 5kHz) and acquired continuously at 20 kHz on a 128-channel DataMax system (RC Electronics) or at 32.5 kHz on a 128-channel Digital Lynx system (Neuralynx Inc.). After recording, local field potential (LFP) was down-sampled to 1250 Hz for additional analysis. For offline spike sorting of unit activity, the wideband signal was digitally high-pass filtered (0.8-5 kHz). Spike sorting was performed automatically, using KlustaKwik (http://klustakwik.sourceforge.net), followed by manual adjustment of the clusters (using "Klusters" software package; http://klusters.sourceforge.net). Neurophysiological and behavioral data were explored using NeuroScope (http://neuroscope.sourceforge.net; Hazan et al., 2006). Further details of recording, and unit separation and cell type classifications are available in (Csicsvari et al., 2003; Diba and Buzsáki, 2007; Mizuseki et al., 2009). For the entorhinal unit data here (used exclusively for the purpose of detecting UP-DOWN state transitions), putative interneurons and principal cells were classified according to the procedure described in Mizuseki et al. 2009. Because of the low number of simultaneously recorded hippocampal units in animals implanted with 96-site probes, we used a simplified method for classification of hippocampal units based on

the shape of spike autocorrelograms; units with a characteristic "bursty" autocorrelogram were classified as principal cells, units lacking a "bursty" autocorrelogram with mean firing rates > 5 Hz were classified as putative interneurons. Hippocampal units with mean firing rates < 0.5 Hz were discarded from the data set. Recording site irregularities (including cross-talk and excessive impedances) were a priori identified and removed from analysis using measures of coherence and normalized power similarity (Diba et al., 2005). Current source density (CSD) was calculated by standard methods (Mitzdorf, 1985). Only CSD calculations centered on three consecutive good channels were used. CSD calculations that would require use of a recording site displaying an irregularity were excluded from further analysis.

2.3.3 Detection of ripples and fast gamma oscillations

The procedures for detection were based on those described earlier (Csicsvari et al., 1999), but with additional refinements in order to minimize false-positive detections and align detected oscillatory events to the peak of the CSD source in the CA1 pyramidal layer. First, the LFP signals from one or more selected channels from the CA1 pyramidal layer were filtered between 50 and 250 Hz, rectified, smoothed with a 3-sample uniform kernel, and then z-score normalized. Candidate oscillatory events (epochs during which this normalized signal exceeded a 2 standard deviation threshold) were detected first. Each candidate event was aligned to the nearest peak of the CA1 pyramidal CSD signal within a +-25 ms window around the midpoint of the detected suprathreshold epoch. Because this alignment procedure can result in the same oscillatory event being detected multiple times, we edited the realigned candidate oscillatory events in order to enforce a minimum 50 ms spacing between events, deleting all but the event with the highest CSD

peak when multiple events occurred within a 50 ms time span. Spectral analysis using multitaper FFT on the wideband LFP and CSD signals (Mitra and Pesaran, 1999; see below) was then performed on each remaining candidate oscillatory event in order to remove false positives. We required that each oscillation in the final dataset have a spectral peak at any frequency between 120 and 200 Hz that is at least 2 standard deviations above the SWS background for that frequency, for power spectra computed using both the LFP and CSD. The frequency at the spectral peak of each remaining oscillatory event was then calculated - if this peak frequency was under 140 Hz, we categorized the oscillatory event as "fast gamma" for the purposes of our analysis; otherwise the event was categorized as a ripple.

2.3.4 Detection of UP and DOWN states in dentate gyrus and entorhinal cortex

Down states in the dentate gyrus ($DOWN_{DG}$) were detected from the CSD trace in the molecular layer of the dentate gyrus. The trace was band-pass filtered between 50 and 100 Hz, rectified, smoothed using a 40 ms uniform kernel, and then normalized. $DOWN_{DG}$ states were defined as periods where the processed normalized signal was at least 0.75 standard deviations below the mean for at least 100 ms. The remaining epochs were considered UP state. Only slow wave sleep episodes were included for the detection of up-down states. The $DOWN_{EC}$-UP_{EC} transitions in EC were detected by using the spiking activity of EC neuron populations. All isolated (clustered) neurons were combined as a single multiple unit (MU) train and smoothed with a 10-msec Gaussian kernel. The $DOWN_{EC}$-UP_{EC} transitions were determined by the following criteria; 1) the smoothed MU activity reached above the UP_{EC} state threshold, defined to be the geometric mean of all non-zero MU firing; 2) the mean MU activity in a 150 msec

window before candidate onset of UP state was below the $DOWN_{EC}$ state threshold, which was defined as 0.2 times UP state threshold and 3) the mean MU activity in a 200 msec window after the onset of the candidate UP state was above the UP_{EC} state threshold (Isomura et al., 2006; Sakata and Harris, 2009). In previous studies, the $DOWN_{EC}$-UP_{EC} transitions in population firing were strongly correlated with increased gamma power and large membrane potential shifts of intracellularly recorded neurons (Isomura et al., 2006; Mukovski et al., 2007).

2.3.5 Multitaper FFT

For spectral analysis of oscillatory patterns, we used a modified version of the multitaper FFT MATLAB package by P. Mitra (Mitra and Pesaran, 1999). Using an FFT window length of 100 ms, over frequencies ranging 50-400 Hz, spectra of individual events contained power estimates over 35 discrete frequency bins. Power spectra were z-score normalized. These z-scored power measurements indicate the number of standard deviations by which power in a given 100 ms window (e.g., a ripple oscillation) differs from average background power during SWS. The normalizing means and standard deviations used in calculating the z-score were derived by randomly triggering at 20,000 different points within slow wave sleep, computing the raw FFT at each of these points, and then calculating the mean and standard deviation of power at each frequency; this procedure was performed independently for every animal and channel analyzed, both CSD and LFP.

2.3.6 Wavelet algorithm

For wavelet analysis, the discrete wavelet transform (65 levels, 1-300 Hz) was computed by using a MATLAB wavelet software package provided by C. Torrence and G. Compo (http://paos.colorado.edu/research/wavelets/software.html). Each level (i.e., frequency) of the wavelet transform was individually normalized by the mean and standard deviation of wavelet power during slow wave sleep episodes. Although the wavelet data for the entire session was normalized, only data from slow wave sleep epochs was used to calculate the normalizing factors in order to avoid bias deriving from differing proportions of slow wave sleep and other behaviors in recording sessions.

2.4 Results

As described earlier, the in situ recording sites in the various anatomical regions and layers could be determined with high spatial resolution (±30 μm) using a combination of spontaneous LFP patterns, multiple unit activity, evoked potentials in response to perforant path and/or commissural stimulation, and post-hoc histological identification of the anatomical position of each recording shank (Csicsvari et al., 2003; Montgomery et al,, 2007).

2.4.1 Segregation and definition of ripple and fast gamma oscillations

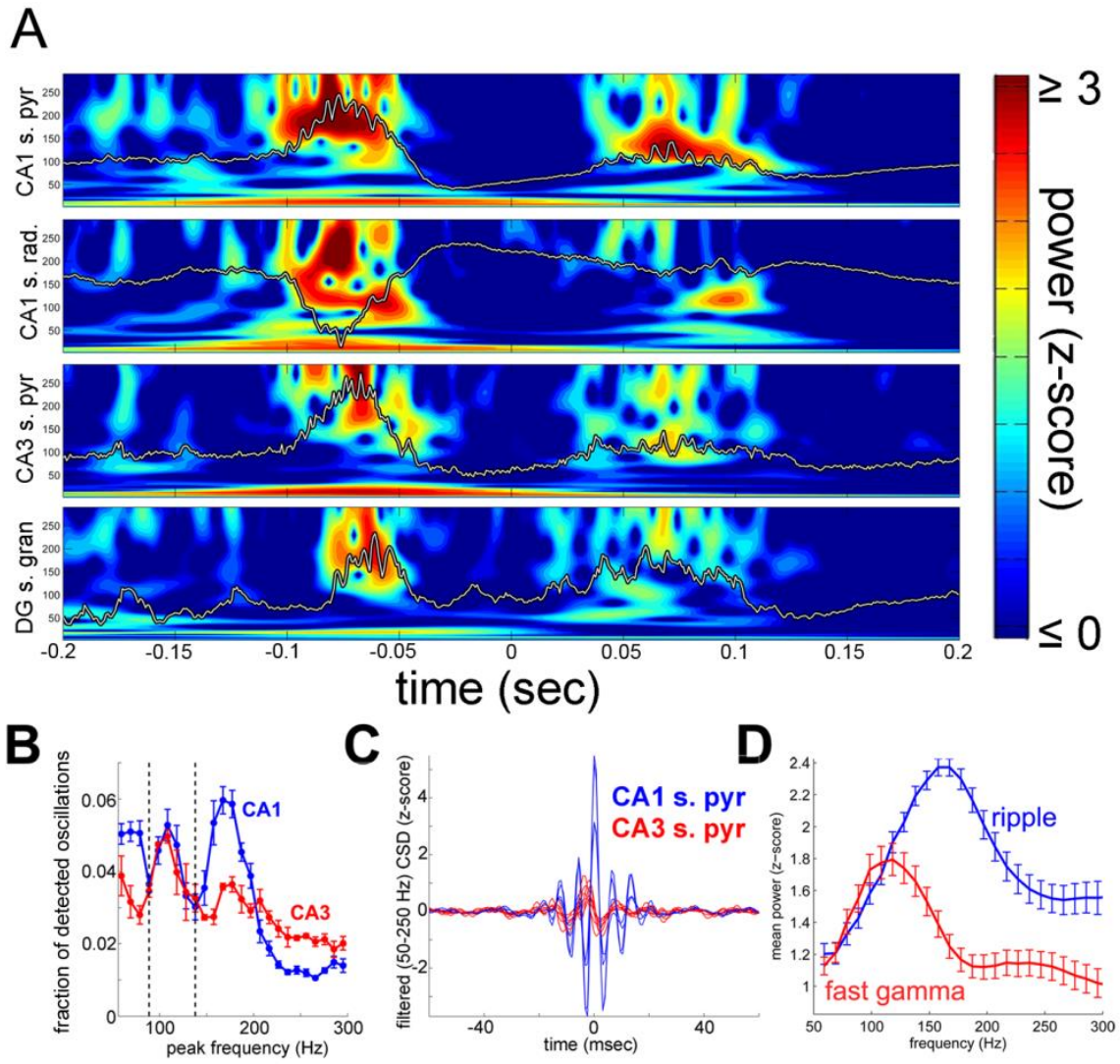

Figure 2.1 Ripples and fast gamma oscillations. A, Example trace of wide-band (1 Hz-10 kHz) current source density (CSD) traces of ripple and fast gamma oscillations from the CA1 str. pyramidale (pyr) and radiatum (rad), CA3 pyramidal layer and dentate granule cell layer (DG. S. gran) in a sleeping rat, overlaid on their respective wavelet spectrograms. B, Distribution of the peak spectral frequency (calculated via FFT) of oscillatory high frequency episodes detected in the CA1 and CA3 pyramidal layers (mean±SEM; n = 9 animals). Dashed lines, minima at 80-90 Hz separating gamma and fast gamma oscillations, and at 140 Hz separating fast gamma (<90-140 Hz) and ripple (>140 Hz) oscillations in CA1. C, Ripple-triggered averages of simultaneously recorded CSD traces from CA1 and CA3 pyramidal layer. For clarity, the amplitude of the CA3 traces has been doubled. Superimposed traces are from four different animals. Note the consistent CA1 vs. CA3 phase relationships across animals, despite different oscillatory frequencies. D, Group mean power spectra of ripple and fast oscillation episodes.

Figure 2.1A illustrates wide-band (1 Hz-5 kHz) current source density (CSD) traces superimposed on time-frequency spectra in CA1 and CA3 stratum pyramidale, CA1 str. radiatum and the granule cell layer during non-REM sleep. In the absence of theta oscillations, LFP patterns in the CA1 pyramidal layer are characterized by relatively silent periods alternating with fast oscillatory events. These transient rhythms can take the form of a faster or slower oscillation in the frequency range of 50-250 Hz, associated with sinks of varying magnitude in CA1 str. radiatum. To segregate and group these oscillations objectively, oscillatory episodes were detected from the 50-250 filtered CA1 stratum pyramidale LFP and the frequency of the peak power was determined for each of the detected events. In the CA1 region, the frequency distribution of the LFP oscillatory episodes was characterized by a definable dip between 130 and 150 Hz, surrounded by distinct peaks at 170-180 Hz and 110 Hz (Fig. 1B). An additional dip at 80-90 Hz was also present in several animals, reflecting a putative boundary between gamma and 'fast' gamma oscillations (Csicsvari et al., 1999b; Canolty et al., 2006; Colgin et al., 2009). Using these boundaries, we defined ripples as fast oscillatory events with peak power >140 Hz, and events with peak power within the 90-140 Hz band as fast gamma (Csicsvari et al., 1999b). During oscillatory episodes (detected in CA1), the distribution of peak frequencies in CA3 showed a similar bimodality, but the main peak occurred in the fast gamma oscillation band, rather than at ripple frequency. Interestingly, similar frequency boundaries between gamma, fast gamma and ripple oscillations have been described in the human brain as well (Canolty et al., 2006; Le Van Quyen et al., 2010). The slower oscillation frequency in the CA3 region, relative to CA1, was also apparent in ripple peak-triggered averages of filtered (50-250 Hz) CA1 pyramidal layer CSD traces

(Fig. 2.1C). Remarkably, the phase of the CA3 traces was consistent across rats, an indication of cross-frequency phase coupling ('n-m' coupling Pikovsky et al., 2001; Tass et al., 1998).

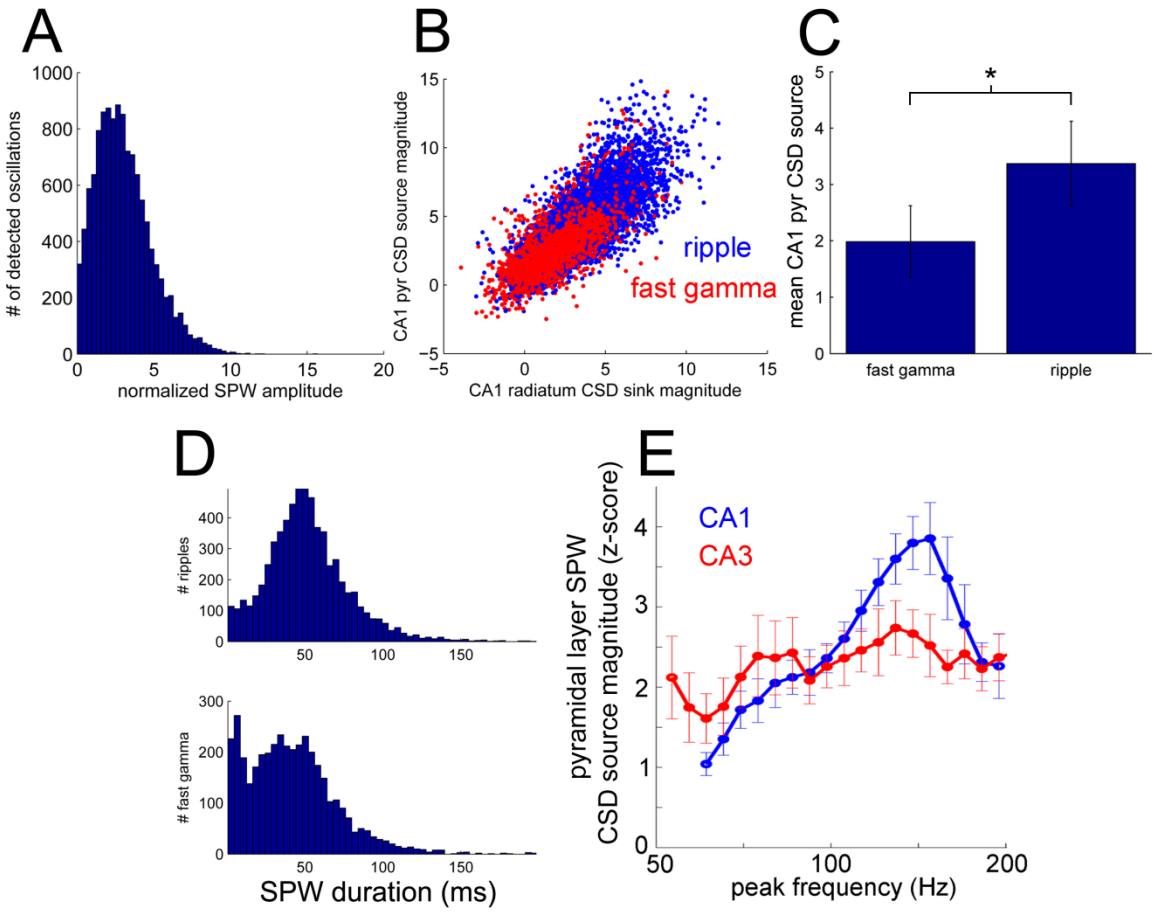

Figure 2.2 Characteristics of ripples and fast gamma oscillations. A, Normalized distribution of SPW sink magnitudes during fast gamma, ripple oscillatory (90-250 Hz) episodes. B, Correlation between sink (CA1 str. radiatum) and source (CA1 pyramidal layer) magnitudes during fast gamma and ripple episodes. C, Magnitude of SPW source during fast gamma and ripple oscillations. D, Distribution of SPW sink duration in str. radiatum. Sink duration was defined as the time period around the detected oscillation where the normalized CSD signal is less than 0.5 standard deviations below the mean. E, Fast oscillation frequency in CA1 and CA3 pyramidal layers as a function of SPW sink magnitude in str. radiatum. Note resonant peak in CA1 at 200 Hz (inverted U relationship). Mean±SEM (n = 6 animals for CA1, n = 4 for CA3).

The distinct frequencies of the CA1 oscillatory episodes (i.e., ripple and fast gamma; Fig. 2.1D) were exploited to examine the potential differential contribution of hippocampal

regions to these rhythms. Examination of the magnitude of SPW sinks in CA1 str. radiatum showed a unimodal distribution (Fig. 2.2A). The magnitude of SPW sink in mid-str. radiatum and the source in the CA1 pyramidal layer were strongly correlated for both ripple events and fast oscillations (Fig. 2.2B; $r > 0.63$ in 6/6 animals, $p < 0.00001$). This high correlation justified the use of SPW source magnitude for further comparisons in all rats, including those in which electrodes were placed only in CA1 pyramidal layer. Both ripples and fast gamma episodes were associated with SPW sources in the CA1 str. pyramidale but ripple-associated sources were of larger magnitude (Fig. 2.2C; $n = 11$, $p < 0.00001$, Wilcoxon rank sum; Fig. 2.3). In addition, the mean duration of SPW sinks was significantly longer for ripple than for fast gamma episodes (Fig. 2.2D; mean duration 51.8 ms vs. 41.8 ms respectively, $n = 6$, $p < 0.00001$, Wilcoxon rank sum; see also Fig 2.3). Comparison between the magnitude of SPW CSD source in the pyramidal layer (i.e., the driving excitatory 'force') and oscillatory frequency revealed an inverted U relationship in CA1. Small amplitude SPWs were associated with fast gamma oscillations, medium size SPWs with either 140 to 170 Hz or >190 Hz ripples, whereas the largest amplitude SPWs consistently co-occurred with 170-180 Hz ripples (Fig. 2.2E). The SPW magnitude-dependence of the oscillation frequency was much weaker in CA3 (Fig. 2.2E).

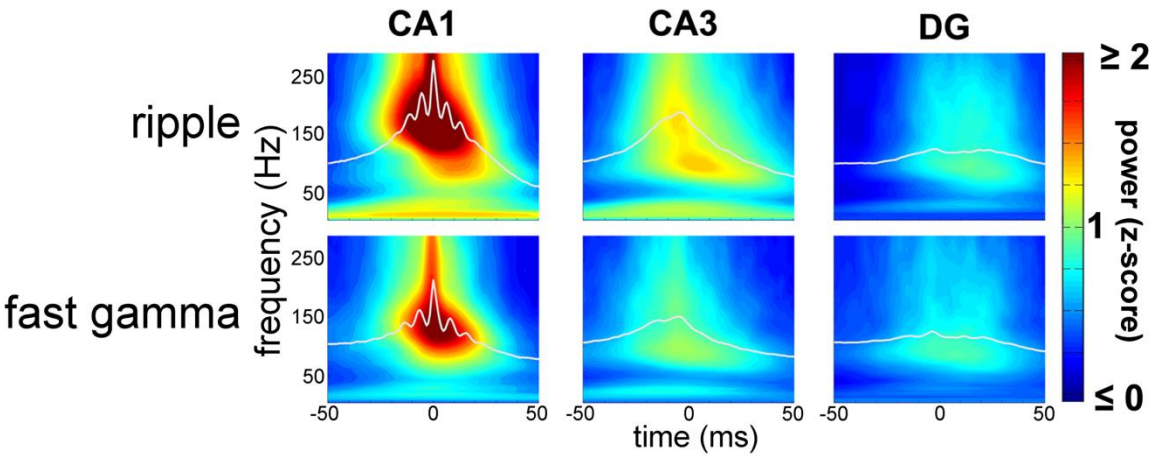

Figure 2.3 Dynamic of oscillatory episodes, illustrated by averaged wavelet spectrograms from a single animal, triggered by ripple peaks and fast gamma oscillation peaks, respectively in the CA1, CA3 pyramidal layer and dentate granule cell layer.

Wavelet analysis of the CSD traces showed that immediately prior to the peak of the CA1 ripples, in CA3 there was elevated spectral power over a wide range of frequencies (~60-250 Hz), but there was no single dominant frequency within this range, indicating that the early part of the CA3 oscillation during ripples lacks consistent rhythmicity (Fig. 2.3). During the latter part of the oscillation in CA3, spectral power showed higher concentration in frequencies around 100 Hz. In the DG, the dominant frequency was about 50 Hz lower than in CA1. Additionally, power was lower in the DG, reflecting less consistency in its co-activation with CA1. Strong power was present at ~10 Hz, especially in CA1, reflecting the duration of the SPW source in the pyramidal layer (Fig. 2.3). During fast gamma oscillations, the frequency difference between CA1 and CA3 regions was rather small, although still apparent (Fig. 2.3). Both ripples and fast gamma episodes displayed a relatively steady frequency oscillation in the first half of the event, followed by a marked frequency deceleration to ~110 Hz during the second half (Fig. 2.3;

Ponomarenko et al., 2008; Nguyen et al., 2009), thus reducing the frequency difference between CA1 and CA3 oscillations.

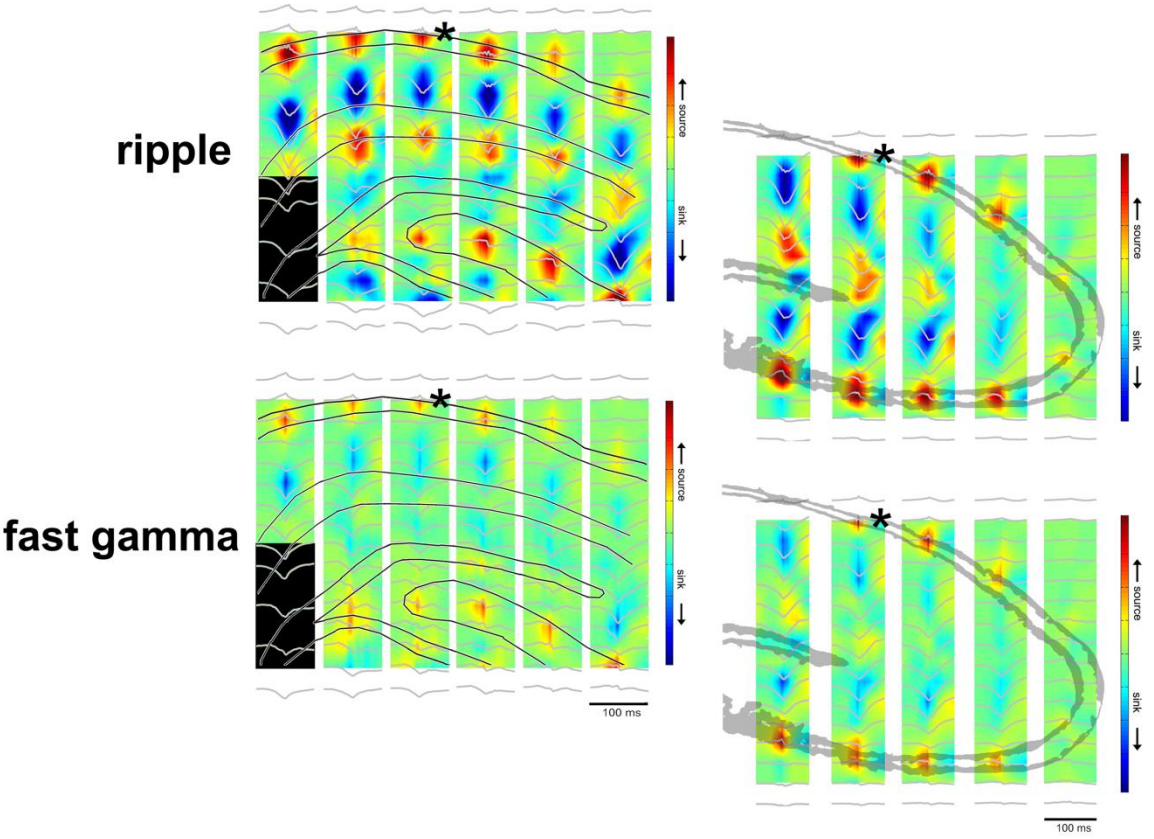

Figure 2.4 Regional distribution of currents associated with ripple and fast gamma oscillation. CSD maps (1 Hz-10 kHz) in two different animals with the average LFP waveforms superimposed (gray traces). Maps were constructed by triggering on the peaks of ripple and fast gamma episodes. *, reference site. Note strong SPWs (sinks) in str. radiatum of CA1 and CA3 and the inner molecular layer of the dentate gyrus during ripples and weaker sinks but with similar spatial distribution during fast gamma oscillations. Sinks in the inner molecular layer of the dentate gyrus possibly reflect activation of excitatory inputs from hilar mossy cells. The most lateral shank in the rat with CA3 sites (bottom) was in the fimbria (not shown).

Using the peaks of the ripple and fast gamma episodes (Experimental Procedures), we constructed CSD maps (Fig. 2.4), which revealed strong ripple-associated SPW sinks in str. radiatum of both CA1 and CA3 regions and smaller ones in the inner molecular layer of the dentate gyrus. The peak of SPW occurred earlier in CA3 than in CA1 by 4.46 ms

on average (n = 5 animals, SEM = 1.14 ms; $p < 0.00001$ in 5/5 animals). SPW-associated current sinks were frequently (but not always) observed in the dentate inner molecular layer. In two out of four animals with simultaneous CA1 and DG recordings, the peak of the dentate sink occurred significantly later than the peak of the CA1 radiatum sink by 5.34 ms (SEM = 1.48 ms, $p < 0.00001$ in 2/4 animals), supporting the CA3 origin of SPWs (Buzsáki et al., 1983; Buzsáki 1986). In the other two animals there was no significant difference between the timing of dentate and CA1 CSD sink peaks. This inconsistency may be due to the relatively crude spatial resolution (100 μm electrode spacing) of the inner molecular layer. The correlation between SPW sink magnitudes in CA1 and CA3 str. radiatum was strong (r = [0.58, 0.51, 0.65, 0.74, 0.69]; $p < 0.00001$ in 5/5 animals) and weaker between CA1 str. radiatum and the dentate inner molecular layer (r = [0.13, 0.30, 0.27, 0.48]; $p < 0.00005$ in 4/4 animals). SPW sink magnitudes in CA3 radiatum and the dentate molecular layer were moderately correlated during ripples (n = 3, $p < 0.01$, r = [0.10, 0.27, 0.29]), but were weakly correlated during fast gamma oscillations (n = 3, $p < 0.01$ in 2/3 animals, $p > 0.05$ in 1/3 animals, r = [0.1, 0.1] where correlation was significant); given the small number of observations this data should be interpreted with caution. Importantly, the magnitude of the SPW sink in CA1 str. radiatum was significantly correlated with ripple power in the CA1 pyramidal layer (r = 0.47; range: 0.30 to 0.55; $p <0.01$ in each of 6 animals). In summary, although CA1 ripples and SPWs are distinct physiological patterns, they are strongly coupled under physiological conditions (Ylinen et al., 1995; Chrobak and Buzsáki, 1996; Csicsvari et al., 2000; Buhl and Buzsáki, 2005).

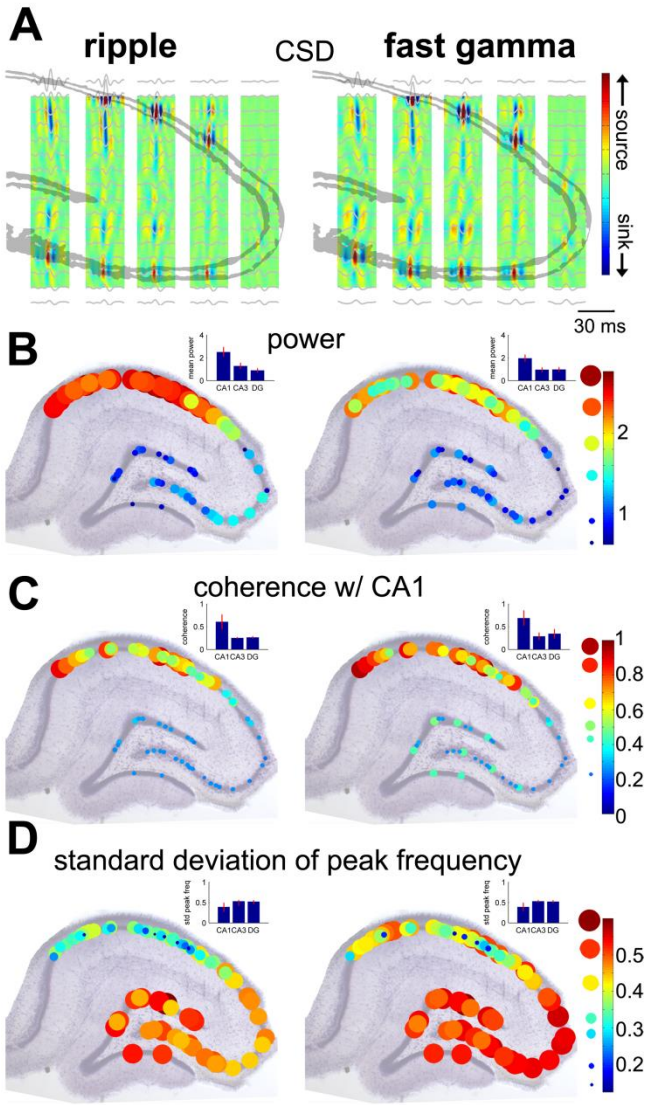

Figure 2.5 Similar and distinct features of ripple and fast gamma oscillations. A, Filtered CSD maps of ripples and fast gamma oscillations from a single animal. Maps were constructed by filtering the CSD signal (50-250 Hz), and then averaging this filtered CSD, triggering on the peaks of ripple and fast gamma episodes. Average filtered (50-250 Hz) LFP traces are overlaid in gray. Note faster oscillations in CA1 compared to CA3 and dentate gyrus. B, Normalized power distribution of ripples (measured at 175 Hz) and fast gamma oscillations (110 Hz) in the cell body layers (n = 10 animals). Histology and CSD information from each animal was used to best align the recording sites from different animals to an idealized hippocampal section perpendicular to the long axis of the hippocampus. The size and color of circles indicate the magnitude of power. C, Regional distribution of phase coherence with the CA1 pyramidal layer. In each animal, coherence values were calculated for all sites in a principal cell layer vs. the most medial CA1 pyramidal layer site available. D, Region-dependence of frequency variability of ripple and fast gamma oscillations. Note stronger power, larger CA1-CA3 difference of coherence and smaller variability of ripples, compared to fast gamma episodes.

Filtered (50-250 Hz) CSD maps of ripples and fast gamma oscillations showed further quantitative differences between these two types of events (Fig. 2.5A). Sinks in proximal CA1 radiatum reflected return currents of the sources in the pyramidal layer. In mid-radiatum, however, the frequency of oscillation was slower, reflecting the oscillation frequency of the CA3 input. To quantify the frequency and power differences, the power of LFP traces at 175 Hz and 110 Hz was determined for ripple and fast gamma episodes, respectively, and data from multiple animals (n = 10) is displayed on the approximate anatomical locations of the recording sites (Fig. 2.5). As expected (Fig. 2.5B,C), LFP power was significantly different across regions ($p < 0.0001$; CA1, CA3, dentate gyrus) and across oscillation types ($p < 0.0005$; ripples vs fast gamma), with a significant region by oscillation type interaction ($p < 0.00001$; ANOVA followed by Tukey's test). The post-ANOVA tests also showed that CA1 power was significantly higher during ripples than fast gamma episodes ($p < 0.0001$) and CA1 power was stronger for both oscillation types compared to CA3 or dentate gyrus (Fig. 2.5B). Phase coherence within the ripple band (measured at 175 Hz) was relatively high for sites within the CA1 pyramidal layer (mean = 0.60, SEM = 0.026, n = 40 recording channel pairings). In contrast, phase coherence between the CA1 and CA3 pyramidal layers (mean = 0.25, SEM = 0.003, n = 17 recording site pairings) and between CA1 pyramidal layer and granule cell layer (mean = 0.27, SEM = 0.005, n = 14 recording site pairings) was significantly lower ($p < 0.00001$; ANOVA). The general pattern of coherence during fast gamma episodes was similar to that of ripples (Fig. 2.5C). However, coherence for fast gamma was significantly higher than for ripples both within CA1 sites (0.68 for fast gamma vs. 0.599 for ripples, $p < 0.00001$, t-test), and between CA1 pyramidal layer and granule cell layer

(0.35 for fast gamma vs. 0.266 for ripples, $p < 0.01$, t-test) but was not significantly different between CA1 and CA3 pyramidal layers. To examine region-dependent variability of peak frequency, the standard deviation of log peak frequency was calculated for each recording site in the cell body layers for both ripple and fast gamma episodes (Fig. 2.5D). Log frequency variation was significantly smaller in CA1 during both ripples and fast gamma episodes than in the CA3 pyramidal layer and granule cell layer ($p < 0.0005$; ANOVA). In addition, the log frequency main effect showed a significantly smaller variation during ripples compared to fast gamma episodes ($p < 0.0001$). The log frequency variation was similar in CA3 and dentate gyrus ($p > 0.05$) and was not significantly different between ripples and fast gamma oscillations ($p > 0.05$).

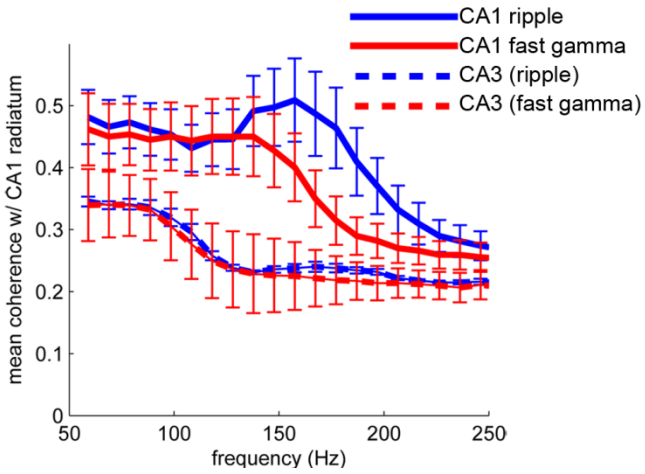

Fig. 2.6 Coherence with CA1 stratum radiatum. During both ripple and fast gamma oscillations, CA1 radiatum is more coherent with the CA1 pyramidal layer than the CA3 pyramidal layer. For each animal with simultaneous recordings of CA1 and CA3 pyramidal layers as well as CA1 radiatum (n = 4), average coherence spectra were calculated for both CA1 and CA3 pyramidal layers vs. a CA1 radiatum channel, for both ripple and fast gamma oscillations, using CSD. Curves plotted here reflect the mean of these averaged spectra across animals; error bars indicate SEM.

To examine further the role of the CA3 region in generating ripples and fast gamma oscillations, coherence between CA1 str. radiatum and the CA3 pyramidal layer CSD

traces was calculated (Fig. 2.6). The coherence between these two regions/layers was low for both ripples and fast gamma oscillations (c < 0.4). In contrast, the coherence between CA1 pyramidal layer and radiatum was significantly higher for both ripples and fast gamma (Fig. 2.6; $n = 4$, $p < 0.00001$, ANOVA). These observations show that ripple and fast gamma oscillations in the CA1 region are not 'transferred' from the upstream CA3 network wave by wave.

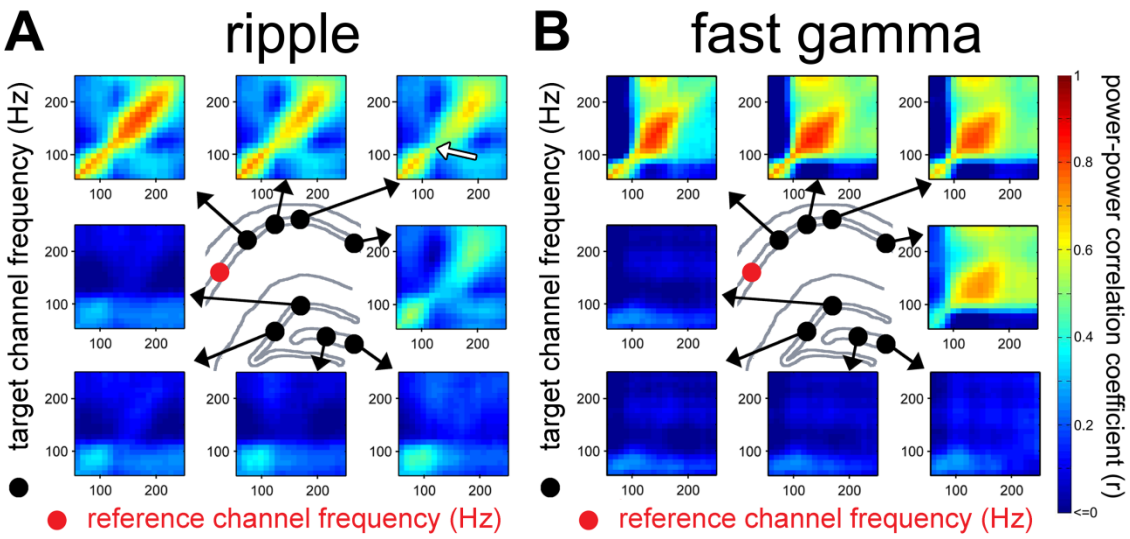

Figure 2.7 Inter-regional power correlations during ripples and fast gamma oscillations. A, Comodugrams during ripples between a reference site (red dot) and other sites in the cell body layers (black dots). Each comodugram plots the matrix of correlation coefficients (r) between the spectral power at the reference site (red dot, x-axis), and power at the target site (black dot, y-axis), for each pairing of frequencies. Note high power correlations in the 140-250 Hz band between CA1 sites and corresponding power increase at <130 Hz in the CA3 and dentate regions. White arrow, correlation discontinuity. B, Same as in A but during fast gamma events.

While ripples and fast oscillations were not highly coherent across hippocampal regions, power changes at different frequencies may co-vary (Fig. 2.3) and such correlations can be revealed by power comodugrams (Buzsáki et al., 2003; Mitra and Bokil, 2007). Power-power correlations showed differences between ripples and fast gamma oscillations, showing minima at 130-140 Hz and 90 Hz, respectively, for CA1-CA1 site

correlations (Fig. 2.7A and B). Power correlations during ripples were high within the CA1 pyramidal layer in the 140 Hz-250 Hz band, although the strength of the correlation decreased with distance (from 0.9 to 0.5 over a 1.5 mm distance in the medio-lateral direction; Fig. 2.7A). Power correlations between CA1 and CA3/DG were consistently low in the ripple band (<0.2). During fast gamma episodes, high power correlations were also confined to the CA1 region (0.6-0.9), associated with a weak increase of power in CA3/DG in the <100 Hz band (Fig. 2.7B). At times of ripple events, the maximum power correlation in the ripple band was accompanied by a minimum power correlation in the fast gamma band (compare Fig. 2.7A and B), indicating that fast gamma and ripple oscillations are competing patterns and do not occur together in the same region at the same time. Overall, these findings demonstrate that while ripples and fast gamma oscillations share the same anatomical substrates and related physiological mechanisms, they also display distinct features.

2.4.2 Neuronal discharges associated with ripple and fast gamma oscillations

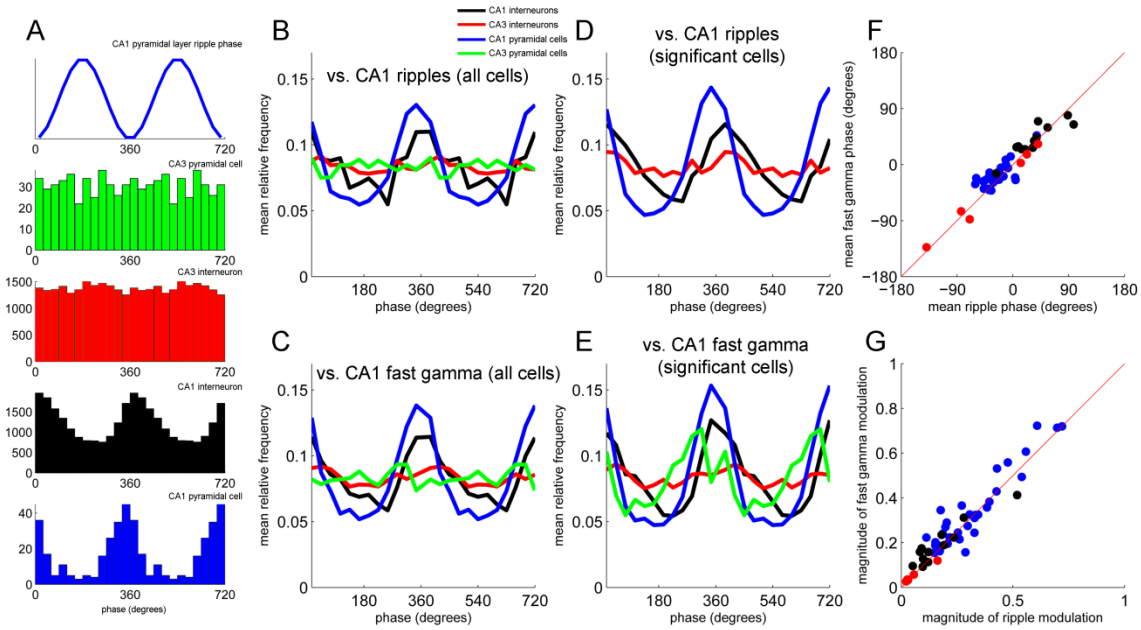

Figure 2.8 Phase-locking of neurons to ripples and fast gamma oscillations. A, Peri-ripple histograms of four simultaneously recorded CA3 and CA1 pyramidal cells and putative interneurons in a representative animal. The discharge of CA1 pyramidal cells and both interneurons (but the CA3 pyramidal cell) was significantly phase locked to ripple oscillations ($p < 0.05$; Hodges-Ajne test for nonuniformity of circular data). B and D, Group histograms for the 4 neurons types during ripples (B) and fast gamma oscillations (D). C and E, Group histograms confined only to significantly phase-locked neurons during ripples (C) and fast gamma oscillations (E). F, Phase relationship of different neuron types during ripples and fast gamma oscillations. G, Relationship between phase-locking magnitude (mean resultant length) of different neuron types during ripples and fast gamma oscillations. Only neurons with significant phase-locking during both ripples and fast gamma oscillations are included.

In agreement with previous studies, the majority of CA1 pyramidal cells were significantly phase-locked to the trough of locally recorded ripple ($p < 0.05$, 38/54 neurons in 4 animals; Hodges-Ajne test for nonuniformity of circular data; Buzsáki et al., 1992), and fast gamma (38/54 neurons; Csicsvari et al., 1999b; Colgin et al., 2009) oscillations (Fig. 2.8). Similarly, 8 of the 9 putative CA1 interneurons were also phase-modulated by both ripples and fast gamma, and the phase preference of the interneuron

population was delayed 60 to 90 degrees relative to the peak firing of CA1 pyramidal neurons (Fig. 2.8A, F; corresponding to 1.3 msec and 2.0 msec delays for ripples and fast gamma, respectively; Csicsvari et al., 1999). Phasic modulation of CA3 pyramidal cells was conspicuously absent during ripples but 3 of the 60 CA3 pyramidal cells showed significant modulation with CA1 fast gamma oscillations. Five of the seven putative CA3 interneurons were significantly phase-locked to both ripples and fast gamma, although their depth of the modulation (mean resultant vector length) was low (Fig. 2.8A, G). The phase preference of the majority of neurons was similar during ripples and fast gamma oscillation (Fig. 2.8F). In addition, the depth of the modulation (i.e., the mean resultant length) remained similar across the two rhythms (Fig. 2.8G). Overall, these unit findings show that while CA3 fast gamma oscillations may contribute to the timing of CA1 neurons, ripples are not 'transferred' wave-by-wave from the CA3 region to CA1. Instead, the build-up of convergent excitation on the dendrites of CA1 neurons produces de novo CA1-specific oscillations.

2.4.3 Contribution of the dentate gyrus to SPW-Rs

A striking difference between SPW-Rs observed in vivo and in vitro is the strong frequency and amplitude regularity of SPW-R events in the slice preparation (Behrens et al., 2007; Foffani et al., 2007; Kubota et al., 2003; Colgin et al., 2005; Maier et al., 2003; Traub and Bibbig, 2000), compared to the irregularly occurring SPW-R in the intact brain (Buzsáki et al., 1983; 1992; Buzsáki 1986; Ylinen et al., 1995; Csicsvari et al., 2000; Nguyen et al., 2009; Le Van Quyen, 2010). The pattern difference may arise from the influence of networks affecting the CA3 region in vivo (Ylinen et al., 1995; Bragin et al., 1995). A candidate dentate event that may exert such an influence is the neocortical slow

oscillation, dominant during slow wave sleep (Steriade et al., 1993; Sirota et al., 2003; Isomura et al., 2006; Battaglia et al., 2004).

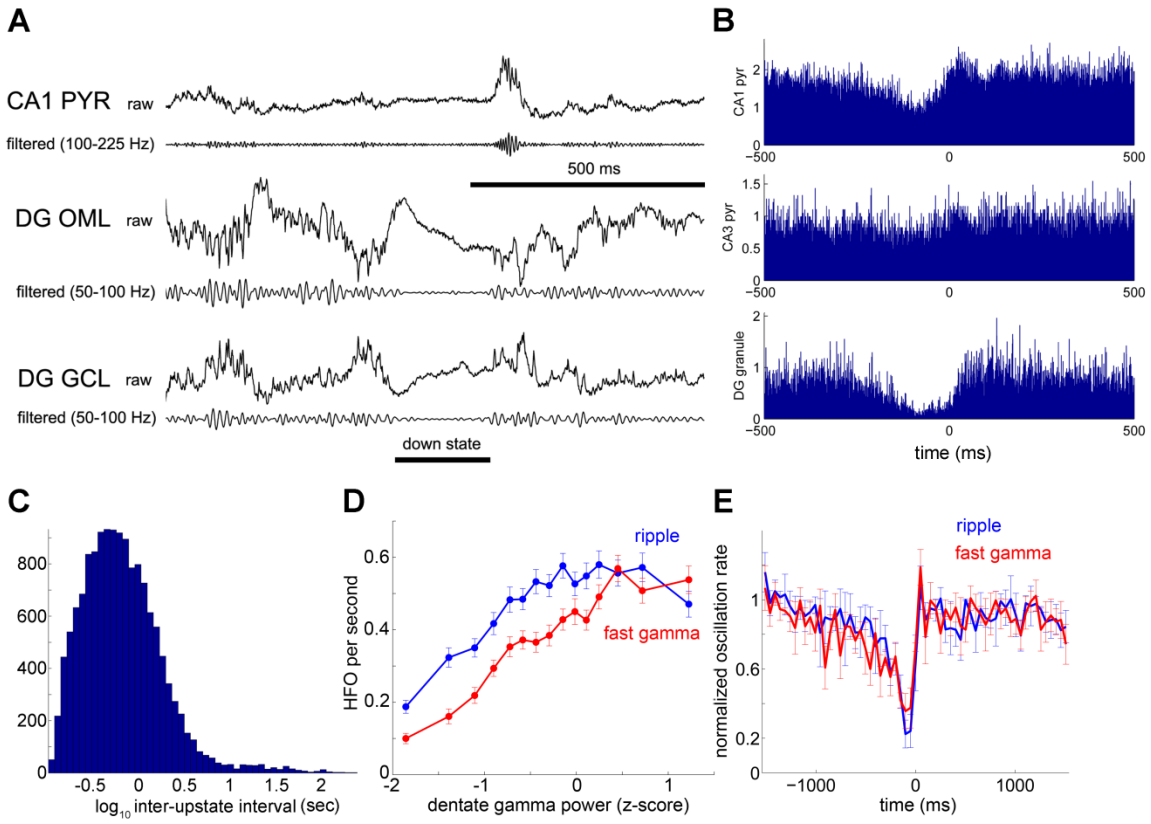

Figure 2.9 Influence of dentate gyrus on CA1 SPW-R. A, Short epochs of wide-band CSD traces (raw, 1 Hz–5 kHz) and their filtered derivatives recorded simultaneously from the CA1 pyramidal layer (CA1 PYR), outer molecular layer (DG OML) and granule cell layer (DG GCL) of the dentate gyrus. Horizontal line indicates a 'DOWN state', defined by the decreased power of gamma band (50-100 Hz) power (see Experimental Procedures). B, Relationship between dentate DOWN states (DOWNDG) and unit discharges of CA 1 and CA3 pyramidal neurons (pyr) and putative dentate granule cells (DG granule). The end of the DOWN state (i.e., DOWN-UP transition) was used as the reference event (time zero). Note strongly decreased discharge activity in the dentate gyrus during DOWNDG. C, Distribution of inter-UP state intervals, determined from DOWNDG-UPDG transitions. D, Occurrence (event/sec, counted in 5 sec bins) of fast gamma and ripple episodes as a function of normalized dentate gamma band power. Note inverted-U relationship. E, Cross-correlogram between DOWNDG and probability of CA1 ripple/fast gamma occurrence. Mean±SEM (n = 4 animals). Note low incidence of ripples and fast oscillation episodes during DOWNDG (i.e., prior to time 0).

To detect the effect of neocortical influence on the hippocampus, the CSD trace recorded in the dentate molecular layer was filtered (50-100 Hz) and rectified, and epochs longer than 100 msec with at least 0.75 standard deviations below the mean power were classified as $DOWN_{DG}$ states (Fig. 2.9A; Isomura et al., 2007). The validity of this arbitrary measure was justified by the correlation of the LFP $DOWN_{DG}$-UP_{DG} changes with unit activity recorded from the dentate gyrus, CA3 and CA1 regions (Fig. 2.9B, n = 4 animals). During $DOWN_{DG}$ states, neurons recorded from the dentate granule cell layer were either silent or fired at a significantly reduced rate relative to baseline ($p < 0.00001$ in 5/5 animals, Wilcoxon signed rank test). This same finding also applied to neurons recorded in the CA1 pyramidal layer and str. oriens ($p < 0.05$ in 3/3 animals), as well as the CA3 pyramidal layer ($p < 0.01$ in 4/4 animals), although the effect was of smaller magnitude in CA3, likely due to the presence of gamma oscillation bursts in the $DOWN_{DG}$ state (Isomura et al., 2007). The temporal distribution of $DOWN_{DG}$ states showed a Poisson-like distribution with a peak between 0.5 to 1 Hz (Fig. 2.9C), possibly reflecting the influence of cortical slow oscillation (Steriade et al., 1993), mediated by the EC (see below). In addition, the dentate UP_{DG}-$DOWN_{DG}$ fluctuations and correlated ripple events had an ultraslow recurrence component between 5 to 15 sec (not shown; Leopold et al., 2003; Sirota et al., 2003). Dentate gamma power was positively correlated with the occurrence frequency of ripple oscillations (Fig. 2.9D; n = 4 animals, r = [0.19, 0.25, 0.25, 0.33], $p < 0.00001$]), as well as fast gamma oscillations (Fig. 2.9D; n = 4 animals, r = [0.28, 0.50, 0.31, 0.26], $p < 0.00001$). Both ripple and fast gamma oscillations occurred at a lower rate in the 250 ms interval preceding $DOWN_{DG}$-UP_{DG}

transitions than in the 250 ms interval after such transitions (Fig 2.9E; $n = 4$, $p < 0.05$, t-test).

2.4.4 Contribution of the entorhinal cortex to SPW-Rs

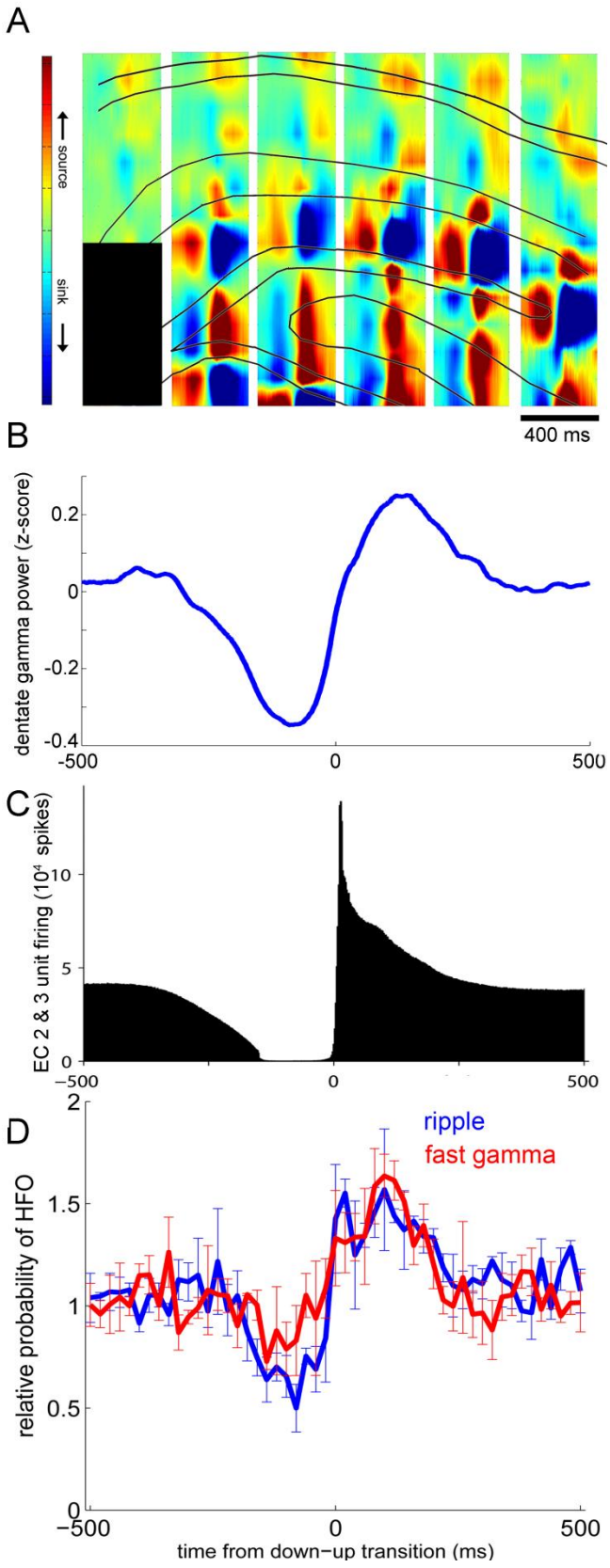
A
source
sink
400 ms
B
dentate gamma power (z-score)
0.2
0
-0.2
-0.4
-500
0
500
C
EC 2 & 3 unit firing (10^4 spikes)
10
5
0
−500
0
500
D
ripple
fast gamma
relative probability of HFO
2
1.5
1
0.5
0
−500
0
500
time from down−up transition (ms)

Figure 2.10 Influence of the entorhinal cortex on CA1 SPW-R A, DOWNDG-triggered CSD map. Note strong sink in the molecular layer (and CA1 str. lacunosum-moleculare), likely reflecting excitatory inputs from the EC. B, Relationship between DOWN-UP transition in EC, defined by onset of unit firing in EC2-EC3 after 150 msec silence (C; see Experimental Procedures), and normalized dentate gamma band (50-100 Hz) power. Note correlated decrease of dentate gamma power and EC unit discharge. D, Cross-correlogram between DOWNEC and probability of CA1 ripple/fast gamma occurrence. Mean±SEM (n = 3 animals).

Previous work has suggested that 'silent' epochs in the dentate gyrus reflect slow oscillation-related changes in the neocortex, conveyed by the EC (Isomura et al., 2007; Hahn et al., 2007; Wolansky et al., 2006). In support of those previous findings, the $DOWN_{DG}$ to UP_{DG} shift-triggered CSD demonstrated strong sinks in the molecular layer of the dentate gyrus and a weaker and delayed sink in the CA1 str. lacunosum-moleculare, the main target layers 2 and 3 of the EC, respectively (EC2, EC3; Fig. 2.10*A*). Conversely, by defining DOWN states in the EC as non-spiking epochs of >150 msec in EC2 and EC3 neurons (Fig. 2.10*C*; Isomura et al., 2006), simultaneous recordings of LFP from the dentate gyrus and unit activity in the EC confirmed that silent epochs in the entorhinal cortex ($DOWN_{EC}$) and dentate gyrus $DOWN_{DG}$ were correlated with each other (Fig. 2.10*B*). After establishing a reliable relationship between silent states in the EC ($DOWN_{EC}$) and the dentate gyrus ($DOWN_{DG}$), we examined the relationship between $DOWN_{EC}$-UP_{EC} shifts and CA1 ripples and fast oscillations. In each rat with both CA1 and EC electrodes (n = 3), the probability of ripple oscillations was significantly lower during $DOWN_{EC}$ states compared to UP_{EC} states (Fig. 2.10*D*; $p <$ 0.01, t-test). The same relationship held for fast gamma oscillations in 2 out of 3 animals. In summary, the EC, directly or by way of the dentate gyrus, can strongly affect the timing of of ripples and fast gamma oscillations.

2.5 Discussion

Our findings show that (1) while hippocampal ripples and fast gamma oscillations are distinct patterns they share multiple physiological mechanisms and anatomical substrate, (2) during both rhythms, the oscillation frequency in CA1 is faster than in CA3, indicating different network resonance in these respective circuits and (3) activity patterns in the EC and dentate gyrus bias the occurrence of both ripples and fast gamma oscillations.

2.5.1 Sharp waves, ripples and fast gamma oscillations are distinct events

SPWs in str. radiatum reflect the depolarization of the apical dendrites of CA1 and CA3 pyramidal cells, due to the synchronous bursting of CA3 pyramidal cells. The population bursts are supported by the spread of excitatory activity in the recurrent CA3 collateral system at times when the burst-suppressive effects of the subcortical inputs are reduced (Buzsáki et al., 1983; Hasselmo and Bower, 1993). The CA3 pyramidal cells, recruited into a SPW event, can broadcast their collective excitation over a large volume of the CA3 and CA1 region (Ylinen et al., 1995). The CA3 output also discharges various interneurons (Csicsvari et al., 1999; 2000; Klausberger et al., 2004; Klausberger and Somogyi, 2008; Ellender et al., 2010), and the interaction between pyramidal cells and interneurons is believed to trigger the ripple oscillation (Buzsáki et al., 1992; Ylinen et al., 1995; Csicsvari et al., 2000; Brunel and Wang, 2003; Foffani et al., 2007; Klausberger et al., 2004). Additional mechanisms, such as gap junction-mediated effects (Draguhn et al., 1998; Schmitz et al., 2001; Traub et al., 2002; 2003; Traub and Bibbig, 2000; Ylinen et al., 1995) and ephaptic entrainment of neurons by the large SPW field

(Anastassiou et al., 2010), may also contribute to the localized ripple episodes (Chrobak and Buzsáki, 1996; Csicsvari et al., 2000). In summary, while the spatially widespread SPWs and the local ripples/fast gamma bursts are strongly linked, they are distinct physiological events and can be dissociated in both normal tissue and pathology (Csicsvari et al., 2000; Leinekugel et al., 2002; Bragin et al., 1999a,b; Buhl and Buzsáki, 2005; Nakashiba et al., 2009).

2.5.2 Ripples and fast gamma oscillations share mechanisms

We found that in the absence of theta oscillations, CA1 can respond in two different ways to CA3 inputs: fast gamma oscillation (~80-140 Hz) or ripple (~140-220 Hz). Their emergence can be intuitively understood as follows. The CA1 and CA3 networks can be conceived of as voltage-controlled oscillators with different response/resonant properties. The coherent SPWs provide the depolarization force and both networks can resonate at either 110 Hz or 170 Hz. While the CA3 region preferentially resonates at <110 Hz, the CA1 favors 170 Hz likely because of its stronger gain properties, as demonstrated here (Fig. 2.1D). Under this hypothesis, weaker excitation would generate ~110-Hz resonance in both regions. Since the oscillations may emerge independently in CA1 and CA3, their frequencies might not perfectly match as shown by the low CA3-CA1 coherence. Nevertheless, because of the small frequency difference, transient phase coupling between the two regions is possible, as demonstrated by the phase-entrainment of individual neurons in both regions (Csicsvari et al., 1999b). At stronger excitation, the CA1 network responds with faster (ripple frequency) oscillation than CA3, due to its steeper input excitation vs. frequency gain.

Anatomical information supports the differential level of excitation in the CA1 and CA3 regions. The axon collaterals of all pyramidal neurons of the CA3a,b, and c subregions target both CA3 and CA1 populations. In contrast, the CA3c subregion sends only limited numbers of collaterals to other CA3 neurons (Ishizuka et al., 1990; Li et al., 1994; Wittner et al., 2007). Therefore, during a CA3 population burst, CA1 neurons are more strongly excited, because of the stronger convergence of CA3 afferents. Another mechanism of the excitatory gain may include inhibition. Previous work has demonstrated that with increasing magnitudes of ripples, the recruitment of CA1 pyramidal cells is more effective than that of interneurons (Csicsvari et al., 1999b). The above hypothesis predicts that excessive excitation of the CA3 network should also generate ripples at the same frequency as in CA1. In support of this prediction, the CA3 region also oscillates at ripple frequency under challenged conditions in vitro and in the epileptic hippocampus in vivo (Behrens et al., 2005; Draguhn et al., 1998; Dzhala and Staley, 2004; Bragin et al., 1999; a, b; 2000; Both et al., 2008; Liotta et al., 2010; Taxidis et al., 2011). The paucity of recurrent excitatory collaterals of CA1 neurons may be an important factor for the observed resonance at ripple frequency (Memmesheimer 2010). In recurrently connected network models, the propagation delays introduce temporal subclustering of neurons and, in turn, the resulting disorganization generates a broadband spectrum (Ibarz et al., 2010), as shown here in the CA3 region. The absence of subclustering mechanisms in CA1 would favor the integration of temporally offset CA3 inputs into a coherent oscillation (Memmesheimer 2010). The dynamically changing balance between excitation and inhibition may also contribute to the ripple band resonance. Overall, our observations suggest that ripples are generated ‘de novo’ in the

CA1 region of the intact hippocampus (Buzsáki et al., 1992; Ylinen et al., 1995; Csicsvari et al., 2002; Buzsáki et al., 2003).

2.5.3 Role of dentate gyrus and entorhinal cortex in timing of SPW-Rs

SPW-like bursts have been also observed in isolated CA3 slices (Behrens et al., 2006; Kubota et al., 2003; Maier et al., 2003; Papatheodoropoulos and Kostopoulos, 2002; Papatheodoropoulos and Koniaris, 2010) and under in vitro conditions, they are super-regular at 2 to 4 Hz (Maier et al., 2003; Kubota et al., 2003; Colgin et al., 2004; 2005; Behrens et al., 2005, 2007; Dzhala and Staley, 2004; Foffani et al., 2007; Colgin et al., 2004, 2005; Pais et al., 2003; Maier et al., 2003; Both et al., 2008; Traub and Bibbig, 2000; Reichinnek et al., 2010; Wu et al., 2005), in contrast to the irregular SPW-R intervals in vivo. The rhythmic recurrence of SPW-Rs in the CA3 network may be explained by an underlying slow relaxation oscillator (Pikovsky et al., 2001; Sirota et al., 2003; Buzsáki, 2006), in which the occurrence of the SPW burst can be advanced by weak inputs in a time- and input magnitude-dependent manner. Our experiments show that inputs from the dentate gyrus and EC time-bias the occurrence of SPW-Rs. We hypothesize that phasic inputs, such as slow oscillations or sleep spindles (Sirota et al., 2003; Isomura et al., 2006; Mölle et al., 2006; 2009; Clemens et al., 2010) can effectively trigger a SPW-R. In support of this hypothesis, slow oscillations were associated with strong sinks in the dentate molecular layer and increased probability of SPW-Rs (see also Battaglia et al., 2004; Isomura et al., 2006).

The hypothesized influence of EC can contribute to the irregular nature of SPW-Rs in vivo. The surge of activity from the EC during UP states can either advance or delay the

next SPW-R event, depending both on the timing and on the relative dominance of excitation vs. inhibition. Such external perturbations can effectively generate irregular patterns due to the interference between the hypothesized SPW-pacing oscillator in the CA3 network and the EC-mediated inputs. Finally, fluctuation of the strength of subcortical inputs may also contribute to the irregular nature of SPW-Rs (Buzsáki 1989; Buzsáki et al., 1983).

2.6 Figure Legends

Figure 2.1

Ripples and fast gamma oscillations. *A*, Example trace of wide-band (1 Hz-10 kHz) current source density (CSD) traces of ripple and fast gamma oscillations from the CA1 str. pyramidale (pyr) and radiatum (rad), CA3 pyramidal layer and dentate granule cell layer (DG. S. gran) in a sleeping rat, overlaid on their respective wavelet spectrograms. *B*, Distribution of the peak spectral frequency (calculated via FFT) of oscillatory high frequency episodes detected in the CA1 and CA3 pyramidal layers (mean±SEM; $n = 9$ animals). Dashed lines, minima at 80-90 Hz separating gamma and fast gamma oscillations, and at 140 Hz separating fast gamma (<90-140 Hz) and ripple (>140 Hz) oscillations in CA1. *C*, Ripple-triggered averages of simultaneously recorded CSD traces from CA1 and CA3 pyramidal layer. For clarity, the amplitude of the CA3 traces has been doubled. Superimposed traces are from four different animals. Note the consistent CA1 vs. CA3 phase relationships across animals, despite different oscillatory frequencies. *D*, Group mean power spectra of ripple and fast oscillation episodes.

Figure 2.2

Characteristics of ripples and fast gamma oscillations. *A*, Normalized distribution of SPW sink magnitudes during fast gamma, ripple oscillatory (90-250 Hz) episodes. *B*, Correlation between sink (CA1 str. radiatum) and source (CA1 pyramidal layer) magnitudes during fast gamma and ripple episodes. *C*, Magnitude of SPW source during fast gamma and ripple oscillations. *D*, Distribution of SPW sink duration in str. radiatum. Sink duration was defined as the time period around the detected oscillation where the normalized CSD signal is less than 0.5 standard deviations below the mean. *E*, Fast oscillation frequency in CA1 and CA3 pyramidal layers as a function of SPW sink magnitude in str. radiatum. Note resonant peak in CA1 at 200 Hz (inverted U relationship). Mean±SEM (n = 6 animals for CA1, n = 4 for CA3).

Figure 2.3

Dynamic of oscillatory episodes, illustrated by averaged wavelet spectrograms from a single animal, triggered by ripple peaks and fast gamma oscillation peaks, respectively in the CA1, CA3 pyramidal layer and dentate granule cell layer.

Figure 2.4

Regional distribution of currents associated with ripple and fast gamma oscillation. CSD maps (1 Hz-10 kHz) in two different animals with the average LFP waveforms superimposed (gray traces). Maps were constructed by triggering on the peaks of ripple and fast gamma episodes. *, reference site. Note strong SPWs (sinks) in str. radiatum of CA1 and CA3 and the inner molecular layer of the dentate gyrus during ripples and

weaker sinks but with similar spatial distribution during fast gamma oscillations. Sinks in the inner molecular layer of the dentate gyrus possibly reflect activation of excitatory inputs from hilar mossy cells. The most lateral shank in the rat with CA3 sites (bottom) was in the fimbria (not shown).

Figure 2.5

Similar and distinct features of ripple and fast gamma oscillations. *A*, Filtered CSD maps of ripples and fast gamma oscillations from a single animal. Maps were constructed by filtering the CSD signal (50-250 Hz), and then averaging this filtered CSD, triggering on the peaks of ripple and fast gamma episodes. Average filtered (50-250 Hz) LFP traces are overlaid in gray. Note faster oscillations in CA1 compared to CA3 and dentate gyrus. *B*, Normalized power distribution of ripples (measured at 175 Hz) and fast gamma oscillations (110 Hz) in the cell body layers (n = 10 animals). Histology and CSD information from each animal was used to best align the recording sites from different animals to an idealized hippocampal section perpendicular to the long axis of the hippocampus. The size and color of circles indicate the magnitude of power. *C*, Regional distribution of phase coherence with the CA1 pyramidal layer. In each animal, coherence values were calculated for all sites in a principal cell layer vs. the most medial CA1 pyramidal layer site available. *D*, Region-dependence of frequency variability of ripple and fast gamma oscillations. Note stronger power, larger CA1-CA3 difference of coherence and smaller variability of ripples, compared to fast gamma episodes.

Figure 2.6

Coherence with CA1 stratum radiatum. During both ripple and fast gamma oscillations, CA1 radiatum is more coherent with the CA1 pyramidal layer than the CA3 pyramidal layer. For each animal with simultaneous recordings of CA1 and CA3 pyramidal layers as well as CA1 radiatum (n = 4), average coherence spectra were calculated for both CA1 and CA3 pyramidal layers vs. a CA1 radiatum channel, for both ripple and fast gamma oscillations, using CSD. Curves plotted here reflect the mean of these averaged spectra across animals; error bars indicate SEM.

Figure 2.7

Inter-regional power correlations during ripples and fast gamma oscillations. *A*, Comodugrams during ripples between a reference site (red dot) and other sites in the cell body layers (black dots). Each comodugram plots the matrix of correlation coefficients (r) between the spectral power at the reference site (red dot, x-axis), and power at the target site (black dot, y-axis), for each pairing of frequencies. Note high power correlations in the 140-250 Hz band between CA1 sites and corresponding power increase at <130 Hz in the CA3 and dentate regions. White arrow, correlation discontinuity. *B*, Same as in A but during fast gamma events.

Figure 2.8

Phase-locking of neurons to ripples and fast gamma oscillations. *A*, Peri-ripple histograms of four simultaneously recorded CA3 and CA1 pyramidal cells and putative interneurons in a representative animal. The discharge of CA1 pyramidal cells and both

interneurons (but the CA3 pyramidal cell) was significantly phase locked to ripple oscillations ($p < 0.05$; Hodges-Ajne test for nonuniformity of circular data). *B* and *D*, Group histograms for the 4 neurons types during ripples (*B*) and fast gamma oscillations (*D*). *C* and *E*, Group histograms confined only to significantly phase-locked neurons during ripples (*C*) and fast gamma oscillations (*E*). *F*, Phase relationship of different neuron types during ripples and fast gamma oscillations. *G*, Relationship between phase-locking magnitude (mean resultant length) of different neuron types during ripples and fast gamma oscillations. Only neurons with significant phase-locking during both ripples and fast gamma oscillations are included.

Figure 2.9

Influence of dentate gyrus on CA1 SPW-R. *A*, Short epochs of wide-band CSD traces (raw, 1 Hz–5 kHz) and their filtered derivatives recorded simultaneously from the CA1 pyramidal layer (CA1 PYR), outer molecular layer (DG OML) and granule cell layer (DG GCL) of the dentate gyrus. Horizontal line indicates a 'DOWN state', defined by the decreased power of gamma band (50-100 Hz) power (see Experimental Procedures). *B*, Relationship between dentate DOWN states ($DOWN_{DG}$) and unit discharges of CA 1 and CA3 pyramidal neurons (pyr) and putative dentate granule cells (DG granule). The end of the DOWN state (i.e., DOWN-UP transition) was used as the reference event (time zero). Note strongly decreased discharge activity in the dentate gyrus during $DOWN_{DG}$. *C*, Distribution of inter-UP state intervals, determined from $DOWN_{DG}$-UP_{DG} transitions. *D*, Occurrence (event/sec, counted in 5 sec bins) of fast gamma and ripple episodes as a function of normalized dentate gamma band power. Note inverted-U relationship. *E*, Cross-correlogram between $DOWN_{DG}$ and probability of CA1 ripple/fast gamma

occurrence. Mean±SEM (*n* = 4 animals). Note low incidence of ripples and fast oscillation episodes during $DOWN_{DG}$ (i.e., prior to time 0).

Figure 2.10

Influence of the entorhinal cortex on CA1 SPW-R *A*, $DOWN_{DG}$-triggered CSD map. Note strong sink in the molecular layer (and CA1 str. lacunosum-moleculare), likely reflecting excitatory inputs from the EC. *B*, Relationship between DOWN-UP transition in EC, defined by onset of unit firing in EC2-EC3 after 150 msec silence (*C*; see Experimental Procedures), and normalized dentate gamma band (50-100 Hz) power. Note correlated decrease of dentate gamma power and EC unit discharge. *D*, Cross-correlogram between $DOWN_{EC}$ and probability of CA1 ripple/fast gamma occurrence. Mean±SEM (*n* = 3 animals).

Section 3- Properties of sharp wave ripples in the waking and sleeping rat

Submitted: Sullivan D and Buzsáki G (2013) Hippocampus.

3.1 Abstract

Sharp waves and ripples (SPW-R) in the hippocampal system are prominent examples of cross-frequency coupling. The spike content of SPW-Rs reflects a compressed template of the dominant spike sequences in waking animals. The forward and reverse nature of the spike sequences during SPW-Rs in the waking and sleeping animal has been debated. Very little is known about the physiological properties of SPW-Rs associated with waking and sleep. We recorded local field potentials of SPW-Rs in the CA1 pyramidal layer of the rat hippocampus during multiple behavioral states: REM sleep (REM-HC), slow wave sleep (SWS-HC), periods of stillness in the home cage (S-HC), running on maze environments (R-M), and periods of stillness while in maze environments (S-M). The peak frequency of ripples was significantly higher during S-M than SWS-HC or S-HC. The amplitude of SPWs and the magnitude and peak frequency of ripples in the CA1 pyramidal layer were significantly correlated during SWS-HC but not during S-M, and SPW amplitude was higher during SWS-HC and S-HC than during S-M. SPW-Rs occurred more frequently during SWS-HC than during any of the other assessed states. During R-M, SPW-Rs were occasionally embedded in the stream of theta waves but only when the rat transiently paused its ambulation. These 'exploratory' SPW-Rs could also be distinguished by their association with distinct sharp waves in str. radiatum. These findings support the view that theta and SPW-Rs are competing physiological patterns.

3.2 Introduction

Large amplitude local field sharp waves (SPWs) in the hippocampus are self-organized, endogeneous patterns, which occur irregularly in the CA1 str. radiatum during behavioral states where there is little or no interaction with the environment, such as immobility, consummatory behaviors, and slow wave sleep (Buzsáki et al., 1983). Synchronous bursting of CA3 pyramidal cells causes a depolarization of the apical dendrites of CA1 pyramidal cells, which is observed in extracellular recordings as a SPW (Fig. 3.1A). The CA3 output during SPWs also discharges various interneurons in CA1 (Csicsvari et al., 1999a; 2000; Klausberger et al., 2003; Klausberger and Somogyi, 2008). In turn, the local interaction between CA1 pyramidal cells and interneurons triggers a short-lived ripple oscillation (SPW-R; O'Keefe and Nadel, 1978; Buzsáki et al., 1992; Ylinen et al., 1995; Csicsvari et al., 2000; Klausberger et al., 2003).

SPW-Rs occur during both waking and sleep, and in terms of the behavioral states in which they are observed, SPW-Rs are the antithesis of hippocampal theta oscillations (Buzsáki, 2005). Theta oscillations are most prominent during navigation and appetitive behaviors, including exploratory walking and running, REM sleep, rearing and head movements but the amplitude and regularity of theta decrease progressively as the animal becomes immobile (Vanderwolf, 1988). During consummatory behaviors, such as eating, drinking and grooming, theta is absent during species-specific, automatic movement patterns but emerges transiently as the animal shifts its position (Vanderwolf, 1988). In a complementary manner, SPW-Rs occur most frequently during slow wave sleep (SWS) but are also present during consummatory behaviors and immobility, including brief pauses of ambulation during exploration (Buzsáki et al., 1983).

Neuronal participation in the population discharge of SPW-R is shaped by the previous experience of the animal and is thought to be a carrier mechanism of 'off-line' consolidation of the memory trace (Buzsáki, 1989; Nadasdy et al., 1999; Wilson and McNaughton, 1994; Foster and Wilson, 2006; Diba and Buzsáki, 2007; O'Neill et al., 2006; 2008; Karlsson and Frank, 2008; 2009; Davidson et al., 2009; Singer and Frank, 2009). The SPW-Rs that may be occasionally observed during navigation were recently termed "exploratory" SPW-Rs (O'Neill et al., 2006) and are thought to play a different physiological and behavioral role than SPW-Rs associated with SWS (Karlsson and Frank, 2009). In support of this view, it had been suggested that the waking experience is replayed backwards by waking SPW-Rs whereas only forward sequences are present during SPW-Rs of sleep (Foster and Wilson, 2006). Subsequently, it was shown that both forward and reversed sequences can be present in SPW-Rs during waking (Diba and Buzsáki, 2007; Davidson et al., 2009). Recently, both forward and reversed sequences of waking activity have been reported during SPW-Rs of SWS (Wikenheiser and Redish, 2013). In addition, selective suppression of SPW-Rs during both sleep (Girardeau et al., 2009; Ego-Stengel and Wilson, 2010) and waking (Jadhav et al., 2012) interferes with learning and memory consolidation, although some differences were noted between the consequences of erasing waking and SWS-related SPW-Rs (Jadhav et al., 2012). Since sleep and waking are fundamentally different brain states (Hobson and Pace-Schott, 2002), and, therefore, SPW-Rs are embedded into different background patterns, we examined the physiological features of waking and sleep-related SPW-Rs.

3.3 Materials and Methods

3.3.1 Animals, Surgery, and Recording

LFP and unit activity were recorded with 8-shank 'octrode' probes of silicon probes from the dorsal CA1 pyramidal layers (four male Long-Evans rats, Mizuseki et al., 2009) or with 2-dimensional silicon probe arrays with 96 monitoring sites covering multiple layers in the CA1, CA3 and dentate regions (four male Long-Evans rats and two male Sprague-Dawley rats; Csicsvari et al., 2003; Montgomery et al., 2007). Surgical procedures have been described in detail elsewhere (Montgomery et al., 2008; Mizuseki et al., 2009). Recordings were carried out while the animal ran on any one of several different behavioral apparatuses (T-maze, linear track, z-maze, zig zag, open field). Theta periods from all maze behaviors were lumped together as RUN (R-M) and periods without theta were concatenated as immobility (S-M). Additional recordings were carried out during sleep, including several epochs of REM sleep (REM-HC) and slow wave sleep (SWS-HC) in the animal's home cage, typically both before and after the behavioral sessions (Mizuseki et al., 2009). Periods in the home cage where the animal was still but not in SWS were classified as stillness in the home cage S-HC. Rapid eye movement sleep (REM) and slow wave sleep episodes were detected offline using the ratio of the power in theta band (5–11 Hz) to delta band (1–4 Hz) of LFP, followed by manual adjustment with the aid of visual inspection of whitened power spectra (using a low-order autoregressive model) and the raw traces (Mizuseki et al., 2009; Grosmark et al 2012). REM epochs were cross-validated with experimenter notes taken during recording to confirm that the rat was immobile and sleeping. During sleep recording, the rat typically curled up in one of the corners of the home cage.

3.3.2 Detection of ripples and multitaper FFT

The procedures for detection of ripples and spectral analysis via multitaper FFT were the same as those described previously (Sullivan et al., 2011). Briefly, LFP signals from one or more selected channels from the CA1 pyramidal layer were filtered between 50 and 250 Hz, rectified, smoothed with a three-sample uniform kernel, and then z-score normalized. Candidate oscillatory events (epochs during which this normalized signal exceeded a 2 SD threshold) were detected first. Each candidate event was aligned to the nearest peak of the CA1 pyramidal CSD signal within a 25-ms window around the midpoint of the detected suprathreshold epoch. Because this alignment procedure can result in the same oscillatory event being detected multiple times, we edited the realigned candidate oscillatory events to enforce a minimum 50 ms spacing between events, deleting all but the event with the highest CSD peak when multiple events occurred within a 50-ms time span. Using multitaper FFT (Mitra and Pesaran, 1999), we calculated the normalized power spectrum for each candidate event. We required that each oscillation in the final data set have a spectral peak at any frequency between 140 and 200 Hz that is at least 2 SDs above the mean SWS background power for that frequency, for power spectra computed using both the LFP and CSD.

3.3.3 Wavelet analysis

For wavelet analysis, the discrete wavelet transform (65 levels, 1–300 Hz) was computed by using a MATLAB wavelet software package provided by C. Torrence and G. Compo (http://paos.colorado.edu/research/wavelets/software.html). For every channel subjected to wavelet analysis, power and phase were calculated and saved for each level (i.e.,

frequency) for each sample (either 1250 or 1252 Hz) for the entire length of the recording. Power at each level (i.e., frequency) of the wavelet transform was individually normalized by the mean and SD of wavelet power during non-REM episodes. Although the wavelet data for the entire session were normalized, only data from non-REM sleep epochs were used to calculate the normalizing factors to avoid bias deriving from differing proportions of non-REM sleep and other behaviors in recording sessions.

3.4 Results

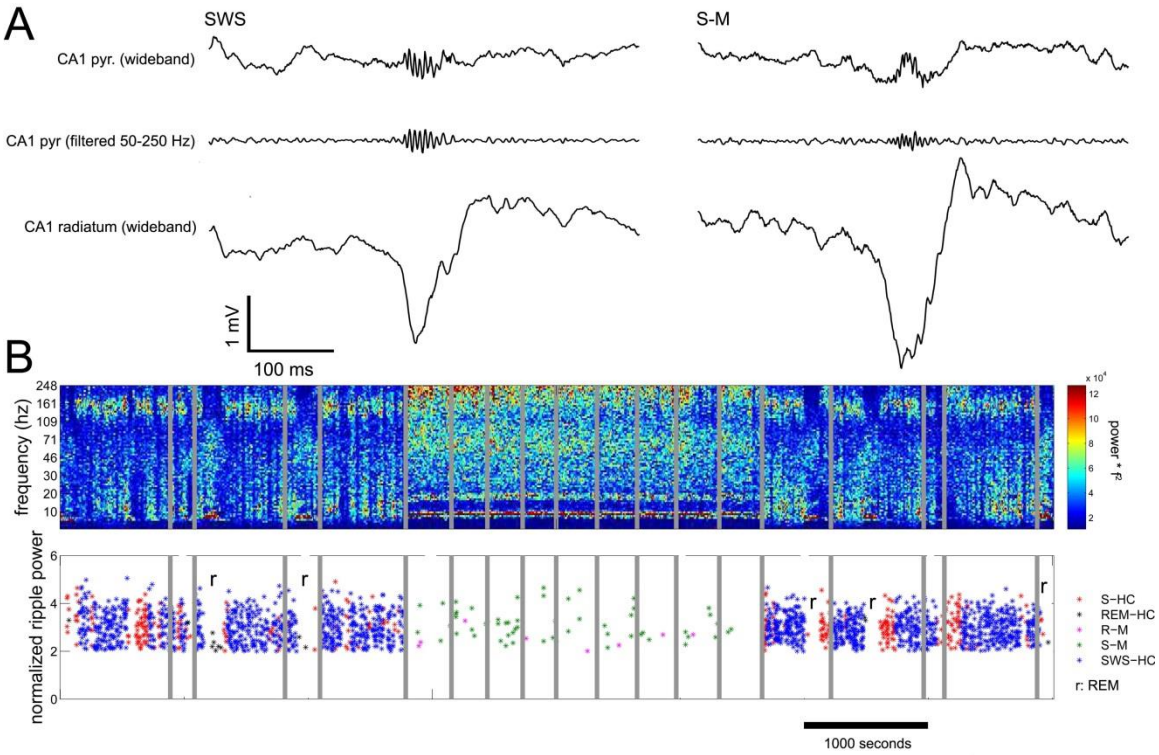

Figure 3.1 SPWs and ripples in the CA1 region during sleep and stillness on the maze. A. Raw traces of wide-band LFP (1-625 Hz) recorded simultaneously from the CA1 pyramidal layer and the mid str. radiatum, together with a band-pass filtered (50-250 Hz) trace of the pyramidal layer signal. SWS, slow wave sleep (SWS); S-M, stillness on the maze. B. Top, time-frequency spectrogram (whitened; log scale) of several hours of recording on the same day from the CA1 region in the home cage (left and right) and maze (middle sessions). Gray lines, gaps in recordings. Note dominant theta power during maze sessions. r, REM sleep episodes of sleep. Bottom, SPW-R events (normalized ripple power) as a function of time/behavior. Each asterisk is a single SPW-R event. SWS-HC, events detected during slow wave (non-REM) sleep in the home cage; S-HC, events detected

during quiet wakefulness in the home cage; REM-HC, events detected during REM sleep in the home cage; S-M, events detected during immobility, drinking in the maze; R-M, events detected during runs in the maze.

We examined the occurrence of SPW-Rs in 5 different situations (Figure 3.1): slow wave sleep in the home cage (SWS-HC), stillness (i.e., immobility) in the home cage (S-HC), REM sleep in the home cage (REM-HC), and running (R-M) and immobility epochs (S-M) in various mazes (see Experimental Methods). SPW-Rs occurred at the highest density during SWS (non-REM), followed by S-HC, followed by transient immobility and drinking periods on the maze (S-M; Fig. 3.1B; 3.4A). During behaviors associated with theta oscillations (R-M and REM-HC), SPW-Rs were absent or rare (see below).

3.4.1 Ripple power and frequency

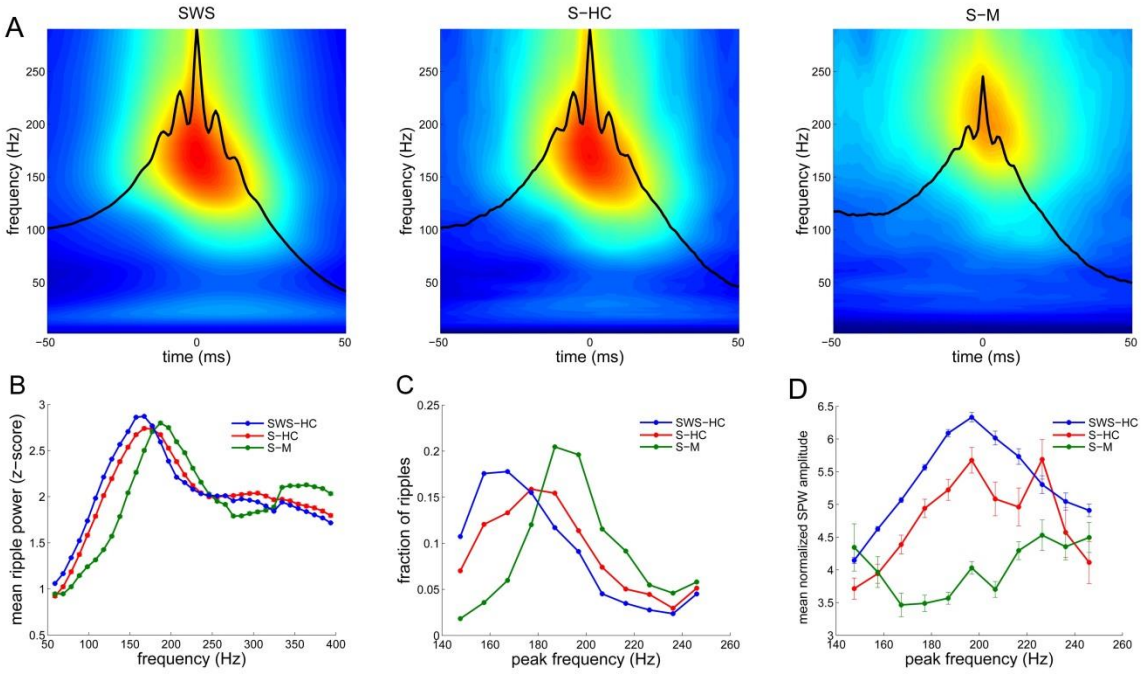

Figure 3.2 SPW-Rs during sleep and waking are different. A. Average wavelet spectrograms of SPW-R-centered epochs from the CA1 pyramidal layer during SWS-HC, S-HC, and S-M. Corresponding averaged CA1 pyramidal layer CSD overlaid in black. Note higher frequency ripple power during S-M. B. Average power spectrum of SPW-Rs during SWS-HC, S-HC, and S-M (mean ± SEM; n = 9 rats). C. Average histogram of the peak spectral frequency (calculated via FFT) of SPW-R events detected during slow wave sleep in the home cage

(SWS-HC) and transient immobility epochs on the maze (mean ± SEM; n = 9 rats). E. Relationship between SPW amplitude and peak ripple frequency in CA1 str. pyr. (mean ± SEM; n = 9 rats).

SPW-Rs in the sleeping rat and those recorded during the pauses of the navigation task were quantitatively different (Fig. 3.2). The most striking difference was the higher frequency of SPW-Rs in the maze (S-M), compared to SPW-Rs recorded in the home cage either during sleep or during stillness (Fig 3.2*A*). To quantify the differences, we first calculated a power spectrum for each detected ripple, and plotted the mean power spectrum for each behavior (Fig. 3.2*B*). SPR-W during SWS-HC had significantly greater peak power in the 140-250 Hz range than during S-HC or S-M ($p < 0.00001$, Kruskal-Wallis one-way non-parametric ANOVA). Second, the mean frequency of each detected SPW-R event was determined and the events were displayed as probability density histograms (Fig. 3.2*C*). Comparing the frequencies of the spectral power peaks, we found that the distributions of SPW-R peak frequency during SWS, S-HC, and S-M were significantly different ($p < 0.00001$; Kruskal-Wallis). While the modal frequency of SPW-Rs was at 167 Hz during SWS-HC, modal ripple frequency was 177 Hz during S-HC, and 187 Hz during S-M.

3.4.2 Ripple frequency, SPW amplitude and the temporal pattern of SPW-R

We examined the relationship between the magnitude of SPWs recorded in the CA1 pyramidal layer and the power and frequency of ripples recorded in the pyramidal layer. As previously described, we used the peak value of the CA1 pyramidal layer current source to quantify the amplitude of the SPW, as this value and the amplitude of the CA1 s. radiatum current sink are highly correlated (Sullivan et al., 2011). SPWs had significantly different magnitudes during SWS, S-HC, and S-M, with the highest

amplitude SPWs during SWS and the lowest magnitude SPWs during S-M ($p < 0.00001$, Kruskal-Wallis). SPW amplitude was correlated weakly, positively, and significantly with the peak frequency of ripple SWS, S-HC, and S-M (Fig 3.2D, $r < 0.12$, $p < 0.00001$). However, whereas there is a clear relationship between SPW amplitude and ripple frequency during SWS and S-HC (Sullivan et al., 2011), the nature of this relationship during S-M is less apparent.

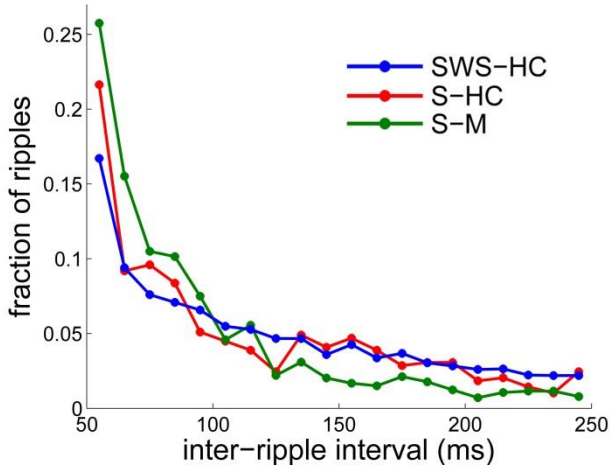

Figure 3.3 Behavior-dependence of SPW-R recurrence. Average histogram of interval between SPW-Rs during sleep (SWS-HC; blue), immobility in the home cage (S-HC), and immobility on the maze (S-M) (mean ± SEM; n = 9 rats) .

The distribution of inter-SPW-R intervals during S-M was significantly different than for during SWS or S-HC (Fig. 3.3; $p < 0.00001$, Kruskal-Wallis). Short (< 100 ms) intervals between SPW-Rs were more common during maze exploration than during sleep or wakefulness in the home cage.

3.4.3 SPW-R during theta oscillations

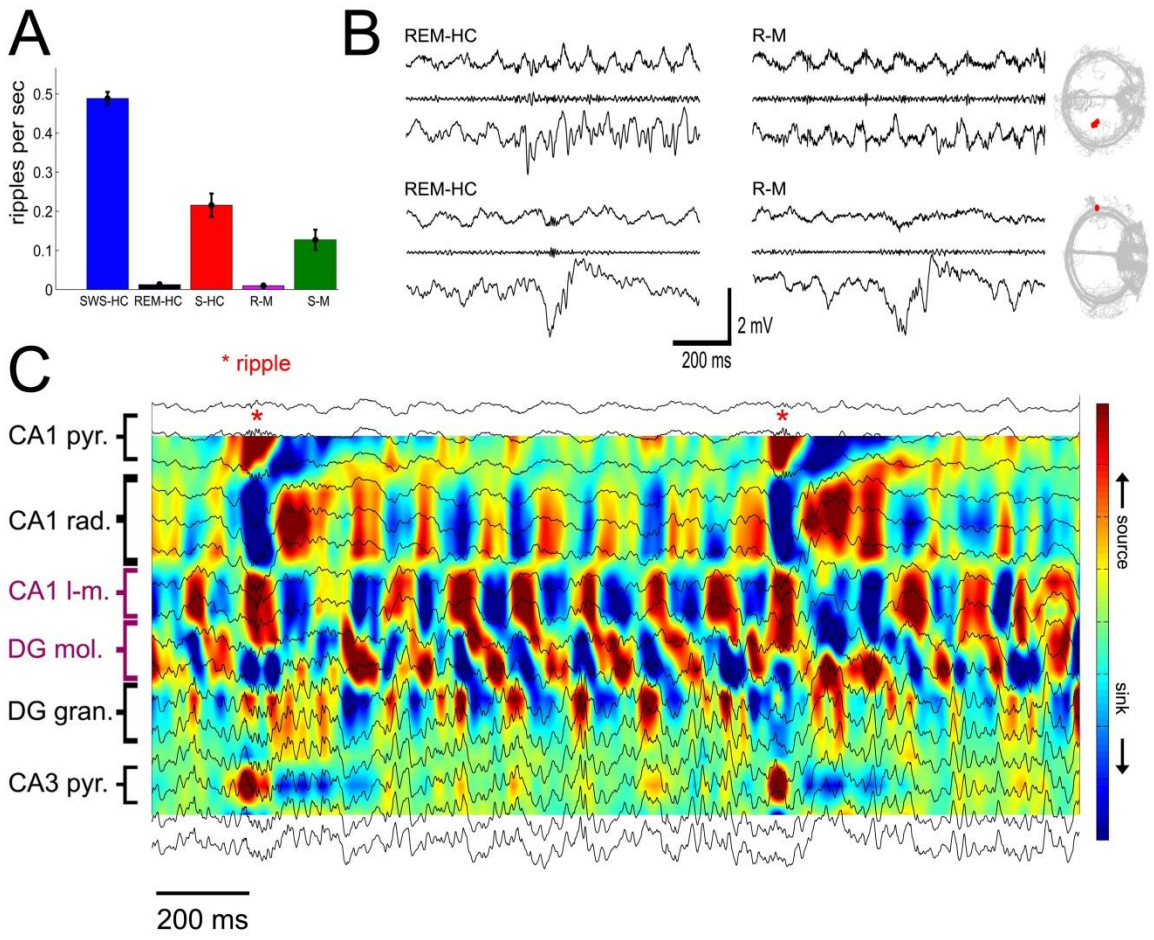

Figure 3.4 Behavior-dependence of SPW-R occurrence. A. Incidence of ripples during different behaviors. SWS-HC, slow wave sleep in home cage; REM-HC, REM sleep in home cage; R-M, running in maze; S-awake still in maze. B. Examples of false SPW-Rs during REM-HC (left), and during R-M (right). The rat's trajectory for the whole R-M session in shown gray; the rat's position during the R-M false SPW-R is shown in red. C. Two-second epoch of activity during REM sleep recorded with one shank of the 96-site linear probe, covering the CA1-CA3-axis. LFP traces (16 sites) are superimposed on the CSD map. Two SPW-Rs were detected (asterisks). Note that in both cases, ripples in the CA1 pyramidal layer are coupled with a large SPW in str. radiatum and a large source in the CA3 pyramidal layer.

Our SPW-R detection algorithm was tuned to detect possibly all SPW-Rs during sleep and immobility (Sullivan et al., 2011). However, we observed that the algorithm also detected false positive 'events' during running and REM sleep (Fig. 3.4). Indeed, SPW-

Rs were also reported during exploration, including theta-associated locomotion (Karlsson and Frank, 2008). The incidence of putative SPW-Rs during the different brain states, as detected by our algorithm, are shown in Figures 3.1 and 3.4A. A small number of putative SPW-Rs were also detected during running in the maze (R-M) and REM sleep (REM-HC). Each of these events was inspected in the original recordings. In most cases, the candidate events during running could be explained by the electromyogram artifacts of the face and neck muscles which 'bled' into the recordings or the presence of large populations bursts of spikes without an explicit rhythmic component, in contrast to the rhythmic multiple spiking during true ripples (Sullivan et al., 2011; Schomburg et al., 2012). In other instances, the stream of theta waves was interrupted, associated with a transient halt of movement (Fig. 3.4). During REM sleep, SPW-Rs were occasionally embedded in a train of theta waves. Examining the trace from the pyramidal layer alone did not reveal an interruption of the theta train. However, in animals with the 96-site probes recordings from dendritic layers were also available. In every case, ripples detected in the CA1 pyramidal layer were coupled with a large sink in CA1 str. radiatum and a strong sink-source pair in the CA3 region (Fig. 3.4), indicating the presence of sharp waves, thus distinct from 'regular' theta waves.

3.5 Discussion

Our findings show that hippocampal SPW-Rs in the waking and sleeping rat differ quantitatively in several parameters. SPW-Rs occur during non-theta states, intermingled with theta waves, yet their physiological origin can be distinguished.

The electrophysiological patterns of waking consummatory behaviors (such as immobility, drinking, eating and grooming) and non-REM (SWS) sleep are different in several ways (Vanderwolf, 1988). Non-REM sleep is characterized by widespread neocortical and paleocortical slow oscillations (Steriade et al., 1993), which can effectively modulate hippocampal activity (Sirota et al., 2003; Wolansky et al., 2006; Isomura et al., 2006; Hahn et al., 2007; Sullivan et al., 2011). This neocortical influence can explain the excess of inter-SPW-R intervals in the 0.2-1.5 sec range during non-REM sleep, compared to immobility in the maze (Sirota et al., 2003; Molle et al., 2009; Sullivan et al., 2011). Another striking difference between the two states was the substantially higher frequency of ripples in the waking animal. Although the mechanisms responsible for adjusting ripple frequency are not well understood (Sullivan et al., 2011; Nguyen et al., 2009; Foffani et al., 2007), the residual subcortical neurotransmitters during transient stops in the maze may be important contributors. This hypothesis is also supported by the observation that ripples are significantly slower in the anesthetized animal, when the release of subcortical neurotransmitters is more strongly attenuated (Hara and Harris, 2002), compared to sleep (Ylinen et al., 1995).

The brain state-dependent dissociation between SPW magnitude on the one hand and ripple power and frequency on the other adds further support to the idea that these event are generated independently and their cross-frequency coupling can be modulated by a multitude of factors. Previous research has shown that the strength of the CA3 drive, as reflected by the magnitude of the CA1 str. radiatum sink, can affect the parameters of ripples and fast gamma oscillations (Sullivan et al., 2011). In addition, SPWs are not invariably associated with pyramidal layer ripples and, vice versa, ripples can

occasionally emerge in the absence of SPWs (Ylinen et al., 1995; Csicsvari et al., 1999b). A robust example of such dissociation is the strong emergence of slower frequency ripples in the CA3-TeTX transgenic mouse, in which CA3 output can be specifically and inducibly controlled (Nakashiba et al., 2008). One possibility for the increased ripple activity in the absence of the CA3 output is that the absence of CA3 pyramidal activity also reduces the drive to CA1 interneurons (Csicsvari at al., 2003) and the more excitable CA1 network can respond more effectively to the intact entorhinal input. In our experiments, the SPW sink magnitude exerted less of a gain on ripple power and virtually no effect on ripple frequency in the waking rat. It is possible that the network resonant properties of the CA1 circuit (Sullivan et al., 2011) are different between waking and sleep states and such resonance may be sharper in the waking animal and limit the frequency-adjusting effects of the input drive. An alternative or complementary explanation is that the forward and reverse sequential replay of waking and sleeping firing patterns (Foster and Wilson, 2006; Diba and Buzsáki, 2007; Davidson et al., 2009; Wikenheiser and Redish, 2013) require different temporal dynamics and these differences are expressed in the faster waking versus slower ripples of sleep. Further experiments examining such potential links explicitly are needed.

No ‘true’ ripples were present during running in the maze. The occasionally detected events were either artifactual or, if present, ripples were always associated with transient halts of locomotion and changes in the stream of theta oscillations. During REM sleep, *bona fide* ripples were routinely detected in every rat. Although overt behavioral change during REM sleep could not assist us in the examination of the circumstances that lead to the emergence of ripples, monitoring the LFP activity in CA1 str. radiatum and the CA3

region showed that theta epochs during REM were quite variable (Montgomery et al., 2008), and interruption of the stream of theta waves could alternate with CA3-CA1 bursts, as reflected by the coupled sharp waves and ripples. Overall, these findings support the hypothesis that theta oscillations and SPW-Rs are competing physiological mechanisms, even though they share overlapping anatomical substrates (Buzsáki et al., 1983; Ylinen et al., 1995; Csicsvari et al., 2003; Sullivan et al., 2011). Depending on the behavioral states, the probability distribution of SPW-Rs and theta waves vary quantitatively from only theta waves during running to only SPW-Rs during immobility and SWS, while in other states an alternating mixture of both patterns can be observed, occasionally in rapid succession.

It is important to emphasize that high frequency activity (‘high gamma’ or epsilon band) can also be present during theta oscillations, coinciding with the phase with maximum spiking activity (Canolty et al., 2006; Colgin et al., 2009; Belluscio et al., 2012; Scheffer-Teixeira et al., 2013). However, in contrast to the rhythmic ripple pattern, the high gamma (or epsilon) power during theta is rarely oscillatory (Schomburg et al., 2012; Scheffer-Teixeira et al., 2013). Importantly, epsilon band power during theta oscillations is present around the trough of the theta waves recorded from the CA1 pyramidal layer (Colgin et al., 2009; Belluscio et al., 2012). In contrast, true ripples are associated with a negative SPW (sink) in str. radiatum and a positive wave (source) in the middle of the CA1 pyramidal layer (Ylinen et al., 1995; Mizuseki et al., 2011). Thus, the mechanisms of high-frequency rhythms during SPW-Rs and theta oscillations may not be identical .

3.6 Figure legends

Figure 3.1

SPWs and ripples in the CA1 region during sleep and stillness on the maze. A. Raw traces of wide-band LFP (1-625 Hz) recorded simultaneously from the CA1 pyramidal layer and the mid str. radiatum, together with a band-pass filtered (50-250 Hz) trace of the pyramidal layer signal. SWS, slow wave sleep (SWS); S-M, stillness on the maze. B. Top, time-frequency spectrogram (whitened; log scale) of several hours of recording on the same day from the CA1 region in the home cage (left and right) and maze (middle sessions). Gray lines, gaps in recordings. Note dominant theta power during maze sessions. r, REM sleep episodes of sleep. Bottom, SPW-R events (normalized ripple power) as a function of time/behavior. Each asterisk is a single SPW-R event. SWS-HC, events detected during slow wave (non-REM) sleep in the home cage; S-HC, events detected during quiet wakefulness in the home cage; REM-HC, events detected during REM sleep in the home cage; S-M, events detected during immobility, drinking in the maze; R-M, events detected during runs in the maze.

Figure 3.2

SPW-Rs during sleep and waking are different. A. Average wavelet spectrograms of SPW-R-centered epochs from the CA1 pyramidal layer during SWS-HC, S-HC, and S-M. Corresponding averaged CA1 pyramidal layer CSD overlaid in black. Note higher frequency ripple power during S-M. B. Average power spectrum of SPW-Rs during SWS-HC, S-HC, and S-M (mean ± SEM; n = 9 rats). C. Average histogram of the peak spectral frequency (calculated via FFT) of SPW-R events detected during slow wave

sleep in the home cage (SWS-HC) and transient immobility epochs on the maze (mean ± SEM; *n* = 9 rats). E. Relationship between SPW amplitude and peak ripple frequency in CA1 str. pyr. (mean ± SEM; *n* = 9 rats).

Figure 3.3

Behavior-dependence of SPW-R recurrence. Average histogram of interval between SPW-Rs during sleep (SWS-HC; blue), immobility in the home cage (S-HC), and immobility on the maze (S-M) (mean ± SEM; *n* = 9 rats) .

Figure 3.4

Behavior-dependence of SPW-R occurrence. A. Incidence of ripples during different behaviors. SWS-HC, slow wave sleep in home cage; REM-HC, REM sleep in home cage; R-M, running in maze; S-awake still in maze. B. Examples of false SPW-Rs during REM-HC (left), and during R-M (right). The rat's trajectory for the whole R-M session in shown gray; the rat's position during the R-M false SPW-R is shown in red. C. Two-second epoch of activity during REM sleep recorded with one shank of the 96-site linear probe, covering the CA1-CA3-axis. LFP traces (16 sites) are superimposed on the CSD map. Two SPW-Rs were detected (asterisks). Note that in both cases, ripples in the CA1 pyramidal layer are coupled with a large SPW in str. radiatum and a large source in the CA3 pyramidal layer.

Section 4 - Relationship between sleep spindles and theta oscillations in the hippocampus

Submitted and under review: Sullivan DW, Mizuseki K, Sorgi T, Buzsáki G (2013) J Neurosci.

4.1 Abstract

Several network patterns allow for information exchange between the neocortex and the entorhinal-hippocampal complex, including theta oscillations and sleep spindles. How neurons are organized in these respective patterns is not well understood. We examined the cellular-synaptic generation of sleep spindles and theta oscillations in the waking rat and during REM sleep by simultaneously recording local field and spikes in the regions and layers of the hippocampus and entorhinal cortex (EC). We show that (1) Current source density analysis reveals that similar anatomical substrates underlie spindles and theta in the hippocampus, although the hippocampal subregions are more synchronized during spindles than theta; (2) the spiking of putative principal cells and interneurons in the CA1, CA3 and dentate gyrus subregions of the hippocampus, as well as layers 2,3, and 5 of medial entorhinal cortex are significantly phase locked to spindles detected in CA1; (3) the relationship between LFP phase and unit spiking differs between spindles and theta; (4) individual hippocampal principal cells generally do not fire in a rhythmic fashion during spindles; (5) power in gamma and epsilon bands of hippocampal LFP is modulated by the phase of spindle oscillations; and (6) unit firing rates during spindles were not significantly affected by whether spindles occurred during non-REM or intermediate sleep. These findings indicate that spindle patterns represent a relatively

simple feed-forward ‘synfire chain’ of excitatory activity from the neocortex to the hippocampus with a relatively random spike content.

4.2 Introduction

Sleep spindles in the neocortex are among the most prominent features of non-REM sleep (Loomis et al, 1935; De Gennaro and Ferrara, 2003; Steriade et al., 1993b). Spindles have been implied in synaptic plasticity and sleep-dependent memory consolidation in both humans and other animals (Sejnowski and Destexhe, 2000; Steriade 2000; Steriade and Timofeev, 2003; Gais et al., 2002; Diekelmann and Born, 2010; Fogel and Smith, 2011; Eschenko et al., 2006; Nir et al., 2011; Miyamoto and Hensch, 2003; Hanlon et al., 2009; Schiffelholz and Aldenhoff, 2002; Khazipov et al., 2004; Schabus et al., 2004), partly because of the ability of thalamocortical spindles to trigger hippocampal sharp wave-ripples (Siapas and Wilson, 1998; Sirota et al., 2003; Isomura et al., 2006; Mölle et al., 2006; Eschenko et al., 2008; Sullivan et al., 2011; Peyrache et al., 2009; 2011; Nishida and Walker, 2007; Clemens et al., 2007; 2010; Johnson et al., 2010). Altered sleep spindle dynamics have been documented in several forms of mental disease (Ferraleli et al., 2007; 2010; Wilson and Argyropoulos, 2012; Wamsley et al., 2012; Vukadinovic 2011; Plante et al., 2012). However, it is not clear whether thalamocortical spindles regularly invade the hippocampus and affect its circuits outside sharp wave ripples, although several observations suggest that this might be the case (Sirota et al., 2003; Isomura et al., 2006; Nir et al., 2011).

Sleep spindles are generated by the interaction between the GABAergic neurons of the thalamic reticular nucleus and the thalamocortical nuclei (Steriade 2000; Steriade et al.,

1993c; Astori et al., 2011; Halassa et al., 2011) and are synchronized across the multiple thalamic nuclei via necortical feedback (Contreras et al., 1996; Gottselig et al., 2002). Sleep spindles can reach the hippocampus either by the direct projection from nucleus reuniens to the distal dendrites of CA1 pyramidal (Herkenham 1978; Wouterlood et al. 1990; Dolleman-Van der Weel et al. 1997) or, by the neocortical-entorhinal cortex path (Wolansky et al., 2006; Isomura et al., 2006; Hahn et al., 2007). If the entorhinal cortex is involved in conveying the neocortical rhythm to the circuits of the hippocampus, a comparison with the mechanisms of theta oscillations is warranted since most theta-associated currents are also generated by the entorhinal inputs (Buzsáki et al., 1983; Alonso and Llinas, 1989; Bragin et al., 1995; Kamondi et al., 1998; Montgomery et al., 2009; Chrobak and Buzsáki, 1998) but in a different brain state. In the present experiments, we investigated the physiological features of sleep spindles and compared their cellular-synaptic generation with those of the theta oscillations in REM sleep and the waking rat. We report that while the anatomical substrates underlying the extracellular current generation of both rhythms are similar, the temporal organization of neuronal firings are qualitatively different during theta and spindle oscillations.

4.3 Materials and Methods

4.3.1 Animals and surgery

Fifteen male Long-Evans rats and one male Sprague-Dawley rat (350-500g; 5-8 months) were used in these experiments. Behavioral training, surgery details and data obtained from subgroups of the present rats have been reported earlier (Csicsvari et al., 2003; Diba and Buzsáki, 2007; Montgomery et al., 2009; Mizuseki et al., 2009, Fujisawa and

Buzsáki 2011). After maze training, recording and stimulation electrodes were implanted. In five rats, a 96-site silicon probe was implanted in the right hemisphere parallel to the transverse axis of the hippocampus (45° parasagittal). These probes had recording sites spaced regularly over a 1.5 x 1.5 mm2 area with six shanks spaced at 300 μm, each with 16 recording sites at 100 μm spacing. A bipolar stimulating electrode was implanted into the angular bundle (perforant path) at 1.0 mm anteroposterior (AP) and 1.0 mm mediolateral (ML) from the junction between lambda and the right lateral ridge, and 3.5 mm dorsoventral from the dura. Another stimulating electrode was implanted in the ventral hippocampal commissure at 1.2 mm AP and 1.0 mm ML from bregma and 3.8 mm from the dura (Csicsvari et al., 2000; Montgomery et al., 2009). Four rats were implanted with 32- and/or 64-site silicon probes in the left or right dorsal hippocampus. The silicon probes, consisting of four or eight individual shanks (spaced 200 μm apart), each with eight staggered recording sites (200 μm spacing), were lowered to CA1 and CA3 pyramidal cell layers (Diba and Buzsáki, 2007) and dentate gyrus. An additional three rats were implanted with a four-shank silicon probe in the right dorsocaudal medial entorhinal cortex (EC) and another four- or eighth-shank probe into the CA1– dentate axis (Mizuseki et al., 2009). One rat was implanted only with a four shank silicon probe in the right dorsocaudal medial entorhinal cortex (Mizuseki et al. 2009). Two rats were implanted with three tetrode microdrives (individually movable tetrodes constructed from 13 μm tungsten wire): one microdrive with three tetrodes targeting right dorsal hippocampal CA1, one microdrive with four tetrodes targeting right visual cortex; and one microdrive with one tetrode targeting the medial septum. One rat was implanted with a 4-shank silicon probe in right dorsal hippocampal CA1 and an 8-shank probe in

PFC (Fujisawa and Buzsáki 2011). Two stainless steel screws inserted above the cerebellum were used as indifferent and ground electrodes during recordings.

Postmortem electrode location was verified using thionin, fluorescent Nissl (Invitrogen), or DAPI (Invitrogen) staining in combination with DiI-labeled (Invitrogen) electrode tracks. Histological reconstruction of electrode tracks is available from Montgomery et al. (2007, 2008), Mizuseki et al (2009), and Fujisawa and Buzsáki (2011). All protocols were approved by the Institutional Animal Care and Use Committee of Rutgers University.

4.3.2 Data collection

After recovery from surgery (~1 week), physiological signals were recorded in the home cage and included waking immobility and sleep epochs. During sleep, the rat curled up in one of the corners with eyes closed. Rapid eye movement (REM) and slow-wave sleep epochs were separated as described previously (Montgomery et al., 2008; Grosmark et al. 2012). During the recording sessions, neurophysiological signals were amplified (1000x), bandpass filtered (1 Hz to 5 kHz), and acquired continuously at 20 kHz on a 128-channel DataMax system (RC Electronics) or at 32.552 kHz on a 128-channel Digital Lynx system (Neuralynx). After recording, the local field potential (LFP) was downsampled to 1250 Hz (DataMax) or 1252 Hz (Neuralynx) for additional analysis. For offline spike sorting of unit activity, the wideband signal was digitally highpass filtered (0.8–5 kHz). Spike sorting was performed automatically, using KlustaKwik (http://klustakwik.sourceforge.net), followed by manual adjustment of the clusters (using “Klusters” software package; http://klusters.sourceforge.net). Neurophysiological and

behavioral data were explored using NeuroScope (http://neuroscope.sourceforge.net) (Hazan et al., 2006). Additional details of recording and unit separation and cell type classifications have been described previously by Csicsvari et al. (2003), Diba and Buzsáki (2007), and Mizuseki et al., (2009). For the entorhinal unit data here, putative interneurons and principal cells were classified according to the procedure described by Mizuseki et al. (2009). Because of the low number of simultaneously recorded hippocampal units in animals implanted with 96-site probes, we used a simplified method for classification of hippocampal units based on the shape of spike autocorrelograms; units with a characteristic "bursty" autocorrelogram were classified as principal cells, and units lacking a "bursty" autocorrelogram with mean firing rates > 5 Hz were classified as putative interneurons. Hippocampal units with mean firing rates < 0.1 Hz were discarded from the data set. Recording site irregularities (including cross talk and excessive impedances) were a priori identified and removed from analysis using measures of coherence and normalized power similarity (Diba et al., 2005). Current source density (CSD) was calculated by standard methods (Mitzdorf, 1985). Only CSD calculations centered on three consecutive good channels were used. CSD calculations that would require use of a recording site displaying an irregularity were excluded from additional analysis.

Recordings were carried out during sleep, including several epochs of REM sleep and slow wave sleep (SWS) in the animal's home cage (Montgomery et al., 2007). In addition, recordings obtained while the animal ran on an open field (200 cm by 100 cm, 180 cm by 180 cm), a linear maze (250 cm long), and an alternation task in the T-maze

(Montgomery et al., 2007; Mizuseki et al., 2009) were also analyzed. Theta periods from all maze behaviors were lumped together as RUN.

4.3.3 Wavelet algorithm

For wavelet analysis, the discrete wavelet transform (65 levels, 1–300 Hz) was computed by using a MATLAB wavelet software package provided by C. Torrence and G. Compo (http://paos.colorado.edu/research/wavelets/software.html). For every channel subjected to wavelet analysis, power and phase were calculated and saved for each level (i.e., frequency) for each sample (either 1250 or 1252 Hz) for the entire length of the recording. Power at each level (i.e., frequency) of the wavelet transform was individually normalized by the mean and SD of wavelet power during non-REM episodes. Although the wavelet data for the entire session were normalized, only data from non-REM sleep epochs were used to calculate the normalizing factors to avoid bias deriving from differing proportions of non-REM sleep and other behaviors in recording sessions. For each unit spike in the datasets, phase relative to a rhythm of interest was calculated by finding the wavelet phase at the frequency with the highest normalized wavelet power within a specified range of frequencies (theta: 4.95-10.02 Hz; spindle: 9.27-17.34 Hz).

4.3.4 Detection of ripples

Ripples were detected via the following procedure: from a single LFP channel in the CA1 pyramidal layer, we calculated mean normalized wavelet power between 97.05 Hz and 196.33 Hz for every sample in the recording. This signal was then smoothed with a 40 ms wide uniform window, and then z-score normalized. Ripples were defined as epochs

during which this z-score normalized signal was at least 2.5 standard deviations above the mean for a duration of at least 30 ms.

4.3.5 Detection of spindles

Spindles were detected via the following procedure: from a single LFP channel in the CA1 pyramidal layer (if available, otherwise entorhinal layer 5 or dentate molecular layer), we calculated the maximum normalized wavelet power in frequencies between 9.27 and 17.34 Hz for every sample in the recording. This signal was then z-score normalized, and epochs where the normalized signal was at least 1.4 standard deviations above the mean for a duration of at least 350 ms were selected. The trough-to-trough duration of each individual cycle was calculated for each preliminary spindle epoch, and any preliminary spindle epoch containing any cycles of duration greater than 125 ms were discarded, as were any spindles detected outside of non-REM sleep.

4.3.6 Coherence

For coherence analysis of spindles, we used a modified version of the multitaper FFT MATLAB package by Mitra and Pesaran (1999). Using a fixed FFT window length of 1 second centered on the midpoints of detected spindles, we calculated coherence over frequencies ranging 1-250 Hz between spindles in the CA1 pyramidal layer and entorhinal layer 5.

4.3.7 Consecutive cycle firing index

In order to quantify the tendency for neurons to fire on consecutive cycles of an oscillation, we created a measure termed consecutive cycle firing index (CCF). For each

neuron, CCF is calculated as the difference between two conditional expectations: the theoretical expectation of the # of spikes, up to 1, that a neuron will fire on a given cycle of an oscillation given that the neuron fired at least one spike on the previous cycle, and the empirically observed value of this expectation. The theoretical conditional expectation assumes that neurons spike in a Poisson distributed pattern at their observed firing rate during the oscillation in question, and is either the neuron's firing rate divided by the mean frequency of the oscillation in question or 1, whichever is less.

4.3.8 Spike phase spectrum

We attempted to identify rhythmic oscillation of single units relative to LFP by transforming spike trains into time series of theta or spindle phase and then estimating the power spectrum of these transformed spike trains via a multitaper FFT (Mizuseki et al., 2009). Our methods were the same as those in Mizuseki et al., except that spike phase was computed via wavelet analysis (see above), and only spikes where instantaneous firing rate (defined as firing rate in a window ± 500 ms from a given spike) was above 5 Hz were included.

4.4 Results

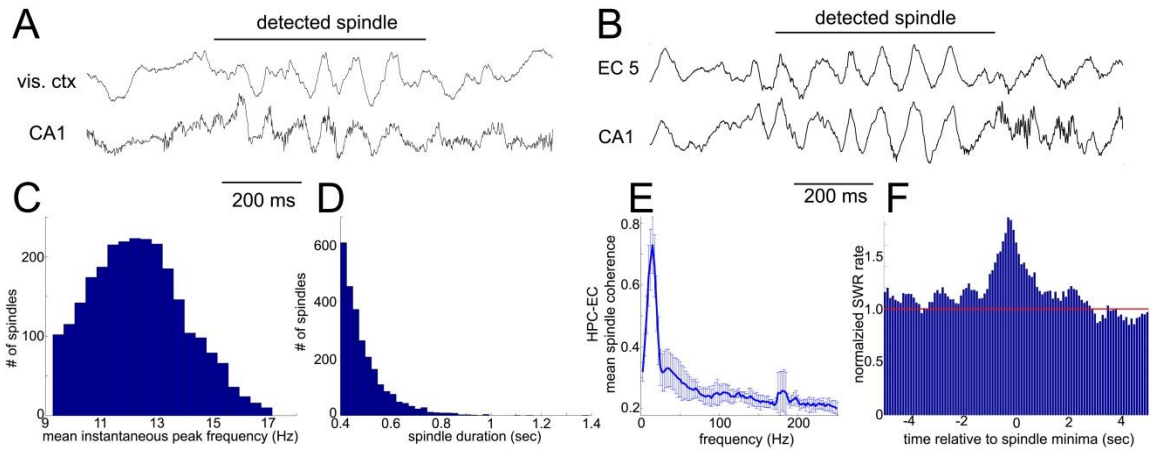

Basic features of sleep spindles. A, Example of filtered (1-626 Hz) LFP traces of a spindle event recorded simultaneously in hippocampal CA1 pyramidal layer and visual cortex. B, Example of filtered (1-625 Hz) LFP traces of a spindle event recorded simultaneously in hippocampal CA1 pyramidal layer and layer 5 of medial entorhinal cortex. Note similar onset, offset, and duration of the spindles in different structures. C, Histogram of mean instantaneous peak frequency of spindles (μ = 12.33 Hz, n = 2579 spindles in 15 rats). D, Histogram of spindle duration (μ = 0.49 sec). E, Average coherence spectrum between spindles in the CA1 pyramidal layer and layer 5 of entorhinal cortex (n = 8 sessions in 2 rats; error bars indicate σ). Note peak coherence value at 15 Hz. F, Cross-correlogram between LFP spindle minima and detected SPW-R events in hippocampal CA1 shows temporal association of these two patterns, peaking at 300 ms preceding individual spindle troughs in CA1, with SPW-R occurrence rate at 187% of baseline (n = 23 sessions in 14 rats).

In support of previous studies (Sirota et al., 2003; Nir et al., 2011), we observed LFP sleep spindles in both hippocampus and EC that occurred simultaneously with spindles recorded in the neocortex (Fig. 4.1A, B). Although sleep spindles had a somewhat variable frequency, their modal peak was 12 Hz in the hippocampus (Fig. 4.1C; mean = 12.37 Hz; *n* = 14 rats), EC (mean = 12.31 Hz; *n* = 4 rats) and the somatosensory-visual cortex (mean = 12.39 Hz, *n* = 2 rats). When spindles were recorded simultaneously in the hippocampus and EC, they were strongly coherent (Fig. 4.1E; > 0.7). Sleep spindles did not have a characteristic duration. The great majority of spindle events were short (95% under 680 ms) while a small minority exceeded 0.8 sec (Fig. 4.1D). The detected spindles

in the hippocampus were not simply volume-conducted from the overlying neocortex since hippocampal units were also phase-locked to the spindles (see below).

4.4.1 CSD profiles of sleep spindles and theta oscillations in the hippocampus

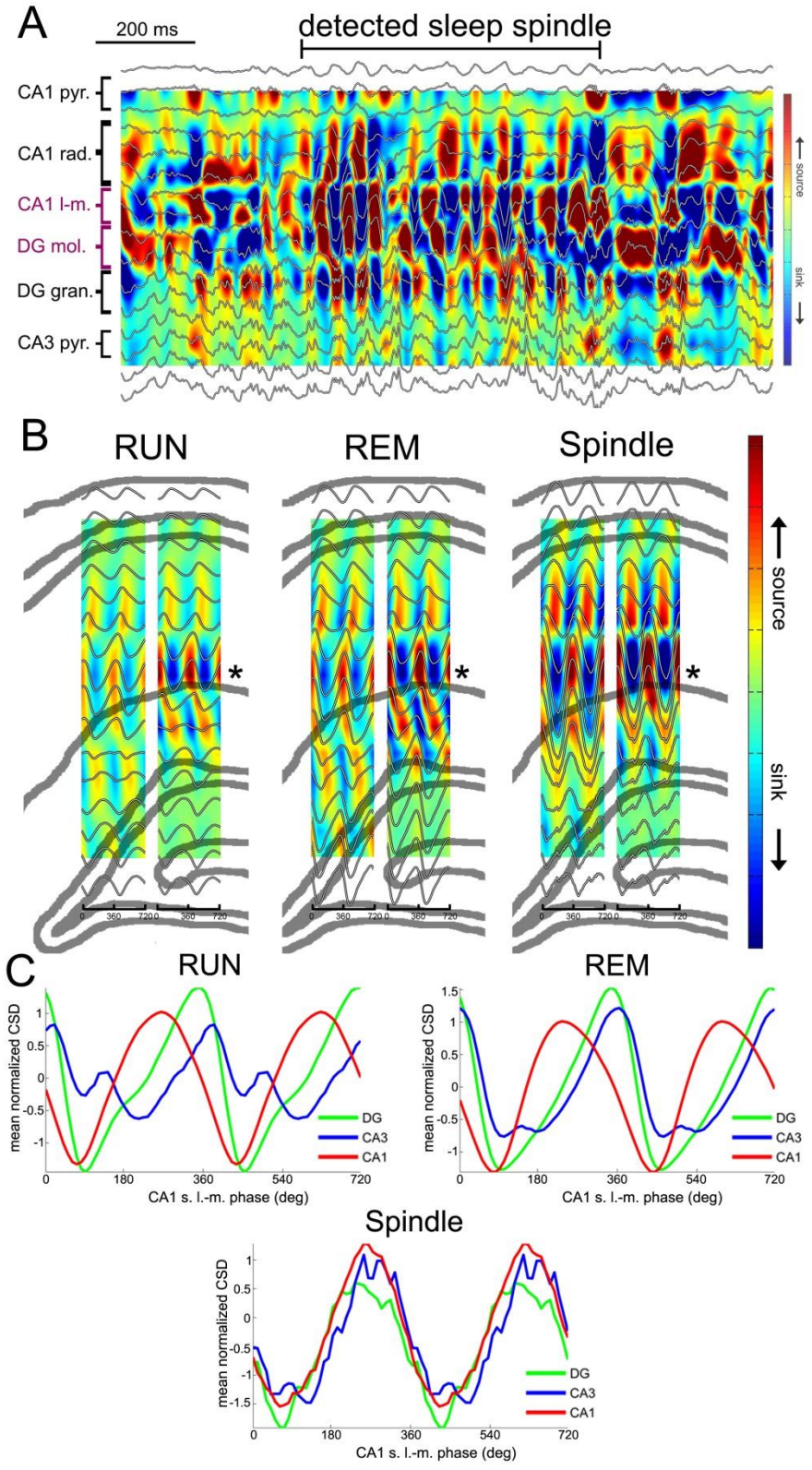

Figure 4.2 Spindle and theta oscillations in the hippocampus. A, Example of wide-band (1 Hz to 1250 Hz) LFP traces of a spindle event, recorded at multiple depths of the CA1-dentate axis and superimposed on the current-source density (CSD) map of the same event. CA1 pyr, pyramidal layer, CA1 rad, stratum radiatum, CA1 l-m, str. lacunosum-moleculare, DG mol, dentate gyrus molecular layer, DG gran, granule cell layer, CA3 pyr, pyramidal layer in the hilar region. B, Average CSD maps in a single animal with superimposed CSD traces during RUN, REM and Spindle. Recordings from two shanks of the silicon probe are shown. Maps and traces were constructed by averaging CSD and LFP traces according to CSD phase in CA1 str. lacunosum-moleculare (phase was partitioned into 10o wide bins). Asterisk indicates reference site. The cycles are calibrated in degrees rather than in time to emphasize the similar depth distributions of the sinks and sources during theta and spindle waves. C, Average normalized CSD as a function of phase in the three hippocampal principal cell layers (n = 5 sessions in 5 rats). Values greater than zero are sources, whereas values less than zero are sinks. Note the enhanced synchrony of CSD in the CA1, CA3 and dentate principal cell layers during spindle oscillations relative to REM or RUN theta.

In four rats with linear probes in multiple hippocampal layers, the laminar distribution of the spindle events could be studied in detail. Current source density (CSD) maps showed that sleep spindles were associated with large sinks in the CA1 str. lacunosum-moleculare and in the dentate molecular layer, with corresponding sources surrounding the sinks (Fig. 4.2A, B). Despite the intermittent nature and higher frequency, the within-hippocampus depth distribution of sinks and sources associated with sleep spindles were remarkably similar to CSD maps of theta oscillations during RUN and REM (Fig. 4.2B; Buzsáki et al., 1986; Brankack et al., 1993; Kamondi et al., 1998; Montgomery et al., 2009). These findings suggest that the synapses and afferent inputs responsible for the bulk of extracellular theta currents during sleep spindles are largely the same as those involved in the current generation of theta oscillations, particularly the layer 2 and layer 3 afferents of the EC, perhaps complemented by the thalamic n. reuniens projection to the CA1 str. lacunosum-moleculare. In contrast to the locations, the timing of the dipoles was different during spindle and theta oscillations (Fig. 4.2C). The currents sources, recorded from the CA1, CA3 pyramidal layer and dentate granule cell layer, showed substantial phase shifts during theta oscillations of RUN and REM, whereas during sleep spindles

they were essentially synchronous, an indication that excitation arrives virtually simultaneously from the entorhinal cortex to all hippocampal regions.

4.4.2 Neuronal discharges associated with sleep spindles and theta oscillations in the hippocampus and EC

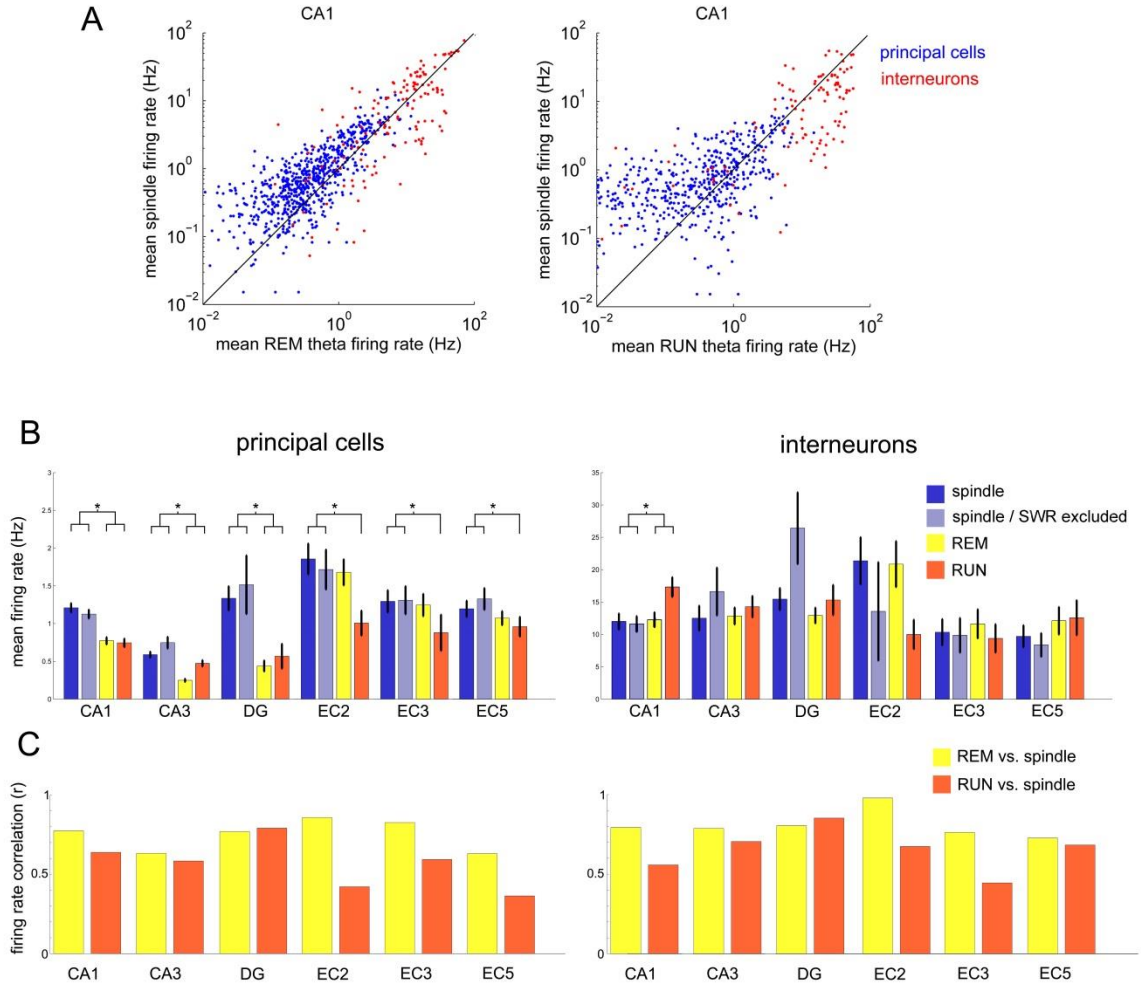

Figure 4.3 Firing rates are correlated across theta and spindle states. A, Correlations between firing rates of CA1 pyramidal cells and interneurons between REM theta and spindle events (left) and RUN theta and spindle events (right). Note log x axis and higher rates during spindle. B, Mean firing rates during RUN, REM and spindle events (with and without ripples excluded from spindle epochs) for all regions and both cell types. Significant differences are shown ($p < 0.00001$). C, Firing rate correlations between spindle and theta states in different regions. All correlations were significant ($p < 0.05$).

Since brain states associated with theta oscillations and sleep spindles are different, we first examined the relationship between firing rates of neurons during these patterns. The mean firing rates of hippocampus principal cells were significantly elevated during the short bouts of sleep spindles compared to theta oscillations of REM and RUN (Fig. 4.3A-C; $p < 0.00001$; Kruskal-Wallis). In the EC, the firing rates of principal cells during spindles were largely similar to those of REM but significantly faster than during RUN (Fig. 4.3B; $p < 0.00001$). Because sleep spindles can occasionally but significantly trigger hippocampal ripples (Fig. 4.1F; Siapas and Wilson 1998; Sirota et al. 2003; Mölle et al, 2006; Peyrache et al., 2011; Phillips et al. 2012), we reexamined the firing rate relationships between spindles and theta after removing spindle episodes associated with ripples from the analysis (here, 32% of spindles detected in the CA1 pyramidal layer contained at least one ripple) . Considering spindles without ripples did not affect the quantitative differences in firing rates between spindles and theta during RUN or REM (Fig. 4.3B). Firing rates during spindles with and without ripples were not significantly different from each other ($p < 0.0001$). The mean firing rates of interneurons did not significantly differ between spindles and either REM or RUN theta, except those of CA1 interneurons, which fired fastest during RUN (Fig. 4.3B; $p < 0.05$).

Despite the firing rate differences across states, a strong, significant firing rate correlation was observed between spindles and REM/RUN for all neurons types and regions (Fig. 4.3A, C; $p < 0.05$). The firing rate correlations generally were higher between spindles and REM (range: 0.65-0.95) than between spindles and RUN (range: 0.40-0.85).

4.4.3 Phase-modulation of spikes during sleep spindles and theta oscillations

The next analysis examined the relationship between unit firing and LFP. A considerable fraction of both principal cells (CA1 = 205/711; CA3 = 42/370; DG = 13/71; EC2 = 26/82; EC3 = 18/106; EC5 = 21/148) and interneurons (CA1 = 80/146; CA3 = 29/69; DG = 45/68; EC2 = 14/27; EC3 = 21/42; EC5 = 22/34) was significantly ($p < 0.05$; Hodges-Ajne test) phase-locked to sleep spindles. These fractions were lower though than those modulated by theta oscillations of RUN (pyramidal cells, CA1 = 438/572; CA3 = 268/357; DG = 28/35; EC2 = 70/82; EC3 = 70/106; EC5 = 81/148; interneurons, CA1 = 112/116; CA3 = 57/59; DG = 31/33; EC2 = 27/27; EC3 = 33/42; EC5 = 30/34) or REM (pyramidal cells, CA1 = 504/711; CA3 = 240/370; DG = 50/71; EC2 = 80/82; EC3 = 80/106; EC5 = 91/148; interneurons, CA1 = 138/146; CA3 = 65/69; DG = 68/68; EC2 = 25/27; EC3 = 36/42; EC5 = 32/34). The lower percentage of significantly modulated neurons during sleep spindles can be partially explained by the overall shorter duration of sleep spindle epochs and the consequent lower number of spikes available for the analysis compared with the long trains of theta waves during REM and RUN.

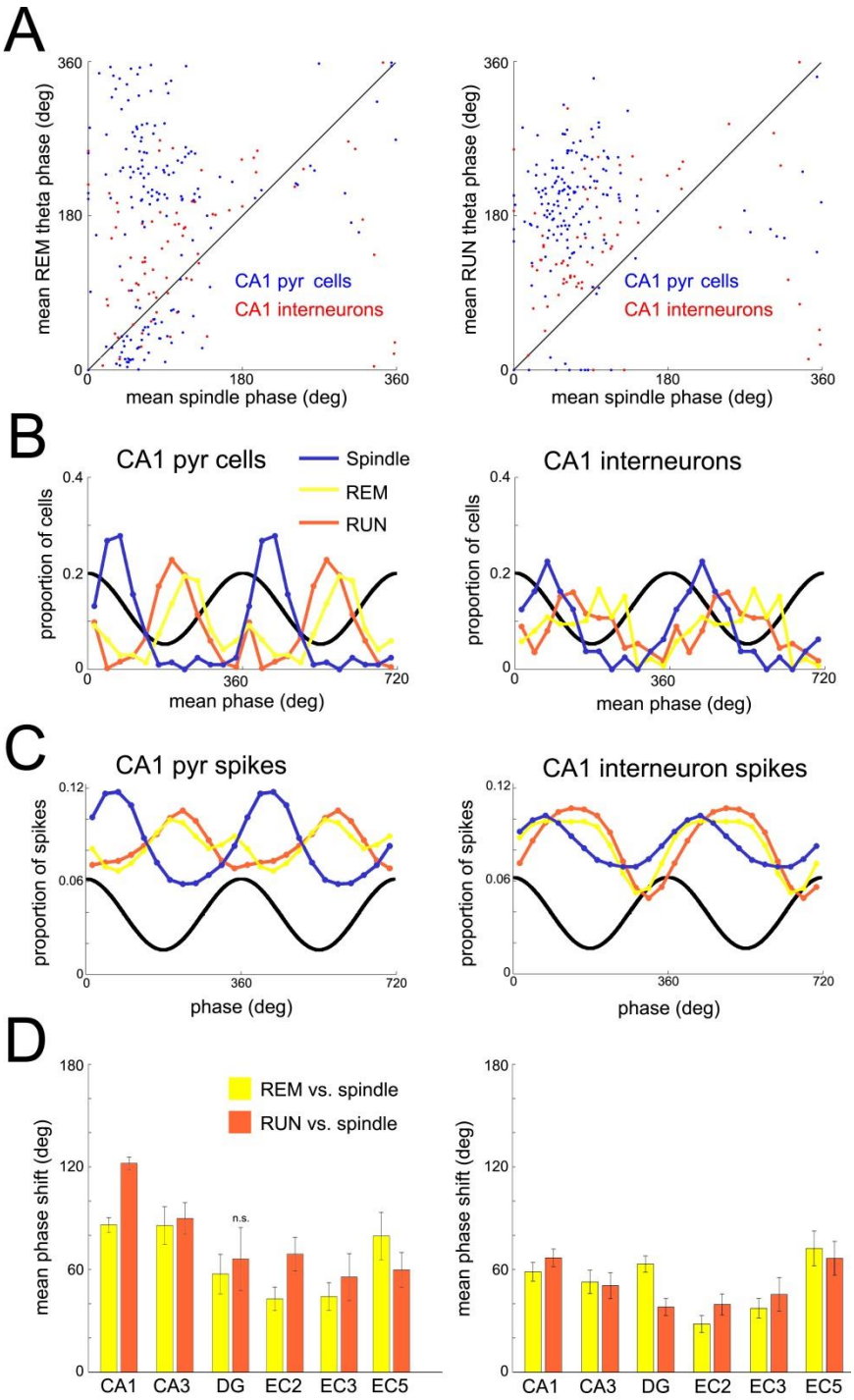

Figure 4.4 Firing phase preferences are different during theta and spindles. A, Correlations between phase preferences of CA1 pyramidal cells and interneurons between REM theta and spindle events (left) and RUN theta and spindle events (right). Each dot is a single neuron with significant phase-locking to both theta and spindles. B, Distribution of phase preferences of significantly phase-modulated CA1 pyramidal cells (left) and interneurons (right). Black sinusoid represents CA1 pyramidal layer LFP. C, Phase distribution of spikes of all CA1 pyramidal cells (left) and interneurons (right). All neurons are included, independent whether they were

significanly phase-locked to the LFP rhythm. D, Mean and SEM phase-shift of the preferred firing phase between REM theta and spindle events and RUN theta and spindle events. All comparisons are significant ($p < 0.0005$) except for DG granule cells between spindle and RUN.

In contrast to the high correlation of firing rates across states in all layers, the spindle vs theta phase relationship of the hippocampal and entorhinal neurons showed important regional differences. For determining the shift of phase preference from theta to spindle, only neurons which passed the Hodges-Ajne test for non-uniformity of circular data ($p < 0.05$) for both REM theta and spindles were included. CA1 principal cells showed a large and significant phase advancement of their preferred spiking during spindle relative to REM and RUN (Fig. 4.4A, B, D; REM vs spindle: 86.11 ± 55.18^{o}; $p < 0.00001$; RUN vs. spindle: 122.10 ± 44.90^{o}; $p < 0.00001$; Wilcoxon signed rank test). Whereas individual CA1 neurons showed a wide range of theta phase preference (Fig. 4.4A), they had a more uniform phase-locking preference to the descending part of the spindle cycle (64.14 ± 42.85^{o})); i.e., following the sink maximum in str. lacunosum-moleculare (Fig. 4.2).. Although the magnitude of phase shift of both principal cells and interneurons between spindle and theta oscillations was generally less in other regions, they were nevertheless significant (Fig. 4.4D; $p < 0.0005$; all regions / cell types / theta types except DG gran for RUN theta, attributable to low n). Another method to examine the phase relationship of spikes and LFP is to generate histograms illustrating the relationship between theta/spindle phase and spiking, independent whether individual neurons are significantly phase-locked to the LFP or not. The theta phase histograms constructed this way showed phase shifts comparable to the phase-preference histograms (Fig. 4.4C).

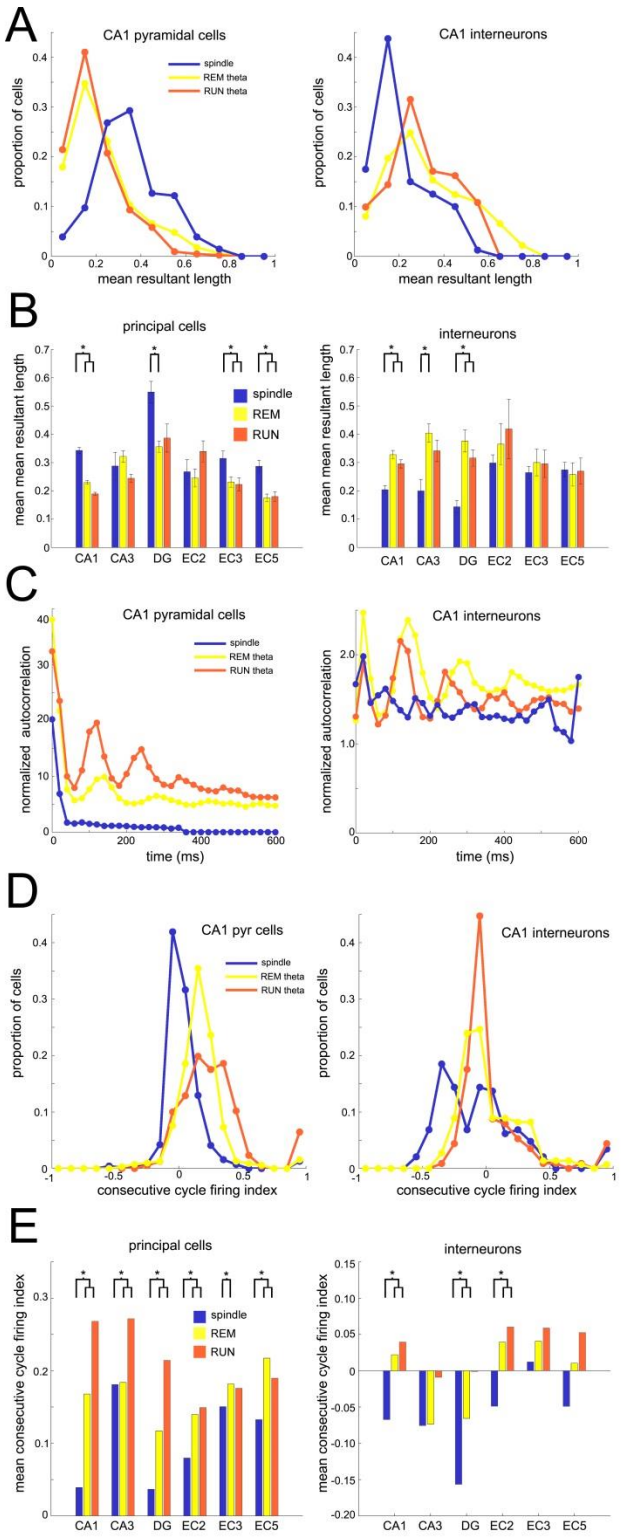

Figure 4.5 EC-hippocampal principal cells fire sporadically but strongly phase-locked during spindles. A, Distribution of mean resultant lengths of phase modulation for CA1 pyramidal cells and interneurons during

RUN and REM theta and spindle events. B, Group means of the mean resultant lengths of phase modulation in different regions. Note stronger phase modulation of principal cells and weaker modulation interneurons in each region. Significant differences are shown ($p < 0.05$). C, Normalized autocorrelograms of CA1 pyramidal cells and interneurons. Note autorhythmicity during both RUN and REM and lack of rhythmic firing during spindle. D, Distribution of consecutive cycle firing (CCF) index of CA1 pyramidal cells and interneurons. Positive numbers indicate that the unit fires on consecutive cycles of the given rhythm more often than predicted by the unit's firing rate alone. Note largely symmetric distribution during spindles for pyramidal cells and negative shift for interneurons due to cycle skipping higher than chance. E, Group means of the CCF index in each region. Note values close to zero for principal cells and negative values for interneurons during spindles. Significant differences are shown ($p < 0.01$).

Among the spindle-modulated neurons, the mean resultant length ('modulation index') of principal cells was significantly higher during sleep spindles compared to theta (Fig. 4.5A, B; $p < 0.05$; except CA3 and EC2 regions), demonstrating a stronger phase-locking of spikes to spindles compared to theta oscillations. Unexpectedly, an opposite relationship was dominant for interneurons, since they were less stongly phase-locked to spindle than to theta oscillations, although this difference reached significance only in the hippocampal regions (Fig. 4.5A, B). Commensurate with the phase-locking results, the spike autocorrelograms of both principal cells and interneurons showed multiple rhythmic peaks in the theta band during REM and RUN (Fig. 4.5C). In contrast, secondary peaks were conspicuously absent during sleep spindles for both principal cells and interneurons (Fig. 4.5C). In the entorhinal cortex, a few units had rhythmic peaks at approximately 5 Hz in their autocorrelograms but only few of these were significantly phase-modulated by sleep spindles (data not shown).

The lack of rhythmicity in the autocorrelograms during spindles, despite strong phase modulation of unit activity, implies that neurons did not reliably fire trains of spikes on consecutive spindle cycles. To quantify this relationship, we introduced a 'consecutive cycle firing index' (CCF; see Experimental Procedures). Positive CCF indicates that the

unit fires on consecutive cycles of the given rhythm more often than predicted by the unit's firing rate alone, zero CCF indicates that the unit fires on consecutive cycles as predicted from firing rate, and negative CCF indicates that the unit fires on consecutive cycles less than predicted by firing rate. Figure 4.5D shows the distribution of CCF for CA1 pyramidal cells and interneurons in spindles, RUN theta, and REM theta – note that CCF distributions for either theta are shifted to the right compared to spindles. For principal cells in all regions, CCF was significantly higher for REM and RUN theta than for spindles (Figure 4.5E; $p < 0.0001$; Kruskal-Wallis). Only interneurons in CA1, DG, and EC2 showed significant differences in CCF, with lower CCF for spindles than theta ($p < 0.01$; Kruskal-Wallis). The irregular participation of neurons in successive spindle cycles is further supported by the Fano factor. The median Fano factor was significantly lower for CA1 pyramidal cells during spindles (F = 1.73) than during either REM (F = 2.06) or RUN (F = 2.11); ($p < 0.00001$; Kruskal-Wallis). This was true for all principal cells in both hippocampus and EC ($p < 0.00001$; except DG where $p = 0.06$) but not for interneurons (except DG but only for REM theta; $p < 0.05$).

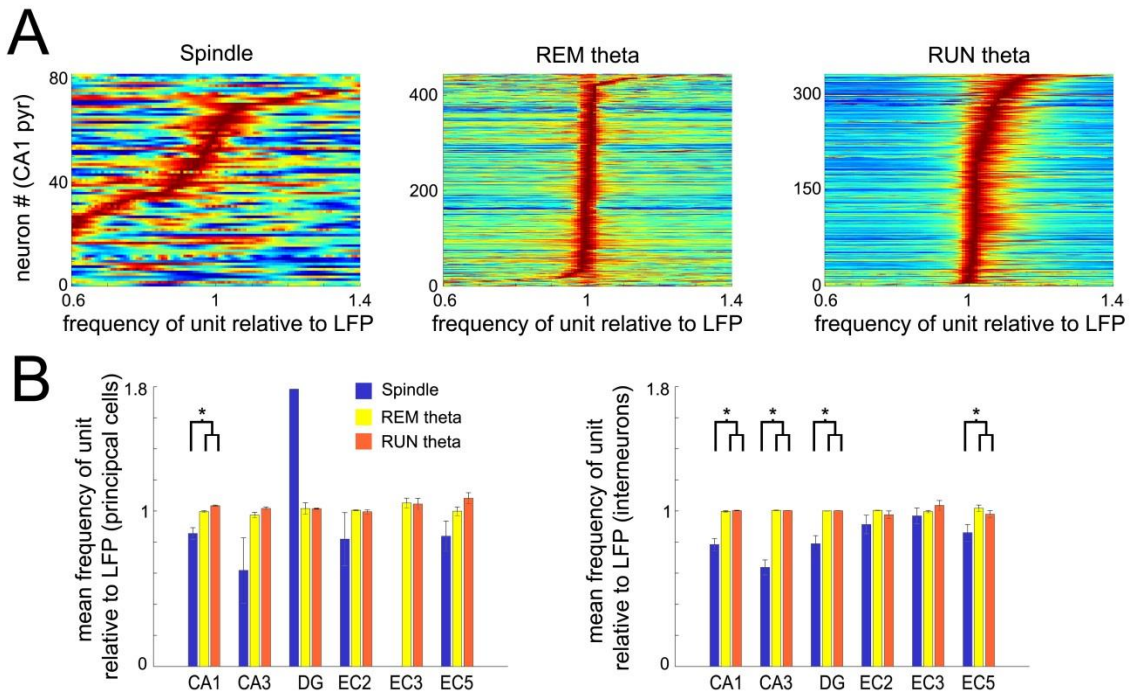

Phase interference of principal cells during theta and spindle oscillations. A, Spike-phase spectra of neurons (Mizuseki et al., 2009; also see materials and methods). Each color-coded row represents the power spectrum of a single CA1 pyramidal neuron, sorted by the magnitude of frequency shift of the power spectral peak. Power spectra were normalized by the amplitude of their peaks. Positive values indicate phase precession (O'Keefe and Recce, 1993). Note phase precession of many neurons during RUN and mainly phase retardation during spindle. B, mean phase interference index (i.e., abscissa of A) for principal cells and interneurons in different regions. Significant differences are indicated. Only 1 DG neuron had significant autocorrelogram during spindle events.

Another quantitative method for the comparison between unit firing and LFP is the 'phase precession index'. Hippocampal and EC2 principal cells show a systematic backward phase shift from late to early phase phases of theta as the rat traverses the place field or 'grid' apexes (O'Keefe and Recce, 1993; Hafting et al., 2008). The phase precession is an indication that the neuron oscillates faster than the reference LFP theta (O'Keefe and Recce, 1993; Maurer et al., 2006; Geisler et al., 2007; Jeewajee et al., 2008) and this phase difference can be expressed in the ''spike phase spectrum'' (Mizuseki et al., 2009). Figure 4.6A illustrates the phase precession index for CA1

pyramidal cells. Many neurons showed spike phase precession during RUN, as indicated by the > 1 index. While hippocampal cells can show phase precession also during REM when individual spike trains are considered (Harris et al., 2002), for most neurons the value was near 1. As expected from the consecutive cycle firing index, only a minority of CA1 pyramidal cells had a spike spectrum index near 1 or > 1 during spindles. Instead, a considerably fraction had values < 1, indicating that CA1 pyramidal neurons oscillated at a frequency below the spindle band. This pattern of firing, in general, also applied to principal cells and interneurons of other regions and layers (Fig. 4.6B). Overall, these results show that principal cells of the hippocampus and EC tend to fire in clusters during theta oscillations of RUN and REM with a high probability of spikes on consecutive theta cycles. In contrast, they fire sporadically during sleep spindles, although the emitted spikes tend to be strongly phase-locked to a restricted phase range of the spindle.

4.4.4 Cross-frequency modulation of LFP gamma power by sleep spindles

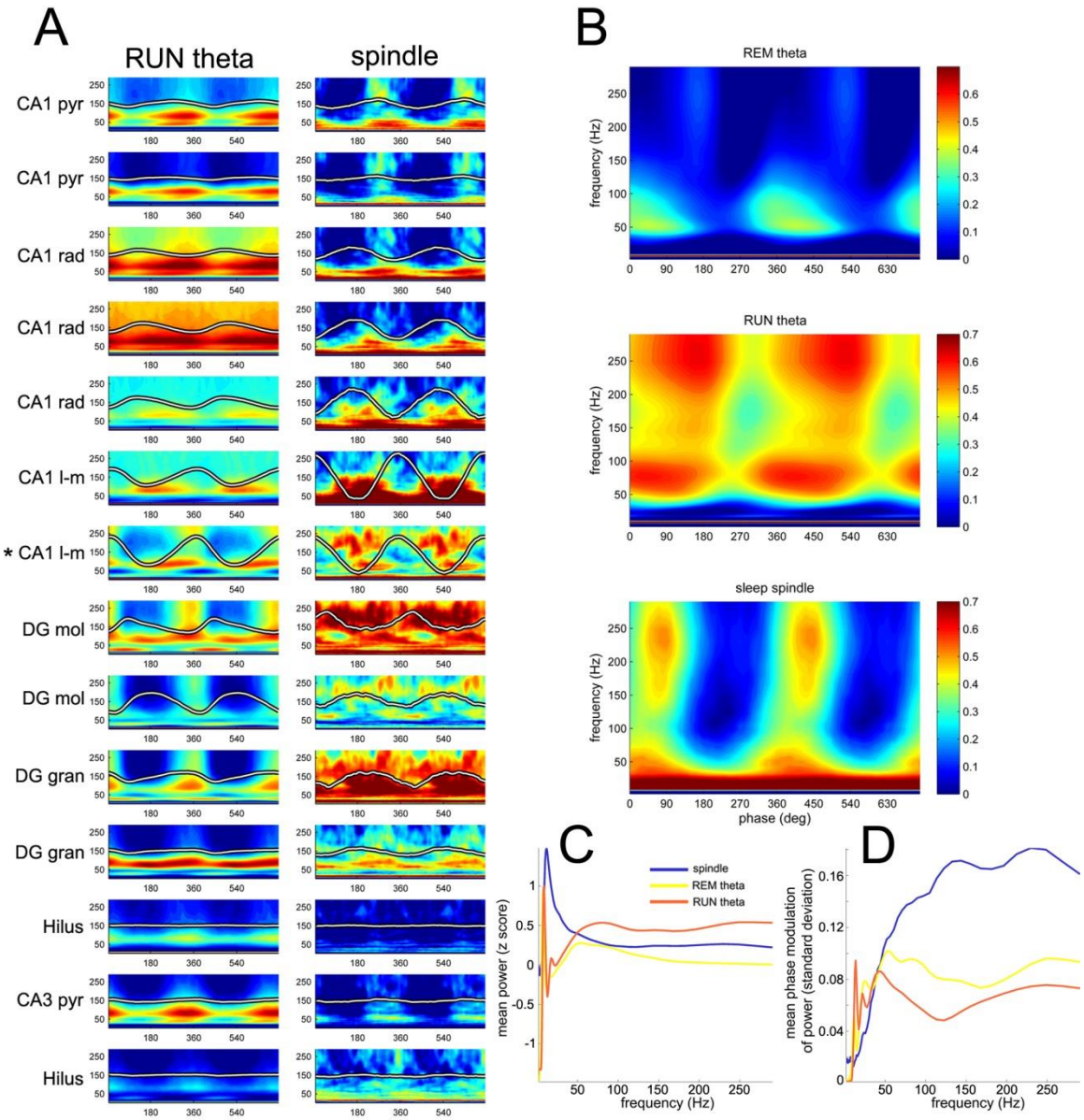

Figure 4.7 Cross-frequency phase-amplitude coupling during theta and spindle oscillations. A, Phase-modulated wavelet maps during theta (RUN) and spindle activity at different depths. Single session CSD traces (as in Fig. 2) are superimposed on the wavelet maps. B, Mean wavelet maps from the CA1 pyramidal layer (n = 23 sessions in 14 rats for REM and spindle; n = 17 sessions in 10 rats for RUN theta). Note dominance of gamma power in the 50-90 Hz band during theta and its lack during spindle events. C, Group mean power spectra for RUN, REM and spindle events. D, Theta and spindle phase modulation of spectral power (standard deviation of power across phase as a function of frequency).

Since a recent study has described spindle phase modulation of gamma power in the neocortex (Ayoub et al., 2012), we examined spindle phase-locking of higher frequency activity in the hippocampus. As reported previously, theta oscillations strongly entrained gamma band (30-90 Hz) and epsilon band (> 90 Hz) activity during RUN (Fig. 4.7; Bragin et al., 1995; Chrobak and Buzsáki, 1998; Canolty et al., 2006; Csicsvari et al., 2003; Colgin et al. 2009; Belluscio et al., 2012; Buzsáki and Wang, 2012). Whereas LFP gamma amplitude during theta oscillations was largest in the hilar region and CA1 str. radiatum (Csicsvari et al., 2003), the strongest gamma band activity during spindles was observed in CA1 str. lacunosum-moleculare and the dentate gyrus (Fig. 4.7A). Group comparison from the CA1 pyramidal layer (spindle and REM theta: n = 23 sessions in 14 rats; RUN theta: n = 17 sessions in 10 rats) revealed differences in theta-gamma band coupling (Fig. 4.7B, C). During RUN and REM, the dominant gamma activity in the CA1 pyramidal layer occurred in the 40-100 Hz band on the descending phase of the theta waves, with additional phase-locking of the epsilon band. During sleep spindles, the epsilon band also showed strong phase-modulation but the dominant gamma band activity was confined to frequencies below 50 Hz (Fig. 4.7C). The oscillatory nature of this lower band is questionable though since within the half-wave of a spindle (~40 msec) not even two cycles of slow gamma events could fit. The epsilon band may largely reflect spiking activity both during theta (Belluscio et al., 2012) and spindle oscillations, since spike and epsilon band modulation shared the same phase range. Frequency bands in which spectral power in the CA1 pyramidal layer is modulated by the phase of spindles and theta are illustrated in figure 4.7D, in which the standard deviation of wavelet power over the 36 10^{o} degree phase bins is plotted as a function of frequency. For REM theta,

the initial two peaks in Fig. 4.7D indicate phase modulation of harmonics at 12 Hz and 25 Hz; subsequent peaks indicate phase modulation of gamma bands centered at 52 Hz and 80 Hz, and the epsilon band at 250 Hz. For RUN theta, the initial two peaks indicate phase modulation of harmonics at 14 Hz and 22 Hz; subsequent peaks indicate phase modulation of a gamma band around 45 Hz, and the epsilon band at 250 Hz. Modulation of power in CA1 by spindle phase shows a different profile, with no clear peaks in the gamma range, but three minor peaks in the epsilon band, suggesting spindle phase modulation of fast gamma (~100 Hz), ripple (~150 Hz), and unit (~250 Hz) activity (ripple epochs were excluded from this analysis but a minority of ripples escaped our detection method).

4.4.5 Spindle recruitment of hippocampal-EC system during intermediate sleep

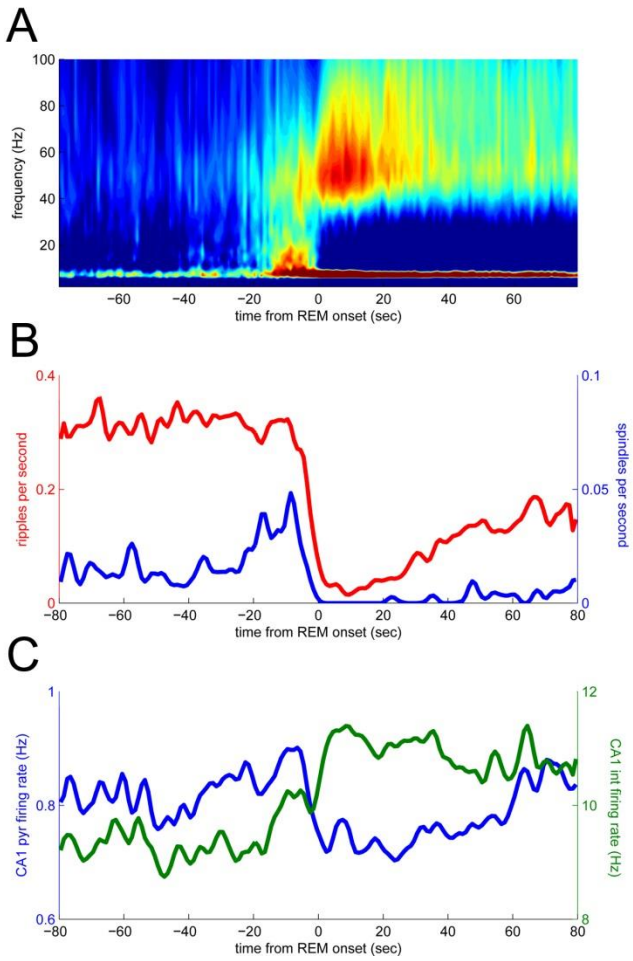

Figure 4.8 Spindles dominate intermediate sleep. A, Time resolved wavelet power changes around non-REM-REM transition recorded from the CA1 pyramidal layers (n = 23 sessions in 13 rats). Note increased spindle power prior to REM onset. B, Averaged ripple rates and detected spindle rates in the same sessions, and C, corresponding firing rate changes of pyramidal cells and interneurons. All REM transitions were used, even ones where there was only a brief gap in between REM episodes.

The different frequencies of LFP sleep spindles and unit firing patterns suggested that the neocortical inputs and intrahippocampal oscillatory patterns can transiently couple and uncouple. This may be particularly eminent during the short intermediate sleep episodes when the neocortex is still in non-REM sleep and the hippocampus switches to theta bouts (Gottesmann, 1973). We defined REM sleep onset by using the power ratio in theta

(5-11 Hz) and delta (1-4 Hz) bands (Experimental Procedures; Mizuseki et al. 2009, Grosmark et al., 2012). Non-REM-REM transitions coincided with a large reduction of sharp wave ripples, increased and decreased discharge of putative interneurons and pyramidal cells, respectively (Fig. 4.8; Grosmark et al., 2012). In agreement with previous observations (Gottesman, 1973), REM sleep was preceded by a surge of sleep spindles, peaking 10-15 sec prior to the onset of hippocampal theta oscillations (Fig. 4.8). In this transitional state, hippocampal activity rapidly and smoothly shifted back and forth between 6-8 Hz theta and spindle frequency oscillations.

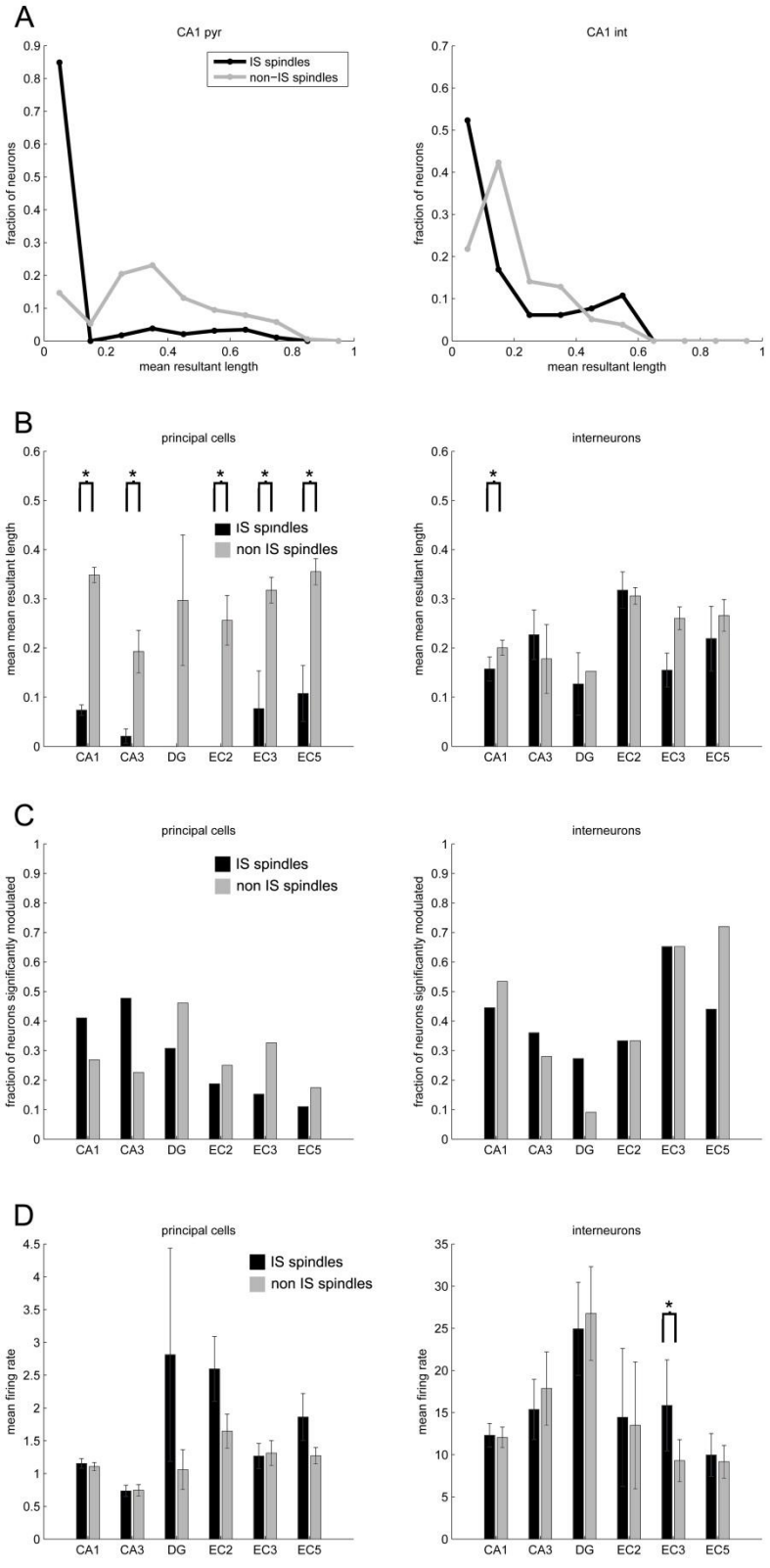
A
CA1 pyr
IS spindles
non−IS spindles
fraction of neurons
mean resultant length
CA1 int
fraction of neurons
mean resultant length
B
principal cells
IS spindles
non IS spindles
mean mean resultant length
CA1
CA3
DG
EC2
EC3
EC5
interneurons
mean mean resultant length
CA1
CA3
DG
EC2
EC3
EC5
C
principal cells
IS spindles
non IS spindles
fraction of neurons significantly modulated
CA1
CA3
DG
EC2
EC3
EC5
interneurons
fraction of neurons significantly modulated
CA1
CA3
DG
EC2
EC3
EC5
D
principal cells
IS spindles
non IS spindles
mean firing rate
CA1
CA3
DG
EC2
EC3
EC5
interneurons
mean firing rate
CA1
CA3
DG
EC2
EC3
EC5

Figure 4.9 Entrainment of EC-hippocampal circuits by sleep spindles during non-REM and intermediate sleep. A, Distribution of the mean resultant lengths (phase-modulation) of CA1 pyramidal cells and interneurons during spindles detected during intermediate sleep (IS spindles) and non-REM sleep (non-IS spindles). B, Average values (and SEM) or the mean resultant length during IS and non-IS spindles. Asterisks indicate significant differences ($p < 0.05$). C, Fraction of significantly modulated neurons during IS and non-IS spindles. D, Firing rates of neurons during IS and non-IS spindle events.

Given the special status of sleep spindles in intermediate sleep, we re-examined the firing pattern relationship of neurons with spindles that occurred during intermediate sleep (defined as the 20 sec period prior to REM onset) and non-REM sleep. Spindle wave modulation of principal cells (i.e., the mean resultant length) was significantly stronger during spindles that occurred during non-REM than intermediate sleep in all regions and layers ($p < 0.05$; Kruskal-Wallis). In the interneuron groups, only the firing rate of CA1 interneurons was significantly different between spindles of non-REM and intermediate sleep (Fig. 4.9A, B). The fraction of significantly phase-modulated neurons were higher in the CA1 and CA3 regions but lower in other regions during spindles of intermediate sleep (Fig. 4.9C). The firing rates of principal cells and interneurons were similar during the two types of spindles in all regions (Fig. 4.9D).

4.5 Discussion

Our findings show that while EC afferents to the hippocampus are involved in the establishment of current generators of both theta oscillations and sleep spindles, the temporal coordination of both the sink-sources of the extracellular currents and unit firing patterns in the EC and hippocampus are quite different. During waking, the entire phase range of theta oscillations is utilized by cell assembly sequences, whereas hippocampal neurons participating in successive waves of sleep spindles are much less organized.

Most principal cells fire relatively synchronously in all hippocampal regions compared to the time-shifted patterns during theta oscillations.

4.5.1 Neocortical-EC-hippocampal propagation of activity during sleep

Our findings support and extend previous observations of activity propagation from the neocortex to EC and hippocampus during non-REM (Isomura et al., 2006; Wolansky et al., 2006; Hahn et al., 2007; Sirota et al., 2003; Mölle et al., 2006; Nir et al., 2011; Logothetis et al., 2012). A large part of this neuronal traffic takes place during sleep spindles (Siapas and Wilson, 1998; Sirota et al., 2003; Eschenko et al., 2006; Isomura et al., 2006; Mölle et al., 2006; Nishida and Walker, 2007; Clemens et al., 2007; 2011; Johnson et al., 2010; Sullivan et al., 2011; Peyrache et al., 2011). Our laminar analyses of the different hippocampal layers and regions showed that the main excitatory dipoles responsible for the excitation of the hippocampal circuits during sleep spindles reside in the CA1 str. lacunosum-moleculare, the dentate molecular layer and possibly the CA3 str. lacunosum-moleculare (Fig. 4.2). Importantly, these same two direct EC pathways, originating from layers III and II, respectively, are also responsible for the largest extracellular currents underlying intrahippocampal theta waves (Buzsáki et al., 1986; Brankack et al., 1993). Indeed, the locations of the sinks and sources of both theta and spindle waves were remarkably similar. However, important differences were also noted. The most important difference was the in the timing of the dipoles. During theta oscillations, the sinks in CA1 str. lacunosum-moleculare and the dentate molecular layer were approximately antiphase, commensurate with the largely antiphase firing of layer II and layer III principal cells (Mizuseki et al., 2009). In contrast, the sinks in these

respective layers were largely synchronous during spindles, in congruence with the in-phase firing of all EC and hippocampal principal neurons.

Our findings indicate that spindle patterns represent a relatively simple feed-forward 'synfire chain' of excitatory activity (Abeles, 1991) from the neocortex to the hippocampus. In contrast, during theta oscillations the regions and layers of the entorhinal-hippocampal system show considerable self-organized autonomy (Mizuseki et al., 2009). The differences between the transiently imposed spindles and the self-organized theta oscillations are even more striking when one examines the spike contents of these rhythms.

4.5.2 Distinct neuronal firing patterns during spindles and theta rhythms

In the absence of theta oscillations, four major network patterns can sustain neuronal spiking in the hippocampus-entorhinal cortex. Among these, sharp wave ripples and gamma-epsilon band oscillation bouts are self-generated and originate in the CA3 system (Buzsáki et al., 1992; Csicsvari et al., 2003; Sullivan et al., 2012). These intrinsic patterns, particularly ripples, give rise to highly organized sequences of neurons largely reflecting cell assembly sequences in the previous waking periods (Wilson and McNaughton, 1994). The remaining two patterns are extrinsic, including slow oscillations (Steriade et al., 1993b) and spindle oscillations. Both extrinsic patterns can drive firing in the EC-hippocampus circuits and interact with the intrinsic sharp wave ripples and gamma oscillations (Isomura et al., 2006; Wolansky et al., 2006; Sirota et al., 2003; Mölle et al. 2006; Nir et al., 2011).

There are at least two possible consequences of the neocortically mediated effects on hippocampal circuits. First, they can provide a random selection of EC-hippocampal neurons. Generating random recruitment of hippocampal neurons could be straightforward if a relatively random constellation of neocortical neurons participates in successive sleep spindle waves and spindle events. Such a mechanism could serve to equalize or 'homogenize' synaptic weights and reduce the excitability across systems that has increased in the waking state (Tononi and Cirelli, 2006). A second possibility is that sleep spindles give rise to consistent and highly organized spike trains in the neocortex, which in turn, could effectively bias not only the time of occurrence but also the neuronal spike content of entorhinal-hippocampal neurons. There is reason to believe that sleep spindles are indeed critical for temporally coordinated neocortical neurons in at least some areas since Johnson et al. (2010) have shown that previously learned neuron spiking sequences in the prefrontal cortex re-occurred mainly during sleep spindles and that the strength of reactivation was correlated with the density of spindles. Against this background, one might expect that the orderly activation of neocortical neurons during spindles would give rise to orderly sequences in EC-hippocampal circuits as well. However, we could not detect reliably repeating patterns. Four different methods, spike autocorrelograms, phase precession, 'consecutive cycle firing index' and the Fano factor, demonstrated the lack of sustained spike trains of single neurons within spindles. The implication of these observations is that in each successive waves of the spindle, largely different sets of principal cells participate. This firing pattern is fundamentally different from theta-related spiking activity. In the waking rat, pyramidal cells fire in multiple theta cycles in their place fields with a precise temporal relationship relative to other

overlapping place neurons (O'Keefe and Recce, 1993). Similarly, neurons during REM sleep pyramidal cells fire clusters of spikes lasting for about a second, reminiscent of the firing patterns in the waking state (Louie and Wilson, 2001). An important role of theta oscillations is to compress representations of the sequentially active neurons into theta-time scale, thus utilize the entire phase space of the cycle (Dragoi and Buzsáki, 2006). Both the cluster firing patterns and the phase space utilization features, characteristic of theta oscillations, are absent during sleep spindles. Instead, neurons fired in a relatively random manner in successive cycles and fired strongly in synchrony, occupying only a small phase range of the spindle waves. The synchronous discharge of EC neurons may explain the higher firing rates of hippocampal principal cells during spindles.

It should be emphasized that while our observations do not demonstrate a simple cycle-to-cycle firing of neurons or their within cycle temporal segregation, we cannot exlude the possibility of higher order relationship among the activated EC or hippocampal neurons. This pattern of activity is in contrast with the orderly sequential firing of neurons during sharp wave ripples (Wilson and McNaughton, 1994; Nadasdy et al., 1999). Thus, it appears that while spindles can affect the timing of occurrence of ripples (Sirota et al., 2003; Peyrache et al., 2011), they do not 'select' which hippocampal neurons participate in ripples. Despite this, it remains a possibility that spindle related firing in the hippocampus can serve to mix previous waking related activity with old and stored information. In this framework, spindles could assist in blending recently acquired information into existing knowledge base (Wagner et al., 2004). Further studies, involving large number of simultaneously recorded cell assemblies from neocortex and hippocampus are needed to address these possibilities (e.g., Ji and Wilson, 2007).

4.6 Figure Legends

Figure 4.1

Basic features of sleep spindles. A, Example of filtered (1-626 Hz) LFP traces of a spindle event recorded simultaneously in hippocampal CA1 pyramidal layer and visual cortex. B, Example of filtered (1-625 Hz) LFP traces of a spindle event recorded simultaneously in hippocampal CA1 pyramidal layer and layer 5 of medial entorhinal cortex. Note similar onset, offset, and duration of the spindles in different structures. C, Histogram of mean instantaneous peak frequency of spindles (μ = 12.33 Hz, n = 2579 spindles in 15 rats). D, Histogram of spindle duration (μ = 0.49 sec). E, Average coherence spectrum between spindles in the CA1 pyramidal layer and layer 5 of entorhinal cortex (n = 8 sessions in 2 rats; error bars indicate σ). Note peak coherence value at 15 Hz. F, Cross-correlogram between LFP spindle minima and detected SPW-R events in hippocampal CA1 shows temporal association of these two patterns, peaking at 300 ms preceding individual spindle troughs in CA1, with SPW-R occurrence rate at 187% of baseline (n = 23 sessions in 14 rats).

Figure 4.2

Spindle and theta oscillations in the hippocampus. *A,* Example of wide-band (1 Hz to 1250 Hz) LFP traces of a spindle event, recorded at multiple depths of the CA1-dentate axis and superimposed on the current-source density (CSD) map of the same event. CA1 pyr, pyramidal layer, CA1 rad, stratum radiatum, CA1 l-m, str. lacunosum-moleculare, DG mol, dentate gyrus molecular layer, DG gran, granule cell layer, CA3 pyr, pyramidal layer in the hilar region. *B,* Average CSD maps in a single animal with superimposed

CSD traces during RUN, REM and Spindle. Recordings from two shanks of the silicon probe are shown. Maps and traces were constructed by averaging CSD and LFP traces according to CSD phase in CA1 str. lacunosum-moleculare (phase was partitioned into 10^{o} wide bins). Asterisk indicates reference site. The cycles are calibrated in degrees rather than in time to emphasize the similar depth distributions of the sinks and sources during theta and spindle waves. *C,* Average normalized CSD as a function of phase in the three hippocampal principal cell layers (n = 5 sessions in 5 rats). Values greater than zero are sources, whereas values less than zero are sinks. Note the enhanced synchrony of CSD in the CA1, CA3 and dentate principal cell layers during spindle oscillations relative to REM or RUN theta.

Figure 4.3

Firing rates are correlated across theta and spindle states. *A,* Correlations between firing rates of CA1 pyramidal cells and interneurons between REM theta and spindle events (left) and RUN theta and spindle events (right). Note log x axis and higher rates during spindle. *B,* Mean firing rates during RUN, REM and spindle events (with and without ripples excluded from spindle epochs) for all regions and both cell types. Significant differences are shown ($p < 0.00001$). *C,* Firing rate correlations between spindle and theta states in different regions. All correlations were significant ($p < 0.05$).

Figure 4.4

Firing phase preferences are different during theta and spindles. *A,* Correlations between phase preferences of CA1 pyramidal cells and interneurons between REM theta and spindle events (left) and RUN theta and spindle events (right). Each dot is a single neuron

with significant phase-locking to both theta and spindles. *B*, Distribution of phase preferences of significantly phase-modulated CA1 pyramidal cells (left) and interneurons (right). Black sinusoid represents CA1 pyramidal layer LFP. *C*, Phase distribution of spikes of all CA1 pyramidal cells (left) and interneurons (right). All neurons are included, independent whether they were significanly phase-locked to the LFP rhythm. *D*, Mean and SEM phase-shift of the preferred firing phase between REM theta and spindle events and RUN theta and spindle events. All comparisons are significant ($p < 0.0005$) except for DG granule cells between spindle and RUN.

Figure 4.5

EC-hippocampal principal cells fire sporadically but strongly phase-locked during spindles. A, Distribution of mean resultant lengths of phase modulation for CA1 pyramidal cells and interneurons during RUN and REM theta and spindle events. B, Group means of the mean resultant lengths of phase modulation in different regions. Note stronger phase modulation of principal cells and weaker modulation interneurons in each region. Significant differences are shown ($p < 0.05$). C, Normalized autocorrelograms of CA1 pyramidal cells and interneurons. Note autorhythmicity during both RUN and REM and lack of rhythmic firing during spindle. D, Distribution of consecutive cycle firing (CCF) index of CA1 pyramidal cells and interneurons. Positive numbers indicate that the unit fires on consecutive cycles of the given rhythm more often than predicted by the unit's firing rate alone. Note largely symmetric distribution during spindles for pyramidal cells and negative shift for interneurons due to cycle skipping higher than chance. E, Group means of the CCF index in each region. Note values close to zero for principal

cells and negative values for interneurons during spindles. Significant differences are shown ($p < 0.01$).

Figure 4.6

Phase interference of principal cells during theta and spindle oscillations. *A*, Spike-phase spectra of neurons (Mizuseki et al., 2009; also see materials and methods). Each color-coded row represents the power spectrum of a single CA1 pyramidal neuron, sorted by the magnitude of frequency shift of the power spectral peak. Power spectra were normalized by the amplitude of their peaks. Positive values indicate phase precession (O'Keefe and Recce, 1993). Note phase precession of many neurons during RUN and mainly phase retardation during spindle. *B*, mean phase interference index (i.e., abscissa of *A*) for principal cells and interneurons in different regions. Significant differences are indicated. Only 1 DG neuron had significant autocorrelogram during spindle events.

Figure 4.7

Cross-frequency phase-amplitude coupling during theta and spindle oscillations. A, Phase-modulated wavelet maps during theta (RUN) and spindle activity at different depths. Single session CSD traces (as in Fig. 2) are superimposed on the wavelet maps. B, Mean wavelet maps from the CA1 pyramidal layer (n = 23 sessions in 14 rats for REM and spindle; n = 17 sessions in 10 rats for RUN theta). Note dominance of gamma power in the 50-90 Hz band during theta and its lack during spindle events. C, Group mean power spectra for RUN, REM and spindle events. D, Theta and spindle phase modulation of spectral power (standard deviation of power across phase as a function of frequency).

Figure 4.8

Spindles dominate intermediate sleep. A, Time resolved wavelet power changes around non-REM-REM transition recorded from the CA1 pyramidal layers (n = 23 sessions in 13 rats). Note increased spindle power prior to REM onset. B, Averaged ripple rates and detected spindle rates in the same sessions, and C, corresponding firing rate changes of pyramidal cells and interneurons. All REM transitions were used, even ones where there was only a brief gap in between REM episodes.

Figure 4.9

Entrainment of EC-hippocampal circuits by sleep spindles during non-REM and intermediate sleep. A, Distribution of the mean resultant lengths (phase-modulation) of CA1 pyramidal cells and interneurons during spindles detected during intermediate sleep (IS spindles) and non-REM sleep (non-IS spindles). B, Average values (and SEM) or the mean resultant length during IS and non-IS spindles. Asterisks indicate significant differences ($p < 0.05$). C, Fraction of significantly modulated neurons during IS and non-IS spindles. D, Firing rates of neurons during IS and non-IS spindle events.

Section 5 – General Discussion

5.1 Ripple oscillations emerge in CA1

Previously, the origin of the ripple oscillation in CA1 was unclear, and the question remained: is the ripple oscillation transmitted from CA3, or does it first emerge in CA1? In-vitro studies have demonstrated the presence of ripple-like oscillations in CA3 (Draguhn et al., 1998; Behrens et al. 2006), suggesting that ripples may first emerge in CA3 and be transmitted to CA1 via the Schaffer collaterals.

The present work argues that despite the presence of a high frequency oscillation in CA3 that coincides with the SPW-R in CA1 (Fig. 2.3), the ripple is generated de-novo in CA1 and is not inherited from CA3. Three lines of evidence suggest this to be the case. First, LFP spectral power at the characteristic ripple frequency (170 Hz) is high in CA1 and lower in CA3, with an abrupt transition at the CA1/CA3 border, and the same pattern holds for CA1-CA3 coherence (Fig 2.5). Second, power-power correlations in the ripple frequency range within CA1 are high, whereas between CA1 and CA3 they are low (Fig. 2.7). Last, and most importantly, we could not find a single CA3 pyramidal cell whose firing was significantly phase modulated by ripples recorded in CA1 (Fig 2.8), which we would expect to find if CA1 ripples were driven by CA3 ripples in a wave-by-wave fashion.

The lack of wave-by-wave coordination between CA3 and CA1 during ripples constrains the role of the ripple oscillation in information transfer between these structures.

Although the set of CA1 neurons that fire during a given SPW-R may be determined in part by the set of upstream CA3 neurons that fire, dynamics at the timescale of the ripple (4-6 milliseconds) likely do not govern the interaction between CA1 and CA3. On the other hand, the present results do not preclude CA1-CA3 interaction during SPW-R at other frequencies; the possibility exists for significant interactions at lower frequencies (e.g., moderate power-power correlations around 100 Hz in Fig 2.7) or cross-frequency phase-amplitude coupling between the ripple oscillation in CA1 and lower frequencies in CA3, including the fast gamma range and also the gamma range (Carr et al. 2012). Although the present work did not examine whether the ripple oscillation organizes communication between CA1 and its downstream structures, the unpublished personal observation that at least some entorhinal neurons are phase modulated by the CA1 ripple suggests that this may be the case.

The mechanism by which ripples emerge in CA1 is unknown. The more 'canonical', connectionism-inspired hypotheses focus on rhythmic, perisomatic $GABA_A$- mediated inhibition as the main driver of the ripple oscillation. In traces of membrane potential from intracellular recordings, ripples are present and their phase reverses around -80 mV, indicative of a chloride conductance mediated mechanism (Ylinen et al. 1995). However, the high spatial coherence across CA1 that exists despite the absence of a common driving ripple frequency input from CA3 suggests that other mechanisms may be at work.

Electrical coupling via gap junctions is one such candidate mechanism. Supporting this, hippocampal interneurons as well as pyramidal cell axons are coupled via gap junctions (Katsumaru et al., 1988; Schmitz et al., 2001), and halothane, a known gap junction blocker, abolishes ripples but leaves sharp waves intact (Ylinen et al., 1995). Modeling

studies have demonstrated that gap junction coupling of pyramidal cell axons is a plausible mechanism for generating the high level of synchrony observed during ripples (Traub et al., 2012).

An important issue is whether CA1 possesses some sort of special property that causes a rhythmic ripple in response to the barrage of excitation delivered by the SPW, or whether CA3 possesses properties that cause it to lack such a rhythmic high frequency oscillation. Perhaps the biggest difference between the anatomies of CA1 and CA3 is the respective absence and presence of mossy fiber input from the dentate gyrus. It is plausible that signaling from the dentate gyrus might disrupt the rhythmicity of the high frequency oscillation that accompanies the SPW in CA3. In the rat, each mossy fiber forms synaptic contacts with on the order of just 15 CA3 pyramidal cells, and due to the very low firing rates of granule cells (Jung and McNaughton, 1993), the activity of different mossy fibers is unlikely to be synchronous. The sparseness and spatial inhomogeneity of mossy fiber excitatory signaling in CA3 may prevent high frequency oscillations from being rhythmically synchronized across long distances in the manner that is observed in CA1. This idea that mossy fiber input prevents CA3 from undergoing a true ripple could be tested experimentally via optogenetic techniques.

The role that the dentate gyrus plays in the initiation of SPW-R remains vague. One of the initial motivations for the Sullivan et al. 2011 study was to find evidence for LFP or unit firing patterns in the DG that would be predictive of SPW-R initiation. Although we found that SPW-R are more likely during up states than down-states detected from DG LFP, this merely suggests, in line with previous work (Isomura et al. 2006) that network states characterized by spiking, as opposed to the near-silence during downstates, are

more conducive to SPW-R initiation. Suppose that SPW-R are indeed initiated by the DG; bursting of just a handful of granule cells firing at high rates could have a powerful effect on the CA3 network (Henze et al., 2002). The strict laminar organization of mossy fiber projections from DG to CA3 implies that such an initiating event could occur anywhere on the septotemporal axis and then propagate along this axis via the CA3 recurrent collaterals. Supporting this idea, data obtained from simultaneous recordings along the septotemporal axis demonstrate that a large fraction of SPW-R are initiated in a localized portion of the septotemporal axis and then propagate toward the septal or temporal pole (Patel, 2013). It would be rare in any of the data analyzed in the present works to have recorded a DG SPW-R initiation simultaneously with SPW-R in CA3 or CA1, as most of the hypothetical initiating events would take place in distant, unrecorded lamina, and would be lost in any measures obtained via event-triggered averaging. Perhaps technical refinements, including optogenetic techniques (Deisseroth, 2011; Stark et al 2012), as well as the ever proceeding scale-up of multi-electrode recording technologies (Berenyi et al., 2011) will clarify this issue.

5.2 Fast gamma may not be distinct from ripples

The first study in the present work (Sullivan et al., 2011) is largely concerned with a bimodality observed in the peak frequency of detected high frequency oscillations (Fig. 2.2) – oscillations with peak frequency above 140 Hz are referred to as ripples, whereas oscillations with peak frequency between 90 and 140 Hz are referred to as “fast gamma”. Nearly every subsequent figure in the study involves a comparison between fast gamma and ripples. The results of the study find numerous quantitative differences between ripples and fast gamma, including that fast gamma compared to ripples has lower spectral

power, lower amplitude sharp waves, and lower amplitude CSD sources and sinks. The lack of any standout qualitative distinction between ripples and fast gamma, along with the absence of any other bimodality that mirrors the peak frequency bimodality, suggests that fast gamma is not a categorically distinct oscillation from ripples, but instead reflects distant, weak, and/or poorly detected ripples. Studies employing multiple electrodes spanning the septotemporal axis and/or both hemispheres would serve to clarify this issue, as would a more thorough analysis of the interaction between LFP phase and frequency and unit firing in both CA1 and CA3.

5.3 SPW-R intermidst active behavior differ from those during sleep and quiescence

The second study in the present work examines differences between SPW-R that occur during quiescent behaviors (e.g., sleep, sitting idly in the home cage) and SPW-R that occur during pauses in otherwise active behavior (e.g., drinking from water wells or sitting in the delay area of a maze running task). Surprisingly, the peak frequency of ripples intermidst active behavior was higher than during quiescent behaviors, and the inverted-U shaped relationship between peak frequency and sharp wave amplitude does not seem to hold for ripples intermidst active behavior.

The possible explanations for these physiological differences in SPW-R according to behavioral state are endless, but amongst them are different levels and balances of neuromodulators, different classes of active interneurons, and different patterns of input from upstream structures. That there are such physiological differences according to behavioral state is consistent with the emerging notion that SPW-R may have different functions in different states. There is ample evidence that during both sleep and waking,

neural firing during SPW-R reflects playback of recent spatial trajectories and is necessary for memory consolidation (Girardeau et al. 2009; Jadhav et al., 2012). During sleep, there is evidence for a process termed "preplay" whereby firing sequences of neurons that will come to represent a given environment are played during SPW-R, perhaps priming the neurons for encoding novel spatial information (Dragoi and Tonegawa, 2011). During the waking state, hippocampal replay sometimes reflects novel manipulation of experienced sequences, including reverse replay (Foster and Wilson, 2006; Diba and Buzsáki, 2007) and novel permutations of paths in a maze environment (Gupta et al., 2010), but it remains to be determined whether the novel arrangement of hippocampal firing sequences originates in the hippocampus itself or in upstream structures. Together, these findings indicate that the function of SPW-R may differ according to the behavioral state of the animal.

Another finding of the second study in the present work is that short intervals between SPW-R are more common intermidst active behavior than during quiescence or sleep. It is not uncommon for multiple ripples to occur in fast succession during a single sharp wave, although current source density analysis shows small amplitude sub-sharp waves corresponding to each ripple (personal observation). This phenomenon may underlie the "slow gamma" that has been reported during SPW-R (Carr et al., 2012). An enticing possibility is that multiple consecutive ripples during waking may reflect the replay of multiple segments of the animal's environment (Gupta et al., 2011).

5.4 The function of sleep spindles is likely different from theta

The third study in the present work is concerned with the function of sleep spindles in the hippocampus. Sleep spindles play a role in plasticity and learning and memory (Sejnowski and Destexhe, 2000; Steriade 2000; Steriade and Timofeev, 2003; Gais et al., 2002; Diekelmann and Born, 2010; Fogel and Smith, 2011; Eschenko et al., 2006; Nir et al., 2011; Miyamoto and Hensch, 2003; Hanlon et al., 2009; Schiffelholz and Aldenhoff, 2002; Khazipov et al., 2004; Schabus et al., 2004), although the role that the hippocampus plays in sleep spindles has never been thoroughly addressed. The main question underlying the third study is whether the sleep spindle oscillation in the hippocampus organizes hippocampal activity in the same manner as the theta oscillation. This hypothesis was motivated in part by the observation that sleep spindles are most common during intermediate sleep (Gottesmann, 1973); a stage that immediately precedes REM sleep (which is dominated by theta oscillations in the hippocampus) – the supposition being that the neuromodulatory regime of REM sleep is being "ramped up" during intermediate sleep and that hippocampal sleep spindles may effectively function like a theta oscillation.

Several lines of evidence support the idea that the patterns of oscillations and neuronal firing in the hippocampus during spindles differ from those during theta. One major difference is that neurons that are phase modulated by spindle oscillations differ in their phase preference relative to theta (Fig. 4.4). Whereas the current sources in the CA3, CA1 and dentate subregions of the hippocampus are asynchronous during theta, they are synchronized during sleep spindles (Fig 4.2). Most importantly, hippocampal cells do not fire in a rhythmic manner during sleep spindles (Fig. 4.5) and do not show any

evidence of spindle phase precession (Fig. 4.6). The phase shift from theta to spindles may arise from a different balance of excitation arriving from upstream sources, particularly the projection to CA1 from the thalamic nucleus reuniens; virtually nothing is known about the physiological impact of this pathway but it is a prime candidate for investigation given the central role of the thalamus in the generation of sleep spindles.

A key caveat in the rejection of a theta-like role for sleep spindles is the weakness of some statistical measures due to low sample sizes. Spindles are very rare compared to SPW-R or theta, and amassing enough data about firing patterns requires long, stable sleep recordings, something that is not often the priority of hippocampal researchers more interested in task-related behavior. Nevertheless, the absence of principal cells that are robustly rhythmically entrained by spindles argues strongly against the hypothesis that sleep spindles are a special case of the theta oscillation.

SPW-R are nearly twice as likely to occur during sleep spindles than during the rest of non-REM sleep -- as is the case with up-states, the increased firing rates of hippocampal principal cells during spindles (Fig. 4.3) may increase the probability of SPW-R initiation. It has been demonstrated that SPW-R affect prefrontal neurons differently depending on whether the SPW-R occurs during or outside a sleep spindle, with certain neurons being less responsive to SPW-R during sleep spindles (Peyrache et al., 2011). Of prime interest is whether sequence replay in the hippocampus is affected by the presence of sleep spindles – might spindles affect the identity of the sequence, or whether the sequence is of place cells or preplay of future place cells? However it turns out, boring is not an apt term to describe the future of this area of research.

Section 6 – Bibliography

Abeles M. (1991) Corticonics: Neural Circuits of the Cerebral Cortex. Cambridge University Press, New-York.

Acsady, L., Arabadzisz, D., Katona, I., and Freund, T. F. (1996). Topographic distribution of dorsal and median raphe neurons with hippocampal, septal and dual projection. Acta Biol. Hung. 47, 9–19.

Acsady L, Kamondi A, Sik A, Freund T, Buzsáki G (1998) GABAergic cells are the major postsynaptic targets of mossy fibers in the rat hippocampus. Journal of Neuroscience 18: 3386-3403.

Alonso A, Llinas RR (1989) Subthreshold Na+-dependent rhythmicity in stellate cells of entorhinal cortex layer II. Nature 342:175-7.

Altman J, Das GD (1965) Autoradiographic and histological evidence of postnatal hippocampal neurogenesis in rats. Journal of Comparative Neurology 124: 319-335.

Alvarado MC, Rudy JW (1995) A comparison of kainic acid plus colchicine and ibotenic acid-induced hippocampal formation damage on four configural tasks in rats. Behavioral Neuroscience 109: 1052-1062.

Amaral DG (1978) A Golgi study of cell types in the hilar region of the hippocampus in the rat. Journal of comparative neurology 182: 851-914.

Amaral DG, Witter MP (1995) Hippocampal Formation. In: The Rat Nervous System (Paxinos G, ed), pp 443-493. San Diego: San Diego Academic.

Amaral DG, Scharfman HE, Lavenex P (2007) The dentate gyrus: fundamental neuroanatomical organization (dentate gyrus for dummies). Progress in Brain Research 163: 3-22.

Anastassiou CA, Montgomery SM, Barahona M, Buzsáki G, Koch C (2010) The effect of spatially inhomogeneous extracellular electric fields on neurons. J Neurosci. 30(5):1925-36.

Astori S, Wimmer RD, Prosser HM, Corti C, Corsi M, Liaudet N, Volterra A, Franken P, Adelman JP, Luthi A (2011) The ca(V)3.3 calcium channel is the major sleep spindle pacemaker in the thalamus. Proc Natl Acad Sci USA 108:13823-8.

Axmacher N, Helmstaedter C, Elger CE, Fell J (2008) Enhancement of neocortical-medial temporal EEG correlations during non-REM sleep. Neural Plast. 2008:563028.

Ayoub A, Mölle M, Preissl H, Born J. (2012) Grouping of MEG gamma oscillations by EEG sleep spindles. Neuroimage. 2012 Jan 16;59(2):1491-500

Bartos M, Vida I, Jonas P (2007) Synaptic mechanisms of synchronized gamma oscillations in inhibitory interneuron networks. Nat Rev Neurosci 8(1):45-56.

Battaglia FP, Sutherland GR, McNaughton BL (2004) Hippocampal sharp wave bursts coincide with neocortical "up-state" transitions. Learn Mem. 11(6):697-704.

Behrens CJ, van den Boom LP, de Hoz L, Friedman A, Heinemann U (2005) Induction of sharp wave-ripple complexes in vitro and reorganization of hippocampal networks. Nat Neurosci. 8(11):1560-7.

Behrens CJ, van den Boom LP, Heinemann U (2007) Effects of the GABA(A) receptor antagonists bicuculline and gabazine on stimulus-induced sharp wave-ripple complexes in adult rat hippocampus in vitro. Eur J Neurosci. 25(7):2170-81.

Belluscio MA, Mizuseki K, Schmidt R, Kempter R, Buzsáki G (2012) Cross-frequency phase-phase coupling between θ and γ oscillations in the hippocampus. J Neurosci 32:423-35.

Berenyi A, Gombkoto P, Jamieson B, Harris TD, Fujisawa G, Buzsáki G (2011) A 256-channel light weight multiplexed data acquisition system for freely moving rodents. Soc Neurosci Abstract 37.937.03.

Both M, Bähner F, von Bohlen und Halbach O, Draguhn A (2008) Propagation of specific network patterns through the mouse hippocampus. Hippocampus. 18(9):899-908.

Bragin A, Jando G, Nadasdy Z, Hetke J, Wise K, Buzsáki G (1995) Gamma (40-100 Hz) oscillation in the hippocampus of the behaving rat. J Neurosci 15:47-60.

Bragin, A., Jando, G, Nadasdy, Z, van Landeghem, M. and Buzsáki, G (1995) Dentate EEG spikes and associated population bursts in the hippocampal hilar region of the rat. Journal of Neurophysiology. 73: 1691-1705.

Bragin A, Engel J Jr, Wilson CL, Fried I, Buzsáki G (1999) High-frequency oscillations in human brain. Hippocampus 9: 137–142

Bragin A, Engel J Jr, Wilson CL, Fried I, Mathern GW (1999) Hippocampal and entorhinal cortex high-frequency oscillations (100–500 Hz) in human epileptic brain and in kainic acid–treated rats with chronic seizures. Epilepsia 40: 127–137.

Bragin A, Wilson CL, Engel J Jr. (2000) Chronic epileptogenesis requires development of a network of pathologically interconnected neuron clusters: a hypothesis. Epilepsia. 41 Suppl 6:S144-52.

Brankack J, Stewart M, Fox SE (1993) Current source density analysis of the hippocampal theta rhythm: associated sustained potentials and candidate synaptic generators. Brain Res 615:310-27.

Brunel N, Wang XJ (2003) What determines the frequency of fast network oscillations with irregular neural discharges? I. Synaptic dynamics and excitation-inhibition balance. J Neurophysiol. 90(1):415-30.

Buckmaster PS, Strowbridge BW, Kunkel DD, Schmiege DL, Schwartzkroin PA (1992) Mossy cell axonal projections to the dentate gyrus molecular layer in the rat hippocampal slice. Hippocampus 2: 349-362.

Buhl DL, Buzsáki G (2005) Developmental emergence of hippocampal fast-field "ripple" oscillations in the behaving rat pups. Neuroscience.134(4):1423-30.

Buzsáki G (1986) Hippocampal sharp waves: their origin and significance. Brain Res. 398(2):242-52.

Buzsáki, G (1989) A two-stage model of memory trace formation: A role for "noisy" brain states. Neuroscience. 31: 551-570.

Buzsáki G (1996) The hippocampo-neocortical dialogue. Cereb Cortex. 6(2):81-92

Buzsáki, G (2002) Theta oscillations in the hippocampus. Neuron. 33:325-340.

Buzsáki G. 2005. Theta rhythm of navigation: link between path integration and landmark navigation, episodic and semantic memory. Hippocampus 15:827-40.

Buzsáki G (2006) Rhythms of the brain. Oxford University Press. New York.

Buzsáki G, Eidelberg E (1983) Phase relations of hippocampal projection cells and interneurons to theta activity in the anesthetized rat. Brain Research 266: 334-339.

Buzsáki G, Draguhn A (2004) Neuronal oscillations in cortical networks Science 304:1926-9.

Buzsáki G, Lopes da Silva F (2012) High frequency oscillations in the intact brain. Progress Neurobiol 98: 241-249.

Buzsáki G, Wang XJ (2012) Mechanisms of gamma oscillations. Annu Rev Neurosci 35:203-35.

Buzsáki G, Moser EI (2013) Memory, navigation and theta rhythm in the hippocampal-entorhinal system. Nat. Neurosci 16:130-38.

Buzsáki G, Leung LW, Vanderwolf CH (1983) Cellular bases of hippocampal EEG in the behaving rat. Brain Res. Rev. 287:139–171.

Buzsáki G, Czopf J, Kondakor I, Kellenyi L (1986) Laminar distribution of hippocampal rhythmic slow activity (RSA) in the behaving rat: current-srouce density analysis, effects of urethane and atropine. Brain Res 265:125-37.

Buzsáki G, Horvath Z, Urioste R, Hetke J, Wise K (1992) High-frequency network oscillation in the hippocampus. Science. 256:1025–1027

Buzsáki G, Buhl DL, Harris KD, Csicsvari J, Czeh B, Morozov A (2003) Hippocampal network patterns of activity in the mouse. Neuroscience. 116:201–211

Buzsáki G, Carpi D, Csicsvari J, Dragoi G, Harris KD, Henze DA, Hirase H (2003) Maintenance and modification of firing rates and sequences in the hippocampus: does sleep play a role? In: Maquet, P., Smith, C., and Stickgold, R. (eds). Sleep and Plasticity. Oxford University Press., Oxford. 247-270

Canolty RT, Edwards E, Dalal SS, Soltani M, Nagarajan SS, Kirsch HE, Berger MS, Barbaro NM, Knight RT (2006) High gamma power is phase-locked to theta oscillations in human neocortex. Science. 313(5793):1626-8.

Carr MF, Karlsson MP, Frank LM (2012) Transient slow gamma synchrony underlies hippocampal memory replay. Neuron 75: 700-13.

Cenquizca LA, Swanson LW (2006) Analysis of direct hippocampal cortical field CA1 axonal projections to diencephalons in rat. Journal of Comparative Neurology 497: 101-114.

Cenquizca LA, Swanson LW (2007) Spatial organization of direct hippocampal field CA1 projections to the rest of the cerebral cortex. Brain Research Reviews 56: 1-26.

Chrobak JJ, Buzsáki G (1996) High-frequency oscillations in the output networks of the hippocampal-entorhinal axis of the freely behaving rat, J. Neurosci. 16:3056–3066.

Chrobak JJ, Buzsáki G (1998) Gamma oscillations in the entorhinal cortex of the freely behaving rat. J Neurosci 18:388-98.

Clemens Z, Mölle M, Eröss, L, Jakus R, Rásonyi G, Halász P, Born J (2010) Fine-tuned coupling between human parahippocampal ripples and sleep spindles. Eur J Neurosci. 2010

Colgin LL, Kubota D, Brucher FA, Jia Y, Branyan E, Gall CM, Lynch G (2004) Spontaneous waves in the dentate gyrus of slices from the ventral hippocampus. J Neurophysiol. 92(6):3385-98.

Colgin LL, Jia Y, Sabatier JM, Lynch G (2005) Blockade of NMDA receptors enhances spontaneous sharp waves in rat hippocampal slices. Neurosci Lett. 385(1):46-51.

Colgin LL, Denninger T, Fyhn M, Hafting T, Bonnevie T, Jensen O, Moser MB, Moser EI (2009) Frequency of gamma oscillations routes flow of information in the hippocampus. Nature. 462(7271):353-7.

Colom LV, Bland BH (1987) State dependent spike train dynamics of hippocampal formation neurons: evidence for theta-on and theta-off cells. Brain Research 422: 277-286.

Contreras D, Destexhe A, Sejnowski TJ, Steriade M (1996) Control of spatiotemporal coherence of a thalamic oscillation by corticothalamic feedback. Science 274:771-774.

Csicsvari J, Hirase H, Czurko A, Mamiya A, Buzsáki G (1999a) Oscillatory coupling of hippocampal pyramidal cells and interneurons in the behaving rat. J. Neurosci. 19:274–287.

Csicsvari J, Hirase H, Czurkó A, Mamiya A, Buzsáki G (1999b) Fast network oscillations in the hippocampal CA1 region of the behaving rat. J Neurosci. 19(16):RC20.

Csicsvari J, Hirase H, Mamiya A, Buzsáki G (2000) Ensemble patterns of hippocampal CA3–CA1 neurons during sharp wave-associated population events, Neuron. 28:585–594.

Csicsvari J, Jameison B, Wise KD, Buzsáki G (2003) Mechanisms of gamma oscillations in the hippocampus of the behaving rat. Neuron 37:311-22.

Davidson TJ, Kloosterman F, Wilson MA. (2009) Hippocampal replay of extended experience. Neuron 63:497-507.

De Gennaro L, Ferrara M (2003) Sleep spindles: an overview. Sleep Med Rev 7:423-440.

Deisseroth K (2011) Optogenetics. Nature Methods 8: 26-29.

Diba K, Buzsáki G (2007) Forward and reverse hippocampal place-cell sequences during ripples. Nat Neurosci. 10:1241-2.

Diba K, Montgomery SM, Harris KD, Buzsáki G (2005) Identification ofsilicon probe irregularities using analysis of in vivo recordings. Soc Neurosci Abstr 31:275.10.

Diekelmann S, Born J (2010) The memory function of sleep. Nat Rev Neurosci 11:114-126.

Dinner DS, Lüders HO, eds (2001) Epilepsy and sleep: physiological and clinical relationships. San Diego, CA: Academic Press.

Dolleman-Van der Weel MJ, Lopes da Silva FH, Witter MP (1997) Nucleus reuniens thalami modulates activity in hippocampal field CA1 through excitatory and inhibitory mechanisms. J Neurosci 17:5640-50.

Dragoi G, Buzsáki G (2006) Temporal encoding of place sequences by hippocampal cell assemblies. Neuron 50:145-57.

Dragoi G, Tonegawa S (2011) Preplay of future place cell sequences by hippocampal cellular assemblies. Nature 469: 397-401.

Draguhn A, Traub RD, Schmitz D, Jefferys JG (1998) Electrical coupling underlies high-frequency oscillations in the hippocampus in vitro. Nature. 394(6689):189-92.

Dupret D, O'Neill J, Pleydell-Bouverie B, Csicsvari J (2010) The reorganization and reactivation of hippocampal maps predict spatial memory performance. Nat Neurosci. 13(8):995-1002

Dusek JA, Eichenbaum H (1997) The hippocampus and memory for orderly stimulus relations. Proceedings of the National Academy of Sciences of the United States of America 94: 7109-7114.

Dzhala VI, Staley KJ (2004) Mechanisms of fast ripples in the hippocampus. J Neurosci. 24: 8896–8906.

Ego-Stengel V, Wilson MA (2010) Disruption of ripple-associated hippocampal activity during rest impairs spatial learning in the rat. Hippocampus. 20(1):1-10.

Ekstrom AD. Kahana MJ, Caplan JB, Fields TA, Isham EA, Newman EL, Fried I (2003) Cellular networks underlying human spatial navigation. Nature 425: 184-188.

Ellender TJ, Nissen W, Colgin LL, Mann EO, Paulsen O (2010) Priming of hippocampal population bursts by individual perisomatic-targeting interneurons. J Neurosci. 30(17):5979-91.

Eschenko O, Mölle M, Born J, Sara SJ (2006) Elevated sleep spindle density after learning or after retrieval in rats. J Neurosci 26: 12914-20.

Eschenko O, Ramadan W, Mölle M, Born J, Sara SJ (2008) Sustained increase in hippocampal sharp-wave ripple activity during slow-wave sleep after learning. Learn Mem. 15(4):222-8.

Ferrarelli F, Huber R, Peterson MJ, Massimini M, Murphy M, Riedner BA, Watson A, Bria P, Tononi G (2007) Reduced sleep spindle activity in schizophrenia patients. Am J Psychiatry 164:483-492.

Ferrarelli F, Peterson MJ, Sarasso S, Riedner BA, Murphy MJ, Benca RM, Bria P, Kalin NH, Tononi G (2010) Thalamic dysfunction in schizophrenia suggested by whole-night deficits in slow and fast spindles. Am J Psychiatry 167:1339-1348.

Foffani G, Uzcategui YG, Gal B, Menendez de la Prida L (2007) Reduced spike-timing reliability correlates with the emergence of fast ripples in the rat epileptic hippocampus. Neuron. 55(6):930-41.

Fogel SM, Smith CT (2011) The function of the sleep spindle: a physiologtical index of intelligence and a mechanism for sleep-dependent memory consolidation. Neurosci Biobehav Rev 35: 1154-65.

Földy C, Yeun Lee S, Szabadics J, Neu A, Soltesz I (2007) Cell type-specific gating of perisomatic inhibition by cholecystokinin. Nat Neurosci 10: 1128-1130.

Foster DJ, Wilson MA (2006) Reverse replay of behavioural sequences in hippocampal place cells during the awake state. Nature. 440(7084):680-3.

Fujisawa S, Buzsáki G (2011) A 4-Hz oscillation adaptively synchronizes prefrontal, VTA, and hippocampal activities. Neuron 72:153-65.

Fyhn M, Molden S, Witter MP, Moser EI, Moser MB (2004) Spatial representation in the entorhinal cortex. Science 305: 1258-64.

Gais S, Mölle M, Helms K, Born J (2002) Learning-dependent increases in sleep spindle density. J Neurosci 22:6830-4.

Geisler C, Robbe D, Zugaro M, Sirota A, Buzsáki G (2007) Hippocampal place cell assemblies are speed-controlled oscillators. Proc Natl Acad Sci USA 104:8149-54.

Gelbard-Sagiv H, Mukamel R, Harel M, Malach R, Fried I (2008) Internally generated reactivation of single neurons in human hippocampus during free recall. Science 322: 96-101.

Girardeau G, Benchenane K, Wiener SI, Buzsáki G, Zugaro MB. (2009) Selective suppression of hippocampal ripples impairs spatial memory. Nat Neurosci 12:1222–1223.

Gottesmann C. Intermediate stages of sleep in the rat (1973) Rev Electroencephalogr Neurophysiol Clin. 65-8

Gottselig JM, Bassetti CL, Achermann P (2002) Power and coherence of sleep spindle frequency activity following hemispheric stroke. Brain 125:373-83.

Graves AR, Moore SJ, Bloss EB, Mensh BD, Kath WL, Spruston N (2012) Hippocampal pyramidal neurons comprise two distinct cell types that are countermodulated by metabotropic receptors. Neuron 76:776-789.

Grosmark AD, Mizuseki K, Pastalkova E, Diba K, Buzsáki G (2012) REM sleep reorganizes hippocampal excitability. Neuron 75:1001-7.

Gulyas, A. I., Görcs, T. J., and Freund, T. F. (1990). Innervation of different peptide-containing neurons in the hippocampus by GABAergic septal afferents. Neuroscience 37, 31–44.

Gulyas AI, Buzsáki G, Freund TF, Hirase H (2006). Populations of hippocampal inhibitory interneurons express different levels of cytochrome c. European Journal of Neuroscience 23:2581-2594.

Hafting T, Fyhn M, Bonnevie T, Moser MB, Moser EI (2008) Hippocampus-independent phase precession in entorhinal grid cells. Nature 453:1248-52.

Hahn TT, Sakmann B, Mehta MR (2007) Differential responses of hippocampal subfields to cortical up-down states. PNAS. 104: 5169-5174.

Halassa MM, Siegle JH, Ritt JT, Feng G, Moore Cl (2011) Selective optical drive of thalamic reticular nucleus generates thalamic bursts and cortical spindles. Nat Neurosci 14:1118-20.

Halasy K. Somogyi P (1993) Subdivisions in the multiple GABAergic innervation of granule cells in the dentate gyrus of the rat hippocampus. European Journal of Neuroscience 5: 411-429.

Han ZS, Buhl EH, Lorinczi Z, Somogyi P (1993) A high degree of spatial selectivity in the axonal and dendritic domains of physiologically identified local-circuit neurons in the dentate gyrus of the rat hippocampus. European Journal of Neuroscience 5: 395-410.

Hanlon EC, Faraguna U, Vyazovsky VV, Tononi G, Cirelli C (2009) Effects of skilled training on sleep slow wave activity and cortical gene expression in the rat. Sleep 32:719-29.

Hara K, Harris RA. 2002. The anesthetic mechanism of urethane: the effects on neurotransmitter-gated ion channels. Anesth Analg. 94:313-8.

Hargreaves EL, Rao G, Lee I, Knierim JJ (2005) Major dissociation between medial and lateral entorhinal input to dorsal hippocampus. Science 308:1792-4.

Harris KD, Henze DA, Hirase H, Leinekugel X, Dragoi G, Czurko A, Buzsáki G (2002) Spike train dynamics predicts theta-related phase precession in hippocampal pyramidal cells. Nature 417:738-41.

Harris KD, Csicsvari J, Hirase H, Dragoi G, Buzsáki G (2003) Organization of cell assemblies in the hippocampus. Nature 424: 552-556.

Hasselmo ME, Bower JM (1993) Acetylcholine and memory. Trends Neurosci. 16(6):218-222.

Hasselmo ME, McClelland JL (1999) Neural models of memory. Current opinion in neurobiology 9: 184-188.

Hazan L, Zugaro M, Buzsáki G (2006) Klusters, NeuroScope, NDManager: A free software suite neurophysiological data processing and visualization. Journal of Neuroscience Methods 155:207-16.

Henze DA, Wittner L, Buzsáki G (2002) Single granule cells reliably discharge targets in the hippocampal CA3 network in vivo. Nat Neurosci 5:790-5.

Herkenham M (1978) The connections of the nucleus reuniens thalami: evidence for a direct thalamo-hippocampal pathway in the rat. J Comp Neurol 177:589-610.

Himanen SL, Virkkala J, Huhtala H, Hasan J (2002) Spindle frequencies in sleep EEG show U-shape within first four NREM sleep episodes. J Sleep Res 11:35-42.

Hobson JA, Pace-Schott EF. 2002. The cognitive neuroscience of sleep: neuronal systems, consciousness and learning. Nat Rev Neurosci. 3(9):679-93.

Huerta PT, Lisman JE (1995) Bidirectional synaptic plasticity induced by a single burst during cholinergic theta oscillation in CA1 in vitro. Neuron 15: 1053-1063.

Huxter JR, Senior TJ, Allen K, Csicsvari J (2008) The phase-specific codes for two-dimensional position, trajectory and heading in the hippocampus. Nature Neuroscience 11:587-594.

Ibarz JM, Foffani G, Cid E, Inostroza M, Menendez de la Prida L (2010) Emergent dynamics of fast ripples in the epileptic hippocampus. J Neurosci. 30(48):16249-61.

Ishizuka N, Weber J, Amaral DG (1990) Organization of intrahippocampal projections originating from CA3 pyramidal cells in the rat. J Comp Neurol. 295(4):580-623.

Isomura Y, Sirota A, Ozen S, Montgomery S, Mizuseki K, Henze DA, Buzsáki G (2006) Integration and segregation of activity in entorhinal-hippocampal subregions by neocortical slow oscillations. Neuron. 52:871-82.

Jadhav SP, Kemere C, German PW, Frank LM. . 2012. Awake hippocampal sharp-wave ripples support spatial memory. Science 336:1454-8.

Jensen O, Lisman JE (1996) Hippocampal CA3 region predicts memory sequences: accounting for the phase precession of place cells. Learn Mem 3: 279-287.

Jewajee A, Barry C, O'Keefe J, Burgess N (2008) Grid cells and theta as oscillatory interference: electrophysiological data from freely moving rats. Hippocampus 18:1175-85.

Ji D, Wilson MA (2007) Coordinated memory replay in the visual cortex and hippocampus during sleep. Nature Neurosci. 10:100–107

Jiruska P, Finnerty GT, Powell AD, Lofti N, Cmejla R, Jefferys JG (2010) Epileptic high-frequency network activity in a model of non-lesional temporal lobe epilepsy. Brain. 133(Pt 5):1380-90

Johnson LA, Euston DR, Tatsuno M, McNaughton BL (2010) Stored-trace reactivation in rat prefrontal cortex is correlated with down-to-up state fluctuation density. J Neurosci. 30(7):2650-61.

Jung MW, McNaughton BL (1993) Spatial selectivity of unit activity in the hippocampal granular layer. Hippocampus 3: 165-182.

Kamondi A, Acsady L, Wang XJ, Buzsáki G (1998) Theta oscillations in somata and dendrites of hippocampal pyramidal cells in vivo: activity-dependent phase-precession of action potentials. Hippocampus 8:244-61.

Karlsson MP, Frank LM (2008) Network dynamics underlying the formation of sparse, informative representations in the hippocampus. J Neurosci. 28(52):14271-81.

Karlsson MP, Frank LM (2009) Awake replay of remote experiences in the hippocampus. Nat Neurosci. 12(7):913-8.

Katsumaru H, Kosaka T, Heizman CW, Hama K (1988) Gap-junctions on GABAergic neurons containing the calcium-binding protein parvalbumin in the rat hippocampus (CA1 regions). Exp Brain Res 73:363-370.

Khazipov R, Sirota A, Leinekugel X, Holmes GL, Ben-Ari Y, Buzsáki G (2004) Early motor activity drives spindle bursts in the developing somatosensory cortex. Nature 432:758-761.

Kiss J, Csaki A, Bokor H, Shanabrough M, and Leranth C (2000) The supramammillo-hippocampal and supramammillo-septal glutatmatergic/aspartatergic projections in the

rat: a combined [3H] D-aspartate autoradiographic and immunohistochemical study. Neuroscience 97: 657-669

Klausberger T, Somogyi P (2008) Neuronal diversity and temporal dynamics: the unity of hippocampal circuit operations. Science. 321(5885):53-7.

Klausberger T, Magill PJ, Marton LF, Roberts JD, Cobden PM, Buzsáki G, Somogyi P (2003) Brain-state- and cell-type-specific firing of hippocampal interneurons in vivo. Nature 421: 844–848.

Krettek, J. E., and Price, J. L. (1977). Projections from the amygdaloid complex and adjacent olfactory structures to the entorhinal cortex and to the subiculum in the rat and cat. J. Comp. Neurol. 172, 723–752.

Kubota D, Colgin LL, Casale M, Brucher FA, Lynch G (2003) Endogenous waves in hippocampal slices. J. Neurophysiol. 89:81–89.

Kudrimoti HS, Barnes CA, McNaughton BL (1999) Reactivation of hippocampal cell assemblies: effects of behavioral state, experience, and EEG dynamics. J. Neurosci. 19(10):4090-4101.

Le Van Quyen M, Staba R, Bragin A, Dickson C, Valderrama M, Fried I, Engel J (2010) Large-scale microelectrode recordings of high-frequency gamma oscillations in human cortex during sleep. J Neurosci. 30(23):7770-82.

Leão RN, Mikulovic S, Leão KE, Munquba H, Gezelius H, Enjin A, Patra K, Eriksson A, Loew LM, Tort AB, Kullander K (2012) OLM interneurons differentially modulated CA3 and entorhinal inputs to hippocampal CA1 neurons. Nat Neurosci 15:1524-30.

Lee AK, Wilson MA (2002) Memory of sequential experience in the hippocampus during slow wave sleep. Neuron. 36(6):1183-94.

Leinekugel X, Khazipov R, Cannon R, Hirase H, Ben-Ari Y, Buzsáki G (2002) Correlated bursts of activity in the neonatal hippocampus in vivo. Science. 296(5575):2049-52.

Leopold DA, Murayama Y, Logothetis NK (2003) Very slow activity fluctuations in monkey visual cortex: implications for functional brain imaging. Cereb Cortex. 13(4):422-33.

Levy WB (1989) Computational Approach to Hippocampal Function. In: Computational Models of Learning in Simple Neural Systems (Hawkins RD, Bower GH, eds), pp 243-305. San Diego : Academic Press .

Levy WB (1996) A sequence predicting CA3 is a flexible associator that learns and uses context to solve hippocampal-like tasks. Hippocampus 6: 579-590.

Li XG, Somogyi P, Ylinen A, Buzsáki G (1994) The hippocampal CA3 network: an in vivo intracellular labeling study. J Comp Neurol. 339(2):181-208.

Liotta A, Caliskan G, Haq RU, Hollnagel JO, Roesler A, Heinemann U, Behrens CJ (2011) Partial disinhibition is required for transition of stimulus-induced sharp wave-ripple complexes to recurrent epileptiform discharges in rat hippocampal slices. J Neurophysiol. 105(1):172-87.

Logothetis NK, Eschenko O, Murayama Y, Augath M, Steudel T, Evrard HC, Besserve M, Oeltermann A (2012) Hippocampal-cortical interaction during periods of subcortical silence. Nature 491:547-53.

Loomis AL, Harvey EN, Hobart G (1935) Potential Rhythms of the Cerebral Cortex during Sleep. Science 81:597-598.

Louie K, Wilson MA (2001) Temporally structured replay of awake hippocampal ensemble activity during rapid eye movement sleep. Neuron 29: 145-56.

Lubenov EV, Siapas AG (2008) Decoupling through synchrony in neuronal circuits with propagation delays. Neuron. 58(1):118-31.

MacDonald CJ, Lepage KQ, Eden UT, Eichenbaum H (2011) Hippocampal “time cells” bridge the gap in memory for discontiguous events. Neuron 71: 737-749.

Maier N, Nimmrich V, Draguhn A (2003) Cellular and network mechanisms underlying spontaneous sharp wave-ripple complexes in mouse hippocampal slices. J Physiol. 550(Pt 3):873-87.

Mann EO, Suckling JM, Hajos N, Greenfield SA, Paulsen O (2005) Perisomatic feedback inhibition underlies cholinergically induced fast network oscillations in the rat hippocampus in vitro. Neuron. 45(1):105-17.

Maurer AP, Cowen SL, Burke SN, Barnes CA, McNaughton BL (2006) Organization of hippocampal cell assemblies based on theta phase precession. Hippocampus 16:785-94.

McClelland JL, McNaughton BL, O'Reilly RC (1995) Why there are complementary learning systems in the hippocampus and neocortex: insights from the successes and failures of connectionist models of learning and memory. Psychol Rev. 102(3):419-57.

McCormick DA, Bal T (1997) Sleep and arousal: thalamocortical mechanisms. Annu Rev Neurosci 20:185-215.

McEchron MD, Bouwmeester H, Tsend W, Weiss C, Disterhoft JF (1998) Hippocampectomy disrupts auditory trace fear conditioning and contextual fear conditioning in the rat. Hippocampus 8: 638-646.

Memmesheimer RM (2010) Quantitative prediction of intermittent high-frequency oscillations in neural networks with supralinear dendritic interactions. PNAS. 107(24):11092-7.

Mitra PP, Bokil H (2007) Observed Brain Dynamics (Hardcover), Oxford University Press.

Mitra PP, Pesaran B (1999) Analysis of dynamic brain imaging data. Biophys J. 1999 76(2):691-708.

Mitzdorf U. (1985) Current source-density method and application in cat cerebral cortex: investigation of evoked potentials and EEG phenomena. Physiol Rev. 65(1):37-100.

Miyamoto H, Hensch TK (2003) Reciprocal interaction of sleep and synaptic plasticity. Mol Interv 3:404-17.

Mizuseki K, Sirota A, Pastalkova E, Buzsáki G (2009) Theta oscillations provide temporal windows for local circuit computation in the entorhinal-hippocampal loop. Neuron. 64(2):267-80.

Mizuseki K, Diba K, Pastalkova E, Buzsáki G. (2011) Hippocampal CA1 pyramidal cells form functionally distinct sublayers. Nat. Neurosci 14:1174-81.

Mölle M, Yeshenko O, Marshall L, Sara SJ, Born J (2006) Hippocampal sharp wave-ripples linked to slow oscillations in rat slow-wave sleep. J Neurophysiol. 96(1):62-70.

Mölle M, Eschenko O, Gais S, Sara SJ, Born J (2009) The influence of learning on sleep slow oscillations and associated spindles and ripples in humans and rats. Eur J Neurosci. 29(5):1071-81.

Montgomery SM, Buzsáki G (2007) Gamma oscillations dynamically couple hippocampal CA3 and CA1 regions during memory task performance. PNAS. 104:14495-500.

Montgomery SM, Sirota A, Buzsáki G. 2008. Theta and gamma coordination of hippocampal networks during waking and rapid eye movement sleep. J Neurosci 28:6731-41.

Montgomery SM, Betancur MI, Buzsáki G (2009) Behavior-dependent coordination of multiple theta dipoles in the hippocampus. J Neurosci. 29(5):1381-94.

Morris RG, Garrud P, Rawlins JN, O'Keefe J (1982) Place navigation impaired in rats with hippocampal lesions. Nature 297: 681-683.

Mukovski M, Chauvette S, Timofeev I, Volgushev M (2007) Detection of active and silent states in neocortical neurons from the field potential signal during slow-wave sleep. Cereb Cortex. 17(2):400-14.

Nadasdy Z, Hirase H, Czurko A, Csicsvari J, Buzsáki G (1999) Replay and time compression of recurring spike sequences in the hippocampus. J Neurosci. 19: 9497-9507.

Nakashiba T, Buhl DL, McHugh TJ, Tonegawa S (2009) Hippocampal CA3 output is crucial for ripple-associated reactivation and consolidation of memory. Neuron. 62(6):781-7.

Nir Y, Staba R, Andrillon T, Vyazovskiy VV, Cirelli C, Fried I, Tononi G (2011) Regional slow waves and spindles in human sleep. Neuron 70:153-169.

Nishida M, Walker MP (2007) Daytime naps, motor memory consolidation and regionally specific sleep spindles. PLoS One 2:e341.

Nguyen DP, Kloosterman F, Barbieri R, Brown EN, Wilson MA (2009) Characterizing the dynamic frequency structure of fast oscillations in the rodent hippocampus. Front Integr Neurosci 3:11.

Nokia MS, Penttonen M, Wikgren J (2010) Hippocampal ripple-contingent training accelerates trace eyeblink conditioning and retards extinction in rabbits. J Neurosci. 30(34):11486-92.

O'Keefe J, Dostrovsky J (1971) The hippocampus as a spatial map. Preliminary evidence from unit activity in the freely-moving rat. Brain Research 34: 171-175.

O'Keefe J and Nadel L(1978) The Hippocampus as a Cognitive Map, Oxford University Press.

O'Keefe J, Reece ML (1993) Phase relationship between hippocampal place units and the EEG theta rhythm. Hippocampus 3:317-30.

O'Neill J, Senior T, Csicsvari J (2006) Place-selective firing of CA1 pyramidal cells during sharp wave/ripple network patterns in exploratory behavior. Neuron. 49(1):143-55.

O'Neill J, Senior TJ, Allen K, Huxter JR, Csicsvari J (2008) Reactivation of experience-dependent cell assembly patterns in the hippocampus. Nat Neurosci. 11(2):209-15.

Pais I, Hormuzdi SG, Monyer H, Traub RD, Wood IC, Buhl EH, Whittington MA, LeBeau FE (2003) Sharp wave-like activity in the hippocampus in vitro in mice lacking the gap junction protein connexin 36. J Neurophysiol. 89(4):2046-54

Papatheodoropoulos C, Koniaris E (2010) a5GABA(A) receptors regulate hippocampal sharp wave-ripple activity in vitro. Neuropharmacology. 2010 Dec 10.

Papatheodoropoulos C, Kostopoulos G (2002) Spontaneous, low frequency (approximately 2-3 Hz) field activity generated in rat ventral hippocampal slices perfused with normal medium. Brain Res Bull. 57(2):187-93.

Pastalkova E, Itskob V, Amarasingham A, Buzsáki G (2008) Internally generated cell assembly sequences in the rat hippocampus. Science 321:1322-7.

Patel J (2013). Oscillatory patterns along the entire septo-temporal axis of the hippocampus in behaving rats. Ph.D. dissertation, Rutgers University.

Penttonen M, Kamondi A, Sik A, Acsady L, Buzsáki G (1997) Feed-forward and feed-back activation of the dentate gyrus in vivo during dentate spikes and sharp wave bursts. Hippocampus 7: 437-450.

Peyrache A, Battaglia FP, Destexhe A (2011) Inhibition recruitment in prefrontal cortex during sleep spindles and gating of hippocampal inputs. Proc Natl Acad Sci USA 108:17207-12

Peyrache A, Khamassi M, Benchenane K, Wiener SI, Battaglia FP (2009) Replay of rule-learning related neural patterns in the prefrontal cortex during sleep. Nat Neurosci. 12(7):919-26

Phillips KG, Bartsch U, McCarthy AP, Edgar DM, Tricklebank MD, Wafford KA, Jones MW (2012) Decoupling of sleep-dependent cortical and hippocampal interactions in a neurodevelopmental model of schizophrenia. Neuron 76:526-33.

Pikovsky A, Rosenblum M, Kurths J (2001) Synchronization: A Universal Concept in Nonlinear Sciences. Cambridge University Press, 2001. ISBN: 0521592852

Plante DT, Goldstein MR, Landsness EC, Peterson MJ, Riedner BA, Ferrarelli F, Wanger T, Guokas JJ, Tononi G, Benca RM (2012) Topographic and sex-related differences in sleep spindles in major depressive disorder: A high-density EEG investigation. J Affect Disord, in press.

Ponomarenko AA, Li JS, Korotkova TM, Huston JP, Haas HL (2008) Frequency of network synchronization in the hippocampus marks learning. Eur J Neurosci. 27:3035-3042.

Quiroga RQ, Reddy L, Kreiman G, Koch C, Fried I (2005) Invariant visual representations by single neurons in the human brain. Nature 435: 1102-1107.

Reichinnek S, Künsting T, Draguhn A, Both M (2010) Field potential signature of distinct multicellular activity patterns in the mouse hippocampus. J Neurosci. 30(46):15441-9.

Ribak CE, Tran PH, Spiegelman I, Okazaki MM, Nadler JV (2000) Status epilepticus-induced hilar basal dendrites on rodent granule cells contribute to recurrent excitatory circuitry. Journal of Comparative Neurology 428: 240-253.

Sakata S, Harris KD (2009) Laminar structure of spontaneous and sensory-evoked population activity in auditory cortex. Neuron. 64(3):404-18.

Schabus M, Gruber G, Parapatics S, Sauter C, Klosch G, Anderer P, Klimesch W, Saletu B, Zeitlhofer J (2004) Sleep spindles and their significance for declarative memory consolidation. Sleep 27:1479-1485.

Scharfman HE (1994) Evidence from simultaneous intracellular recordings in rat hippocampal slices that area CA3 pyramidal cells innervate dentate hilar mossy cells. Journal of Neurophysiology 72: 2167-2180.

Scharfman HE (2007) The dentate gyrus: a comprehensive guide to structure, function, and clinical implications. Progress in brain research 163.

Scheffer-Teixeira R, Belchior H, Leão RN, Ribeiro S, Tort AB. 2013 On high-frequency field oscillations (>100 Hz) and the spectral leakage of spiking activity. J Neurosci. 33:1535-9.

Schiffelholz T, Aldenhoff JB (2002) Novel object presentation affects sleep-wake behavior in rats. Neurosci Lett 328:41-44.

Schmitz D, Schuchmann S, Fisahn A, Draguhn A, Buhl EH, Petrasch-Parwez E, Dermietzel R, Heinemann U, Traub RD. (2001) Axo-axonal coupling. a novel mechanism for ultrafast neuronal communication. Neuron 31(5):831-840.

Schomburg EW, Anastassiou CA, Buzsáki G, Koch C. 2012. The spiking component of oscillatory extracellular potentials in the rat hippocampus. J Neurosci 32:11798-811

Scoville WB, Milner B (1957) Loss of Recent Memory after Bilateral Hippocampal Lesions. Journal of Neurology, Neurosurgery & Psychiatry 20: 11-21.

Sederberg, PB, Schulze-Bonhage A, Madsen JR, Bromfield EB, McCarthy DC, Brandt A, Tully, MS, Kahana MJ (2007) Hippocampal and neocortical gamma oscillations predict memory formation in humans. Cereb. Cortex 17 1190–1196.

Sejnowski TJ, Destexhe A (2000) Why do we sleep? Brain Res 886:208-223.

Seress L and Mrzljak L (1987) Basal dendrites of granule cells are normal features of the fetal and adult dentate gyrus of both monkey and human hippocampal formations. Brain Research 405: 169-174.

Siapas AG, Wilson MA (1998) Coordinated interactions between hippocampal ripples and cortical spindles during slow-wave sleep. Neuron. 21(5):1123-8.

Siapas AG, Lubenov EV, Wilson MA (2005) Prefrontal phase locking to hippocampal theta oscillations. Neuron 46:141-151.

Sik A, Penttonen M, Buzsáki G (1997) Interneurons in the hippocampal dentate gyrus: an in vivo intracellular study. European Journal of Neuroscience 9: 573-588.

Singer AC, Frank LM (2009) Rewarded outcomes enhance reactivation of experience in the hippocampus. Neuron. 64(6):910-21.

Sirota, A., Csicsvari, J. Buhl, D. and Buzsáki, G (2003) Communication between neocortex and hippocampus during sleep in rats and mice. PNAS. 100:2065-2069.

Skaggs WE, McNaughton BL (1996) Replay of neuronal firing sequences in rat hippocampus during sleep following spatial experience. Science. 271(5257):1870-3.

Skaggs WE, McNaughton BL, Wilson MA, Barnes CA (1996) Theta phase precession in hippocampal neuronal populations and the compression of temporal sequences. Hippocampus 6:149–172.

Sloviter RS, Valiquette G, Abrams GM, Ronk EC, Sollas EC, Paul LA, Neubort S (1989) Selective loss of hippocampal granule cells in the mature rat brain after adrenalectomy. Science 243: 535-538.

Solstad T, Boccara CN, Kropff E, Moser MB, Moser EI (2008) Representation of geometric borders in the entorhinal cortex. Science 322:1865-8.

Squire LR (1987) Memory and Brain. Oxford University Press.

Staba RJ, Wilson CL, Bragin A, Fried I, Engel J Jr (2002) Quantitative analysis of high-frequency oscillations (80-500 Hz) recorded in human epileptic hippocampus and entorhinal cortex. J Neurophysiol. 88(4):1743-52.

Stark E, Koos T, Buzsáki G (2012) Diode-probes for spatiotemporal optical control of multiple neurons in freely-moving animals. J Neurophys 108:349-63.

Steriade M (2000) Corticothalamic resonance, states of vigilance and mentation. Neuroscience 101:243-276.

Steriade M, Timofeev I (2003) Neuronal plasticity in thalamocortical networks during sleep and waking oscillations. Neuron 37:563-576.

Steriade M, Contreras D, Curro Dossi R, Nunez A (1993b) The slow (< 1 Hz) oscillation in reticular thalamic and thalamocortical neurons: scenario of sleep rhythm generation in interacting thalamic and neocortical networks. J Neurosci 13:3284-3299.

Steriade M, McCormick DA, Sejnowski TJ (1993c) Thalamocorical oscillations in the sleeping and aroused brain. Science 262:679-85.

Steriade M, Nuñez A, Amzica F (1993) A novel slow (< 1 Hz) oscillation of neocortical neurons in vivo: depolarizing and hyperpolarizing components. J Neurosci. 13(8):3252-3265.

Sullivan D, Csicsvari J, Mizuseki K, Montgomery S, Diba K, Buzsáki G (2011) Relationships between hippocampal sharp waves, ripples, and fast gamma oscillation: influence of dentate and entorhinal cortical activity. J Neurosci 31:8605-16.

Suzuki SS, Smith GK (1987) Spontaneous EEG spikes in the normal hippocampus. I. Behavioral correlates, laminar profiles and bilateral synchrony. Electroencephalogr Clin Neurophysiol 67:348–359.

Swanson LW, Wyss JM, Cowan WM (1978) An autoradiographic study of the organization of intrahippocampal association pathways in the rat. Journal of Comparative Neurology 181: 435-442.

Swanson, L. W., Köhler, C., and Björklund, A. (1987). The limbic region. I. The septohippocampal system. In “Handbook of Chemical Neuroanatomy” (Björklund, A., Hökfelt, T., and Swanson, L. W., Eds.), Vol. 5, Part I., pp. 125–227. Elsevier, Publisher, Amsterdam.

Tass, P., Rosenblum, M.G., Weule, J., Kurths, J., Pikovsky, A.S., Volkmann, J., Schnitzler, A., Freund, H.J (1998) Detection of n:m Phase Locking from Noise Data: Application to Magnetoencephalography. Phys. Rev. Lett. 81 (1998) 3291–3294

Taxidis J, Coombes S, Mason R, Owen MR (2011) Modeling sharp waveripple complexes through a CA3-CA1 network model with chemical synapses. Hippocampus. Advance online publication. Retrieved March 30, 2011. doi:10.1002/hip.20930.

Timofeev I, Grenier F, Steriade M (2001) Disfacilitation and active inhibition in the neocortex during the natural sleep-wake cycle: an intracellular study. Proc Natl Acad Sci U S A 98:1924-1929.

Tononi G, Cirelli C (2006) Sleep function and synaptic homeostasis. Sleep Med Rev 10:49-62.

Traub R, Bibbig A (2000) A model of high frequency ripples in the hippocampus based on synaptic coupling plus axon-axon gap junctions between pyramidal neurons. J Neurosci 20:2086–2093.

Traub RD (2003) Fast Oscillations and Epilepsy. Epilepsy Curr. 3(3):77-79.

Traub RD, Draguhn A, Whittington MA, Baldeweg T, Bibbig A, Buhl EH, Schmitz D (2002) Axonal gap junctions between principal neurons: a novel source of network oscillations, and perhaps epileptogenesis. Rev Neurosci. 13(1):1-30.

Traub RD, Schmitz D, Maier N, Whittington M, Draguhn A (2012) Axonal properties determine somatic firing in a model of in vitro CA1 hippocampal sharp wave/ripples and persistent gamma oscillations. Eur J Neurosci 36: 2650-2660.

Treves A, Rolls ET (1994) Computational analysis of the role of the hippocampus in memory. Hippocampus 4: 374-391.

Tsodyks MV, Skaggs WE, Sejnowski TJ, McNaughton BL (1996) Population dynamics and theta rhythm phase precession of hippocampal place cell firing: a spiking neuron model. Hippocampus 6:271-280.

Tukker JJ, Fuentealba P, Hartwich K, Somogyi P, Klausberger T (2007) Cell type-specific tuning of hippocampal interneuron firing during gamma oscillations in vivo. Journal of Neuroscience 27: 8184-8189.

Vanderwolf CH. 1988. Cerebral activity and behavior: control by central cholinergic and serotonergic systems. Int Rev Neurobiol. ;30:225-340.

Vertes RP and McKenna JT (2000) Collateral projections from the supramammillary nucleus to the medial septum and hippocampus, Synapse 38: 281-293.

Vertes RP, Hoover WB, Viana Di Prisco G (2004) Theta rhythm of the hippocampus: subcortical control and functional significance. Behavioral Cognitive Neuroscience Reviews 3: 173-200.

von Krosigk M, Bal T, McCormick DA (1993) Cellular mechanisms of a synchronized oscillation in the thalamus. Science 261:361-364.

Vukadinovic Z (2011) Sleep abnormalities in schizophrenia may suggest impaired trans-thalamic cortico-cortical communication: towards a dynamic model of the illness. Eur J Neurosci 34:1031-9.

Wagner T, Axmacher N, Lehnertz K, Elger CE, Fell J. (2010) Sleep-dependent directional coupling between human neocortex and hippocampus. Cortex 46:256–263.

Wamsley EJ, Tucker MA, Shinn AK, Ono KE, McKinley SK, Ely AV, Goff DC, Stickgold R, Manoach DS (2012) Reduced sleep spindles and spindle coherence in schizophrenia: mechanisms of impaired memory consolidation? Biol Psychiatry 71:154-61.

Wang XJ (2010) Neurophysiological and computational principles of cortical rhythms in cognition. Physiol Rev. 90(3):1195-268.

Whittington MA, Cunningham MO, LeBeau FE, Racca C, Traub RD (2011) Multiple origins of the cortical gamma rhythm. Dev Neurobiol. 71(1):92-106.

Wikenheiser M., Redish AD. 2013. The balance of forward and backward hippocampal sequences shifts across behavioral states. Hippocampus. 23: 22-9

Wierzynski CM, Lubenov EV, Gu M, Siapas AG (2009) State-dependent spike-timing relationships between hippocampal and prefrontal circuits during sleep. Neuron 61:587-96.

Wilson MA, McNaughton BL (1994) Reactivation of hippocampal ensemble memories during sleep. Science. 265(5172):676-9.

Wilson S, Argyropoulos S (2012) Sleep in schizophrenia: time for closer attention. Br J Psychiatry 200:273-4.

Witter MP, Groenewegen HJ, Lopes da Silva FH, Lohman AH. (1989) Functional organization of the extrinsic and intrinsic circuitry of the parahippocampal region. Prog Neurobiol. 33(3):161-253.

Wittner L, Henze DA, Zaborszky L, Buzsáki G (2007) Three-dimensional reconstruction of the axon arbor of a CA3 pyramidal cell recorded and filled in vivo. Brain Struct Funct. 212:75-83.

Wolansky T, Clement EA, Peters SR, Palczak MA, Dickson CT (2006) Hippocampal slow oscillation: a novel EEG state and its coordination with ongoing neocortical activity. J Neurosci. 26(23):6213-29.

Wouterlood FG, Saldana E, Witter MP (1990) Projection from the nucleus reuniens thalami to the hippocampal region: light and electron microscopic tracing study in the rat with the anterograde tracer phaseoulus vulgaris-leucoagglutinin. J Comp Neurol 296:179-203.

Wu C, Asl MN, Gillis J, Skinner FK, Zhang L (2005) An in vitro model of hippocampal sharp waves: regional initiation and intracellular correlates. J. Neurophysiol. 94, 741e753.

Ylinen A, Bragin A, Nadasdy Z, Jando G, Szabo I, Sik A, Buzsáki G (1995) Sharp wave-associated high-frequency oscillation (200 Hz) in the intact hippocampus: network and intracellular mechanisms. J Neurosci. 15:30–46.

Zhao C, Deng W, Gage FH (2008) Mechanisms and functional implications of adult neurogenesis. Cell 132: 645-660.

DAVID W. SULLIVAN

479 Manila Ave #3, Jersey City NJ 07302 | 201-284-9909 | Sullivan.dw@gmail.com

EDUCATION

Rutgers University, Newark NJ
Ph.D. in Neuroscience **expected 2013**
Dissertation: Inter-regional synchronization in the hippocampal system by oscillations: unit and LFP studies

University of Virginia, Charlottesville VA
B.S. in Computer Science **2001**
Thesis: Vine: a tool for analysis of excitation in a neural network model of hippocampal CA3

TEACHING EXPERIENCE

Rutgers University
Teaching Assistant: Psychology 101 **2007**
Held a weekly 90 minute review and demonstation lecture

Teaching Assistant: Foundations in Neuroscience **2006**
Held a review session prior to each exam

LAB EXPERIENCE

Dr. Gyorgy Buzsaki, Rutgers University
Ph.D. Student **August 2004 – March 2013**
Surgery room manager, lab meeting coordinator

Dr. Laszlo Zaborszky, Rutgers University
Rotating Ph.D. student **January 2007 – April 2007**

Dr. William B Levy, University of Virginia
Research Assistant **June 2000 - July 2004**

PUBLICATIONS

Sullivan DW, Buzsaki G (**2013**) Properties of sharp wave ripples in the waking and sleeping rat. Manuscript under preparation.

Sullivan DW, Mizuseki K, Sorgi A, Buzsaki G (**2013**) Relationships between sleep spindles and theta oscillations in the hippocampus. Submitted.

VandeCasteele M., S M, Royer S, Belluscio M, Berényi A, Diba K, Fujisawa S, Grosmark A , Mao D, Mizuseki K, Patel J, Stark E, Sullivan D, Watson B, Buzsáki G. (**2012)** Large-scale recording of neurons by movable silicon probes in behaving rodents. Jove March 2012.

Sullivan DW, Csicsvari J, Mizuseki K, Montgomery SM, Diba K, Buzaski G (**2010**) Relationships between hippocampal sharp waves ripples, and fast gamma oscillation: influence of dentate and entorhinal cortical activity. J Neurosci 31:8605-8616

Gundlfinger A, Breustedt J, Sullivan D, Schmitz D (**2010**) Natural spike trains trigger short- and long-lasting dynamics at hippocampal mossy fiber synapses in rodents. PLoS One 5:e9961.

Levy WB, Sanyal A, Rodriguez P, Sullivan DW, Wu XB (**2005**) The formation of neural codes in the hippocampus: trace conditioning as a prototypical paradigm for studying the random recoding hypothesis. Biol Cybern 92:409-26.

Sullivan DW, Levy WB (**2004**) Quantal synaptic failures enhance performance in a minimal hippocampal model. Network 15:45-67.

Shon AP, Wu XB, Sullivan DW, Levy WB (**2002**) Initial state randomness improves sequence learning in a model hippocampal network. Phys Rev E 65:031914.